Experimental and numerical modelling of sewage surge during urban flooding

Auteur : Fontaine, Fantine
Promoteur(s) : Dewals, Benjamin
Faculté : Faculté des Sciences appliquées
Diplôme : Master : ingénieur civil des constructions, à finalité spécialisée en "urban and environmental engineering"
Année académique : 2018-2019
URI/URL : http://hdl.handle.net/2268.2/6805

Experimental and numerical modelling of sewage surge during urban flooding

Report submitted as part requirement for the Degree of Master in Civil Engineering

by Fantine Fontaine

Advisor: B. Dewals
Members of the Jury : P. Archambeau, S. Erpicum, J. Shucksmith
Academic coordinator : J.-M. Franssen

University of Liège - Faculty of Applied Sciences

Academic year 2018-2019

Acknowledgements

I would like to thank my friends and family for the moral support and encouragements. Thanks to my housemates for the proper introduction to South Yorkshire and English culture, the discoveries in Peak District and exciting nights in Sheffield. Special thank to Matthew for reading and commenting the report. To Mathilde, thank you for the support during the last few days. Last but not least, I would like to thank the British government for delaying Brexit while I was still in the United Kingdom.

I would like to thank Martin and Paul in the lab for fixing when needed and set up everything. To Matteo Rubinato, thank you for the great help during the tests, for showing me all the tips and sharing your expertise on the subject. I would like to thank James Shucksmith for the continuous supervision and comments throughout my work in Sheffield. I would like to thank Benjamin Dewals for the support in the numerical simulations and the great and important reviews at the end of the study. Finally, I would like to thank all the members of the jury for taking the time to be a part of this Master Thesis.

Abstract

With the increasing of urban flood events, drainage models are more and more useful to assess the risk associated with those events. Linking discharge equations are implemented in order to estimate the exchange flow rate between the surface and a pipe system. The discharge coefficient is the only empirical parameter used in those equations. Its estimation is then very important. This Master Thesis aims to continue the work of Rubinato et al. (2017) [12] whose perspective was to perform more unsteady state tests in order to conclude about the adequation of the estimated discharge coefficient in those events.

The work done for this Master Thesis starts with the conduction of 50 steady and 48 unsteady state experimental tests. The analysis of the steady state tests ends with the evaluation of an appropriate discharge coefficient for all the possible scenarios. Two numerical models are confronted to the experimental results by using the previously fitted discharge coefficients in the linking equations. One is modelling the configuration with a uniform flow and the other, more complex, is a 2D software solving the dynamic shallow-water equations (Wolf). The numerical model presents acceptable results compared to the experimental data.

The discharge coefficients are implemented in the uniform flow model with the unsteady state tests results after its validation for the steady state events. The model matches the experimental results with a low tendency to overestimate the exchange flow rate. The results improve with a high exchange flow rate or with a longer duration of the event.

All recorded data gathered during this study can be found on the following link : `https://drive.google.com/drive/folders/16HAIfZQsXmxB4pJ4pIFNRCjNkdV3QKFv?usp=sharing`

Contents

List of notations

ΔE : total energy loss between two points

A_m : manhole area

C_i : Discharge coefficient

D_m : manhole diameter

E : total energy head

Fr_s : surface flow Froude number

h : water depth

h_{exp} : experimental water depth

h_p : water depth in the manhole used for calculations

h_s : water depth of the surface used for calculations

$h_s(h_{exp})$: surface water depth taken from the upstream surface experimental water depth

$h_s(h_u)$: surface water depth calculated from a uniform flow model (Manning)

$h_s(h_{wolf})$: surface water depth calculated by Wolf software

h_u : uniform water depth

K : energy loss coefficient

L : surface width

n : Manning coefficient

P : pressure head

Q : flow rate

Q_1 : upstream surface flow rate in the facility

Q_3 : upstream pipe flow rate in the facility

Q_4 : downstream pipe flow rate in the facility

Q_{exp} : measured flow rates in the facility

Q_e : exchange flow rate

$Q_e(Q_{exp}) = Q_4 - Q_3$: exchange flow rate calculated from experimental flow rates

$Q_e(h_{exp}, C_i)$: exchange flow rate calculated from the linking equations with the experimental surface water depth and a discharge coefficient

$Q_e(h_u, C_i)$: exchange flow rate calculated from the linking equations with the uniform water depth and a discharge coefficient

$Q_e(h_{wolf}, C_i)$: exchange flow rate calculated from the linking equations with the surface water depth calculated by Wolf software and a discharge coefficient

Re_p : pipe flow Reynolds number

s : slope

v : velocity

Z_{crest} : surface elevation relative to the pipe hydraulic head

1 Introduction

Urban flood events are becoming more and more significant and frequent. Urban drainage models are used to assess the risk associated with those events. Those models either use linking discharge equations to estimate the exchange flow rate between the pipe network and the free surface above or head loss equations to assess the local head losses in manholes. Those equations rely on a number of empirical parameters. Lots of studies have been conducted to quantify the parameters needed to model urban flooding. This report first goes through significant results relating to this research. The conclusion made by Rubinato et al. (2017) [12] stated that there was a lack of information about the quantification of head losses in unsteady events. This Master Thesis focuses on the subject by conducting a larger range of unsteady state tests which are compared to a numerical model.

The first phase comprising of the experimental work is conducted in a facility provided by the University of Sheffield (UK). It represents a typical UK road linked to a pipe network by a single manhole, constructed with a 1/6 geometrical scale. The first objective is the calibration of the instruments which is required to produce quality data. After that, a number of steady state tests are performed and compared with the previous results (Rubinato et al. (2017) [12]). After the conduction of steady state tests, new experimental tests focusing on unsteady state conditions are performed with more configurations than in the previous research. The tests are conducted by looking at different types of unsteady events in peak surge and duration. A total of 98 tests are performed (50 steady state and 48 unsteady state tests).

The second part of the report concentrates on numerical modelling. A first model is implemented which calculates the results taking into account a uniform flow configuration. All the tests are simulated in this model. With the help of Wolf software, developed by the University of Liège (BE), a second set of results is collected but this time only for a small amount of tests. This software is a hydraulic numerical 2D model solving the fully dynamic shallow-water equations.

Finally, analysis and comparison of the experimental and numerical results are made. The analysis studies the accuracy of exchange flows equations implemented with one parameter gathered by the experiments : the discharge coefficient. Two approaches are made in order to define the best discharge coefficient, considering two different estimations of the head pressure in the manhole. The main objective of this Master Thesis is to define a discharge coefficient implemented in a numerical model that would represent the actual exchange flow between a sewer and a surface with the best accuracy.

2 Literature review

This chapter contains a summary of the literature regarding unsteady state studies in similar conditions as well as findings about the quantification of energy losses.

2.1 Vertical exchanges in unsteady state scenarios

Saldarriaga et al. (2012) [14] studied the behaviour of the flow inside a manhole connected to one inlet and one or two outlets depending on the configuration considered. This model is represented on Figure 2.1, the three pipes attached to the manhole can be positioned differently or even removed. 188 tests were conducted in total.

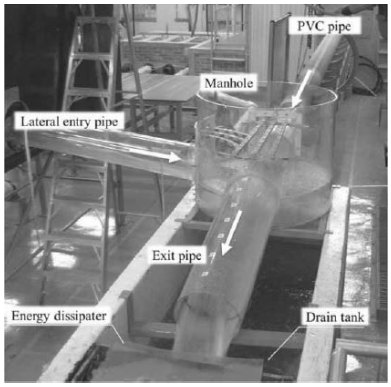

Figure 2.1: Geometry of the model used by Saldarriaga et al. (2012) [14]

The conclusion of this report stated the presence of three types of standing waves in the hydraulic behaviour of a manhole.

Another paper (Bazin et al. (2014) [2]) studied the interaction between a surface and a sewer system. The facility used for this research consists on a modelled street with two sidewalks connected to a drainage system by a series of manholes on each side of the street. Figure 2.2 shows the experimental model.

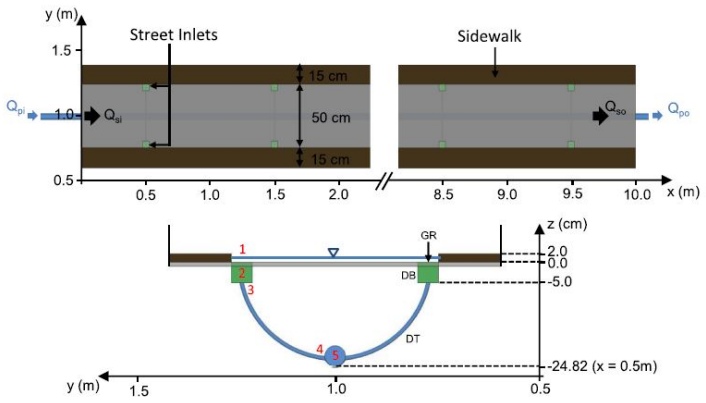

Figure 2.2: Geometry of the model used by Bazin et al. (2014) [2]

The experimental procedure included steady state tests (twelve drainage scenarios and four overflow scenarios) as well as two unsteady state tests. In the unsteady state cases, numerical results matched the experimental ones, however, no comparison can be made because the main characteristics of the tests were limited. For example, the model consisted of a pipe junction (with no manhole), the scenarios conducted only represented pressurised pipe conditions, the range of Reynolds numbers tested was quite limited, etc.

Fraga et al. (2017) [5] conducted an experiment on a real scaled model of a street section. This study modeled the rainfall with the help of diffusers located above the surface. Figure 2.3 indicates the geometry of the model used for those experiments.

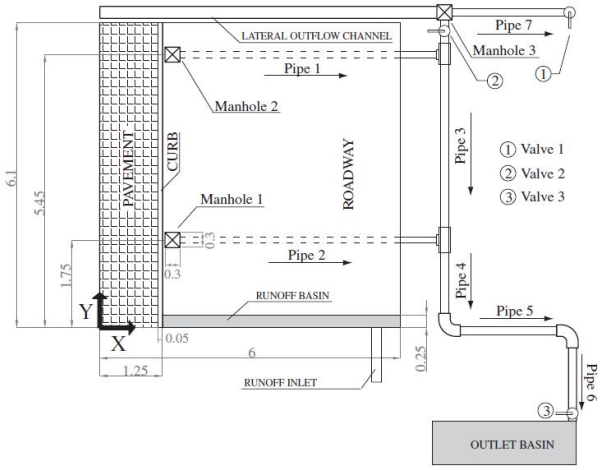

Figure 2.3: Geometry of the model used by Fraga et al. (2017) [5]

This research used the same linking equations as the ones used in Rubinato et al. (2017) [12] (see Section 2.3) and the research in this Master Thesis (see Section 4.1). The numerical model predicted the flow rates in all the pipes with the accuracy given in Figure 2.4, however, no information about the discharge coefficient was given.

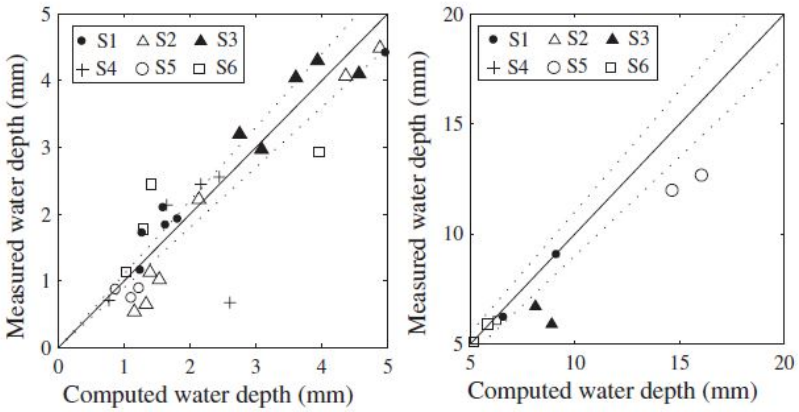

Figure 2.4: Comparison between numerical and experimental results of Fraga et al. (2017) [5]

2.2 Energy loss coefficient

The studies made by Marsalek (1984) [7] focused on characterising the energy losses in different types of junctions in order to quantify the effects of the junction geometry. One of the configuration tested is the same as the one used in this project (circular manhole ; junction M1). The different configurations tested are shown in Figure 2.5. The upstream and downstream pipe diameters were identical for all the tests, with an internal diameter of $152mm$. The circular manhole had an internal diameter of $293mm$ which results in a ratio of $D_{manhole}$ over D_{pipe} of 1.92. In the facility used in this project, the ratio is 3.2, however, the results could still be compared as Sangster et al. (1958) [15] concluded in their research that the loss coefficient do not increase that much for ratios larger than 2. In his research, Marsalek (1984) [7] also tested different manholes with smaller diameter and this previous conclusion is what brought him not to test manholes wider than $2D_{pipe}$. For this report, only the larger manhole tested by Marsalek (1984) [7] will be of interest.

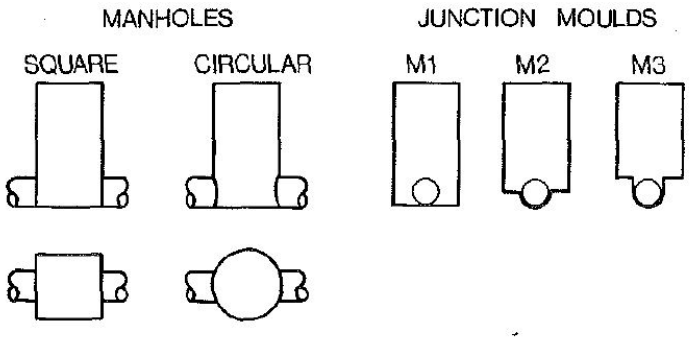

Figure 2.5: Geometries tested by Marsalek (1984) [7]

Those tests were conducted in steady state conditions. In order to quantify the head loss coefficient, the head loss ΔE was expressed as a difference of the total energy head ($E = z + p + \frac{v^2}{2g}$) between points downstream and points upstream of the junction. It was then compared to the expression of $\Delta E = K\frac{v^2}{2g}$ in a graph so that the head loss coefficient K could be found.

The test results showed that, for a circular manhole with a M1 junction (see Figure 2.5) the mean value of the head loss coefficient is 0.208 in a 95% confidence limit of 0.195 to 0.221.

An other interesting study was performed by Wang et al. (1998) [16]. This research tried to determine the effect of four parameters on the head loss coefficient K : Reynolds number, surcharge depth, relative inflows and pipe diameter. The model consisted of a junction of four pipes (three inlets and one outlet), see Figure 2.6. The model had a $1/6$ scale and a $1/1000$ slope (such as the experimental model used in this present research). In order to compare the research done by Wang et al. (1998) [16] to the present one, lateral junction b has to be eliminated from the model and lateral junction a can be presented as the inflow coming from the surface (see Section 3.1 for more information on the model for this research). Even so, it remains a difference with the present work in the fact that the flow coming from pipe a would have to be vertical.

The results of this study showed that the head loss coefficients do not depend on the Reynolds number or the surcharge level. Figure 2.7 indicates the results for this research (open squares) compared with the results of Marsalek (1984) [7] previously cited (filled triangles).

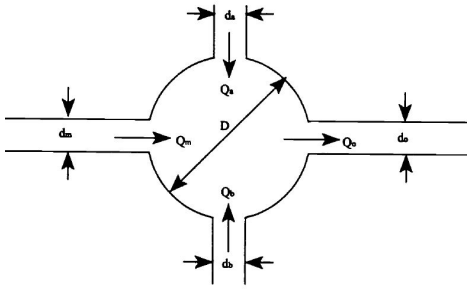

Figure 2.6: Geometry of the model used by Wang et al. (1998) [16]

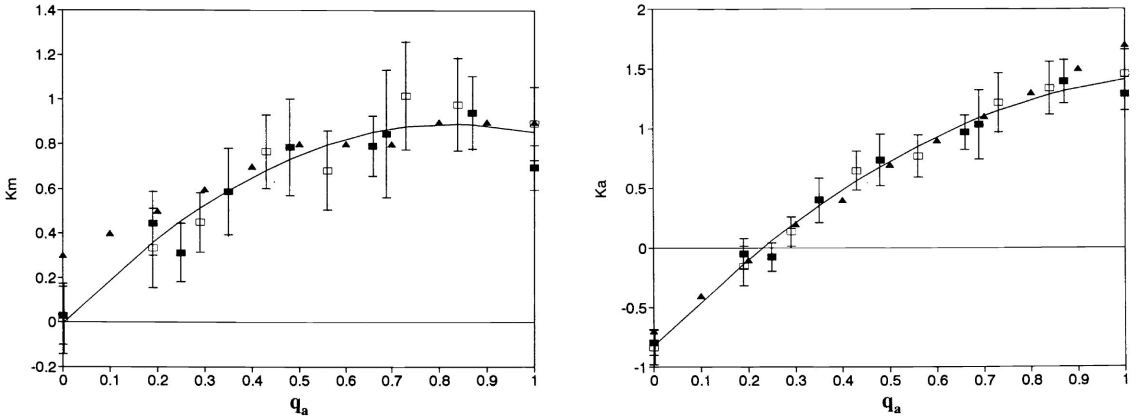

Figure 2.7: Variation of the loss coefficient K_m for the inlet pipe m (left) and K_a for the inlet pipe a (right) depending on the inflow a - Wang et al. (1998) [16] : open squares ; Marsalek (1984) [7] : filled triangles

O'Loughlin et al. (2002) [8] mentioned several conditions that can influence the head losses in manholes. It could be related to geometry of the manhole (number of them, diameter and angle of the pipes reaching the manhole(s) as well as their position from one to another) or flow characteristics (in the pipe system and on the surface). The conclusion of their study mentioned that flow in a manhole is extremely complex to calculate with known methods and developments of theoretical concepts has to be made in order to achieve accurate expressions. Moreover, as energy loss coefficients are derived from steady state tests, sometimes, they do not apply well in unsteady state scenarios.

Pfister et al. (2014) [10] also used the same approach as Marsalek (1984) [7] to calculate the energy loss coefficient by comparing the total energy loss between two points ΔE to $v^2/2g$. The tests were conducted for a 45° and a 90° manhole junction and provided good expressions of the head loss coefficients.

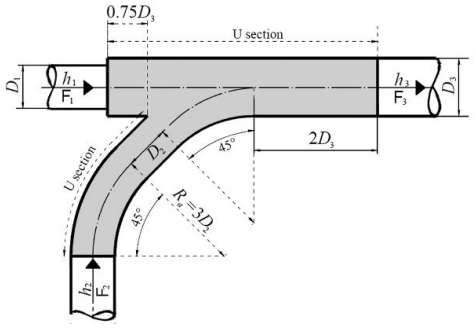

Figure 2.8: Geometry of the 90° junction in Pfister et al. (2014) [10]

It is important to notice that the method is often used in scientific papers. However, the results of this study in term of values are not of interest for this project as the geometry is quite different (the 90° turn is made horizontally and not vertically as in the facility used in this research and the shape of the junction is not as direct, see Figure 2.8).

2.3 Experiments done in the same facility

Several tests were conducted on the experimental model used for this project. The experimental facility is detailed at Section 3.1.

Originally, the facility was set up for the PhD Thesis of Dr. M. Rubinato [11]. This research had the objective to design an experimental model that can provide numerous information about pressure, flow rates and velocities in a single pipe connected to a surface by a single manhole. This facility allowed the application of different scenarios, in steady or unsteady state conditions.

The research done by Rubinato provided several new information : (1) the quantification of energy losses in a manhole during steady state conditions, (2) the quantification of exchange flows between a surface and a sewer through a single manhole, (3) the quantification of discharge coefficients and (4) the performance of numerical hydraulic models during unsteady state events. All results were, after that, published in different papers that this Section will review.

Using the same facility, several papers were published of which two are interesting for this research. First, Rubinato et al. (2017) [12] conducted experiments in steady and unsteady conditions in order to quantify the value of discharge coefficients for a large amount of hydraulic conditions. This was the first study leading to this quantification. They also confronted their results to a 2D numerical model using shallow water equations for the surface flow coupled with a model for the sewer flow both linked through general weir/orifice equations. Those equations will be used in this research as well (see Section 4.1).

A series of tests were conducted in order to generate different scenarios. Figure 2.9 details the four scenarios.

- Scenario 1 : Flow on the surface with no flow in the pipe system (or small flow not inducing surcharge of the sewer), resulting in a surface to sewer flow exchange. This scenario corresponds to the application of a weir equation.
- Scenario 2 : Surface to sewer exchange with both a flow on the surface and in the sewer system. This corresponds to the application of a submerge weir or submerge orifice equation.
- Scenarios 3 and 4 : The sewer system overflowing on to the surface. This configuration can happen if there is either flow on the surface (Scenario 3) or not (Scenario 4), both resulting in a sewer to surface exchange. Those scenarios correspond to the application of an orifice equation.

Those scenarios were, at first, generated in steady state conditions with several tests. After that, nine tests were conducted to generate all of those scenarios in unsteady state conditions.

The discharge coefficients found for the steady state tests were the following : between 0.493 and 0.587 for the weir equation ; between 0.054 and 0.057 for the submerged weir equation ; between 0.159 and 0.174 for the orifice equation. The paper concluded that those coefficients can be used as they correctly reproduce the behaviour of the exchange flow between a surface and a sewer in steady state conditions.

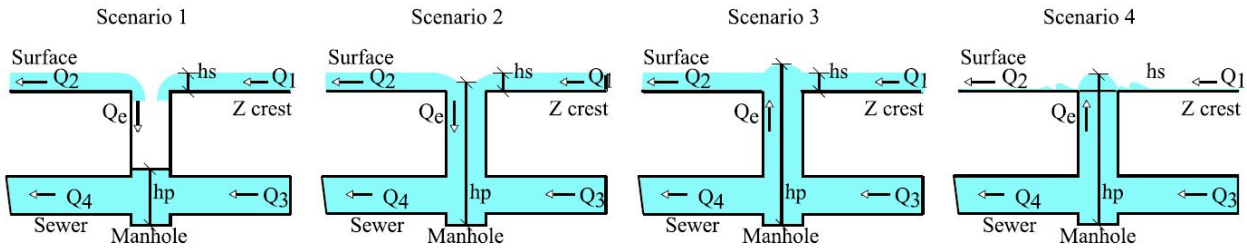

Figure 2.9: Scenarios tested in the experiments done by Rubinato et al. (2017) [12]

As for unsteady conditions, the small number of tests conducted could not lead to a proper conclusion. It was seen that the numerical model using the previously calibrated discharge coefficient, overestimated the amount of exchanged flow rate. This was assumed to be caused by the additional head losses not existing in steady state conditions.

The second interesting paper had the objective to quantify the energy losses in a surcharging manhole (Rubinato et al. (2018) [13]). In this paper, the experimental results were confronted to a numerical model called Sipson (Djordjevic et al. (2005) [4]). This paper also compared the results obtained by the application of a lid on the manhole.

By plotting the relationship between the head losses and velocity head, they managed to evaluate the value of the head loss coefficient. It was found that the sewer to surface energy loss coefficient was not affected by neither the flow on the surface nor the conditions in the pipe, downstream of the manhole. However, the sewer energy loss, while not affected by the flow on the surface, was directly dependent on the the closure of the pipe system downstream of the manhole. The mean of the total head loss coefficient K varies from 0.81 to 1.14 with an obstruction downstream in the pipe system from 50% to 85%.

The conclusion of this paper stated that the results were conclusive for this configuration and could be an alternative to usual quantification of vertical exchanges such as the one used in the previous paper (Rubinato et al. (2017) [12]). It was also said that further work should focus on the variability of this coefficient regarding other configurations and geometry of the manhole. It was also showed that numerical modelling was not able to provide good results when the surcharging conditions were more complex.

The main objective of this present work is to perform more unsteady state condition tests in order to observe the behaviour of those tests. Conducting those experiments should reply to the request of information observed in the studies previously cited.

3 Experimental model

In this chapter, the experimental modelling is explained. First, the facility as well as the instruments used for the collection of data are detailed then, their calibration is performed to obtain the best data outcome from the main data collection software (*LabView*). Finally, the procedure of the experiments iq explained for the steady and unsteady state tests.

3.1 Model characteristics

The model facility is built in the Hydraulic Laboratory of the University of Sheffield (UK) and represents a surface of $4m$ by $8.2m$ with a slope of 0.001 connected to a sewer pipe system through a single manhole. The pipe system has an internal diameter of $75mm$. The manhole is circular with a diameter of $240mm$ and is $478mm$ long under the bed of the flume. The pipe system is going through the manhole with one inflow and one outflow junction.

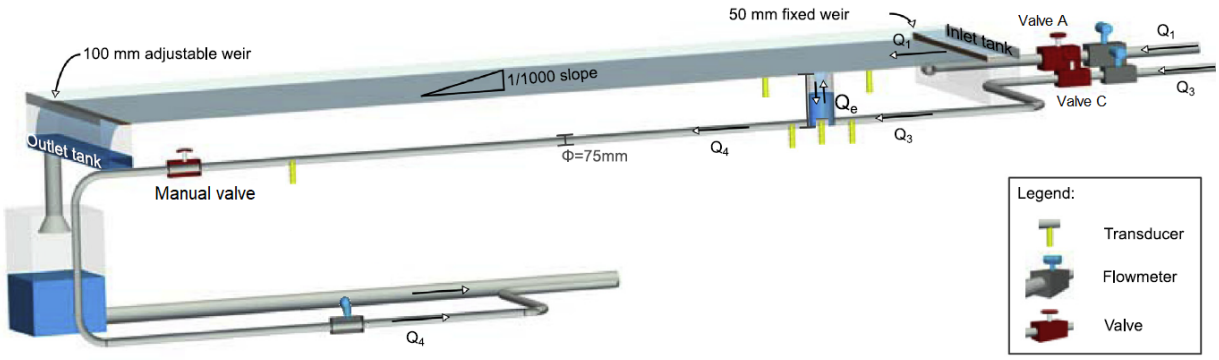

Figure 3.1: Scheme of the experimental facility [12]

Figure 3.1 shows the different instruments that will be used during the tests and Figures 3.2 and 3.3 show the actual facility. There are : two automated valves controlling the upstream flows on the surface (Valve A) and in the pipe system (Valve C); one manual valve downstream of the pipe system; three flow meters, two upstream (measuring Q_1 for the surface and Q_3 for the sewer) and one downstream (measuring Q_4 for the sewer) of the facility; two pressure transducers on the surface (measuring $P_{surface,up}$, $710mm$ from the centre of the manhole and $P_{surface,dn}$, $1010mm$ from the manhole) and four in the pipe system (measuring $P_{sewer,up}$, $P_{sewer,dn}$ as well as $P_{manhole}$ at the centre of the manhole and $P_{sewer,dn2}$ just before the manual valve). In Section 3.2, those instruments will be detailed further.

The experimental model is based on a typical UK drainage system. It is designed and constructed with a 1/6 geometrical scale. This model is governed by a Froude similitude meaning that the Froude number should remain identical in the experimental data and at real scale. All the factors are located in Table 3.1. For more detailed calculations, see the PhD Thesis of Dr. M. Rubinato [11] at Section 3.1.

Figure 3.2: Actual experimental facility : surface from downstream (left) and downstream pipe system (right)

Figure 3.3: Actual experimental facility : upstream pipe system (left) and manhole (right)

Measurements	Scale
Lengths	1/6
Time	1/2.45
Velocities	1/2.45
Volume flows	1/88.18

Table 3.1: Froude similitude for the experimental model

The valves control the flow rate that will enter the system. Valve A controls the flow entering the surface bed while Valve C controls the flow in the pipe system (Figure 3.4). They are controlled by *LabView* system and can open within a range of $[0 - 165](-)$, 165 being completely open. Those valves are butterfly valves, controlling the flow with the rotation of a disk.

There is also a manual valve at the end of the pipe system allowing it to obstruct the flow downstream of the manhole.

Figure 3.4: Valve A (left) and Valve C (right)

3.2 Instrumentation

There are several instruments that are used for measurements during the experiment. In this section, a small description of all of them is done followed by their calibration procedure and results.

3.2.1 Flow meters

There are two flow meters for the surface, one upstream and one downstream. It is the same for the flow meters for the pipe system. There are two types of flow meters as seen in Figure 3.5. Both of them are electromagnetic *MAG900* flow meters, supplied by *Arkon Flow System* (UK). the error of this flow meter is 0.5% of the maximal flow rate ($11l/s$) meaning a maximal $+-0.055l/s$ error.

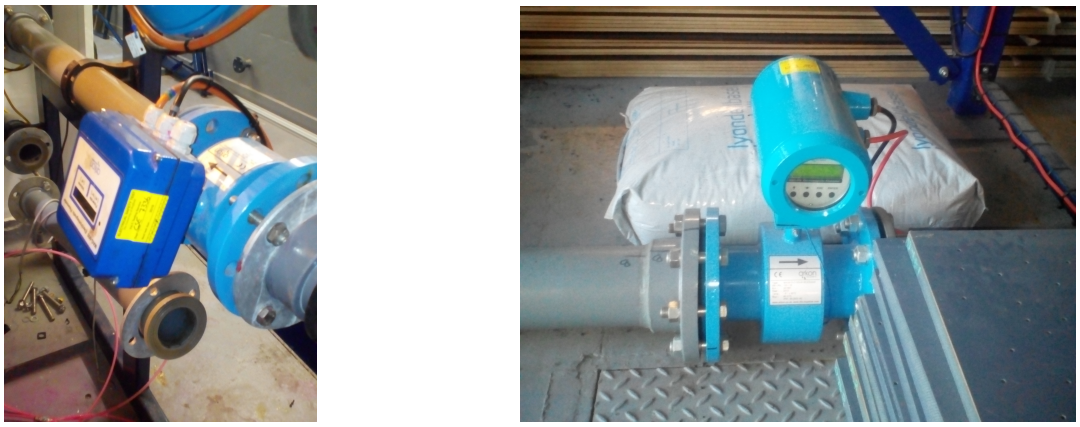

Figure 3.5: Two types of flow meters in the model

For the flow meter calibrations, the valve is opened from 100 to 165 with a step of 5. The openings have to be increased and preferably with no going back to avoid an hysteresis phenomenon. First, the flow is generated for the considered valve opening for at least 3 minutes. After this time, once the flow stabilised, it is observed directly on the flow meter and written down every 5 seconds for 3 minutes during which the computer records its electrical signal. The average of all the data is calculated for each valve opening. Finally, a graph comparing the measured flow rate (in l/s) and the electrical signal (in A) is drawn.

In order to have a meaningful mean, a comparison between a usual mean and one removing the values above or below 5% of the usual mean is made. It is found that sometimes, it is required to

remove some terms in the evaluation of the mean. It is, however, only useful for a small number of results as most of the values are very similar.

The same method is followed for the surface and the pipe flow meters. In order to perform the calibration of the pipe flow meters, Valve A is shut down and vice versa for the surface flow meters.

While doing the calibrations of the water tank (see next paragraph) for a 165 opening, it is discovered that the upstream and downstream pipe flows do not correspond. It is discovered that some of the pipe flow went to the surface. Closer look on when it started, showed that only with an opening of 165 of the valve, the water started to appear on the surface. Conclusion, the calibrations of the pipe system instruments do not take into account the last measurement with the biggest opening of the valve.

Figures 3.6 and 3.7 show the results of the pipe flow meters calibrations.

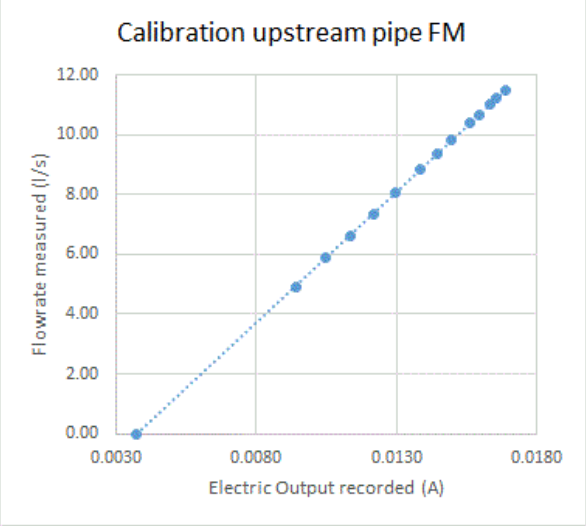

Figure 3.6: Calibration of the upstream flow meter for the pipe

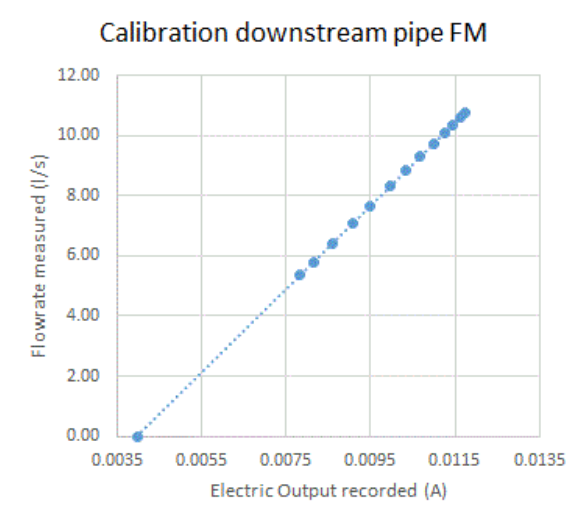

Figure 3.7: Calibration of the downstream flow meter for the pipe

From those graphs a linear equation can be fitted that is be added to the main data acquisition program. Those equations are :

$$y = 874.18x - 3.2788 \tag{3.1}$$

for the upstream flow meter and

$$y = 1388.6x - 5.5337 \tag{3.2}$$

for the downstream flow meter (x being the recorded signal in A and y the corresponding flow rate in l/s).

The surface flow meters can be calibrated following the same method. Figure 3.8 shows the results of the upstream surface flow meter calibration.

The linear equation fitted from this graph can be used to transform the electrical signal from the flow meter to an exact flow rate. This equation is :

$$y = 868.87x - 3.4577 \tag{3.3}$$

for the upstream flow meter (x being the recorded signal in A and y the corresponding flow rate in l/s).

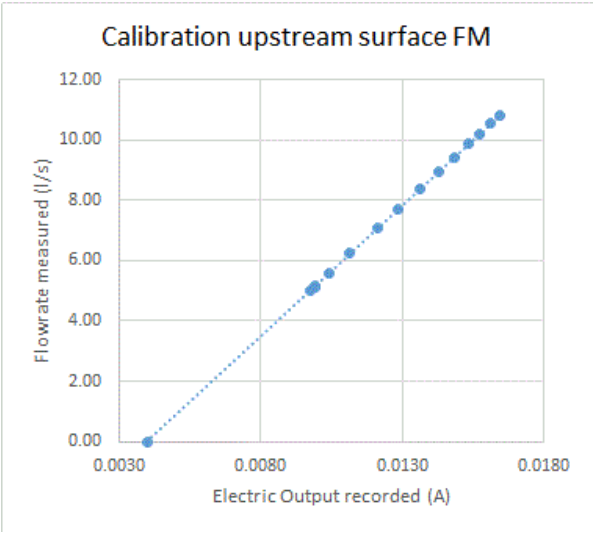

Figure 3.8: Calibration of the upstream flow meter for the surface

3.2.2 Measuring tank

The measuring tank collects water downstream of the model. Figure 3.9 shows the bar outside the tank used to assess the volume of water inside the tank.

Figure 3.9: Water tank gauge

Recorded upstream and downstream flows can present some differences. In order to decrease the error between them, a coefficient is applied to the recorded values. The method consists of measuring the flow of a measuring tank located at the end of the system and comparing it to the recorded flows. This method is applied only to the pipe flow meters as the water coming out of the surface, unfortunately, does not go into a measuring tank.

The method is the following. Valve C is opened increasingly from 100 to 165 with a 5 step interval. Then, the speed at which the tank is filled is measured. In order to do that, the time between two marks on the bar coming out of the tank (spaced from 1 foot) is observed (Figure 3.10). 849.505 (specific constant for this tank for a 1 foot measurement) is divided by this duration and it gives the measured flow in the tank for each valve opening. This process is repeated three times in order to average the results.

As said in the previous paragraph, results for the 165 opening are not taken into account due to a leak of water from the pipe to the surface.

Figure 3.10: Measurements on the water tank gauge

Comparing the electrical signal recorded and measured flow in the tank, an error value is calculated.

$$Error = \frac{Recorded\ flow - measured\ tank\ flow}{measured\ tank\ flow} \times 100 \tag{3.4}$$

In order to decrease this error, a correction factor is applied to the recorded flow rates. This factor is calculated by dividing each recorded flow rate by the measured flow rate in the tank and taking an average of this value. It is found that the factors for the upstream and downstream pipe flow meters are 1.132 and 1.095 and will be multiplied to Equations 3.1 and 3.2.

Figure 3.11 shows the difference between the flows with and without the correction factor. Figure 3.12 shows the evolution of the error with or without the application of the factor.

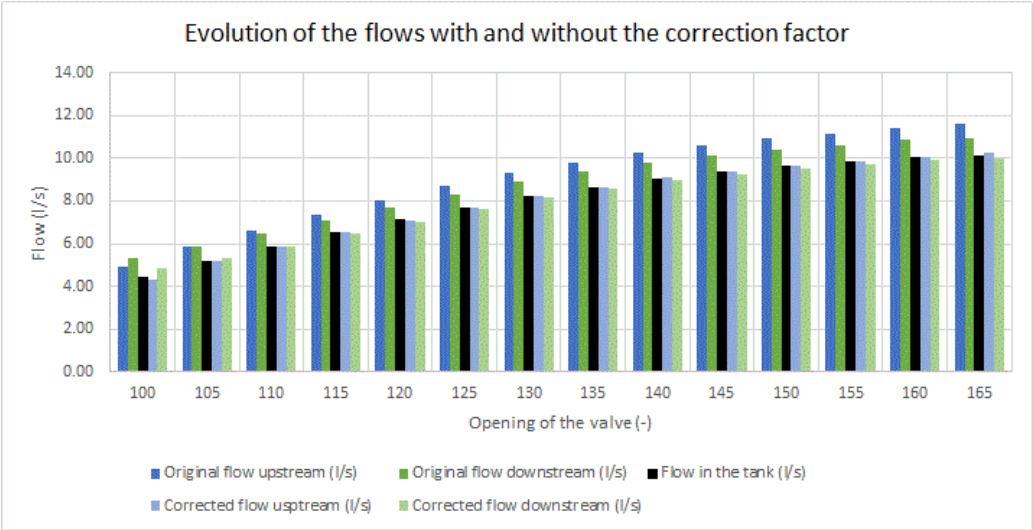

Figure 3.11: Evolution of the pipe flows with and without the application of the correction factor

The error is significantly reduced by the application of this factor. Apart from the smallest opening, all the errors are below 3%.

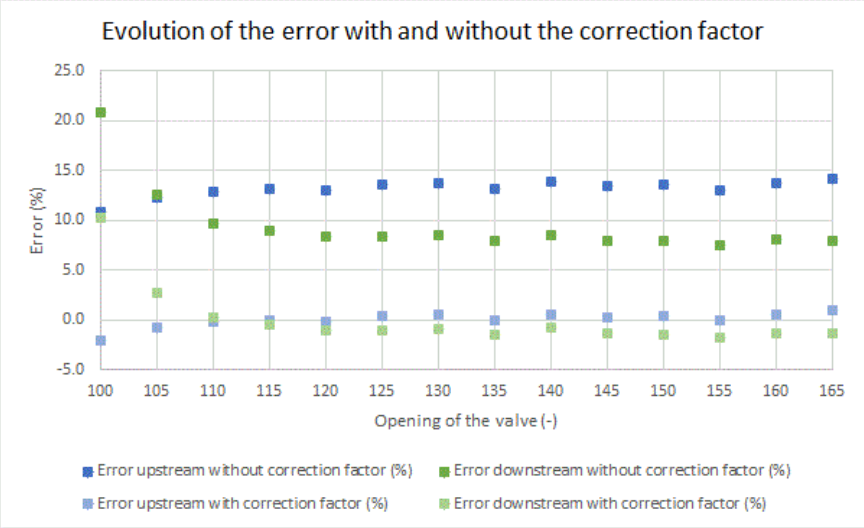

Figure 3.12: Evolution of the error with and without the application of the correction factor

3.2.3 Pressure transducers

Two types of pressure transducers are found in the system, the ones recording the pressure of the surface and the ones for the pipe system. The pressure transducers for the surface can record a range of [0-100]mm while the others can record a [0-600]mm range (Figure 3.13). All of the pressure transducers used in this facility are *Series 5000 GEMS* sensors. Furthermore, the error of the pressure transducers is 0.2% of the maximal water depth ($100mm$ for the surface pressure transducer and $500mm$ for the pipe pressure transducers) meaning a +- $0.2mm$ error for the surface water depth and +- $1mm$ for the pipe pressure head.

Figure 3.13: Pressure transducer

The last calibrated instruments are the pressure transducers. The same methodology is followed for the two types but the range of water height above them is be the same, as the ones for the pipe system are assessed with a container of the same size of the manhole (height of 478mm), the ones for the surface are measured with a smaller container having a maximum height of 100mm (Figure 3.14).

In order to calibrate the pressure transducers, they are attached under the containers and the electrical signal is recorded for every 25mm of water up to 478mm for the bigger one and every 10mm up to 100mm for the small one.

Figures 3.15 to 3.20 show the results for each calibration.

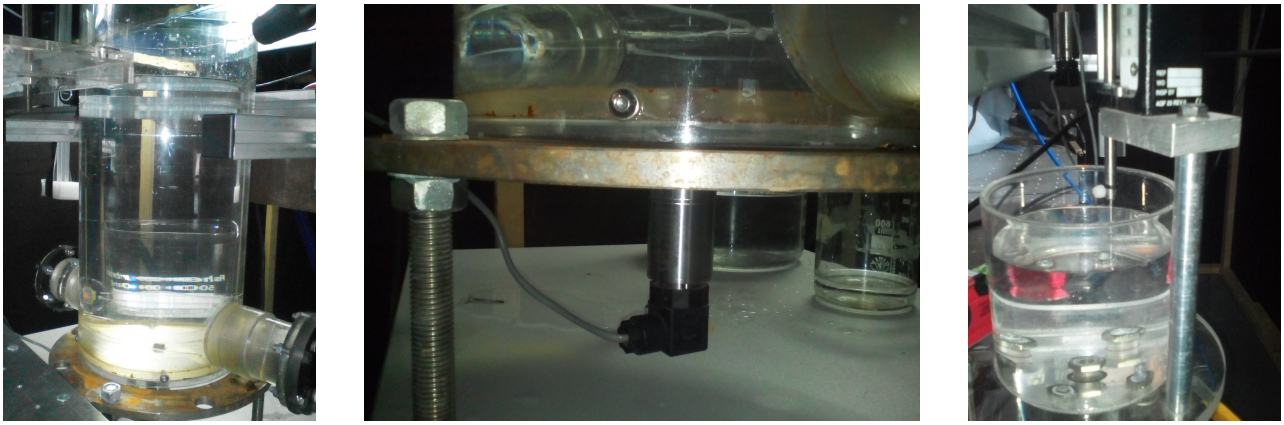

Figure 3.14: Calibration of the pipe and surface pressure transducers

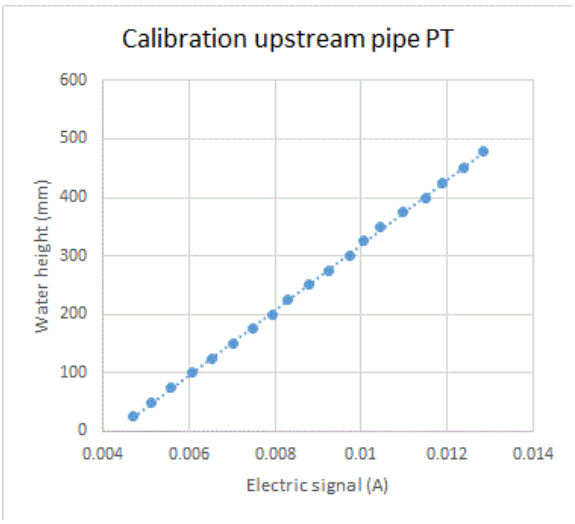

Figure 3.15: Calibration of the upstream pipe pressure transducer

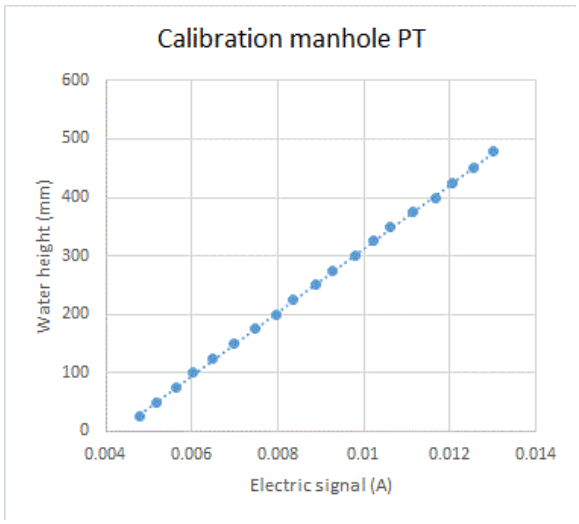

Figure 3.16: Calibration of the pressure transducer inside the manhole

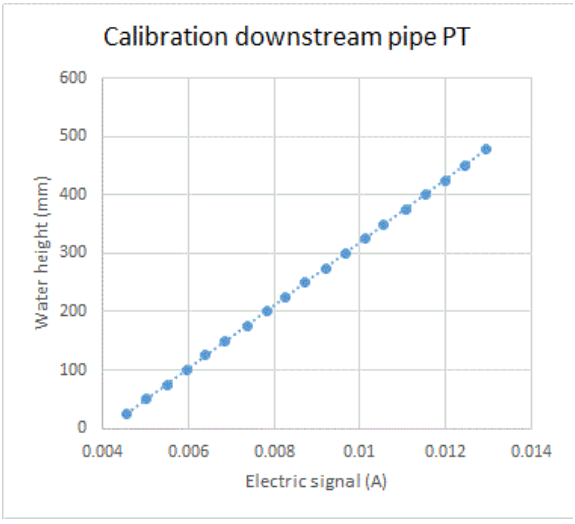

Figure 3.17: Calibration of the downstream pipe pressure transducer

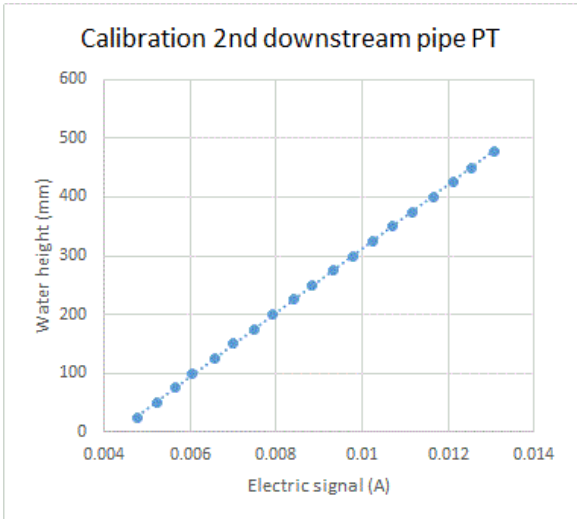

Figure 3.18: Calibration of the second downstream pipe pressure transducer

From these results, an equation is fitted to represent the interaction of the recorded signal with the actual pressure in the model. The equations found are listed below.

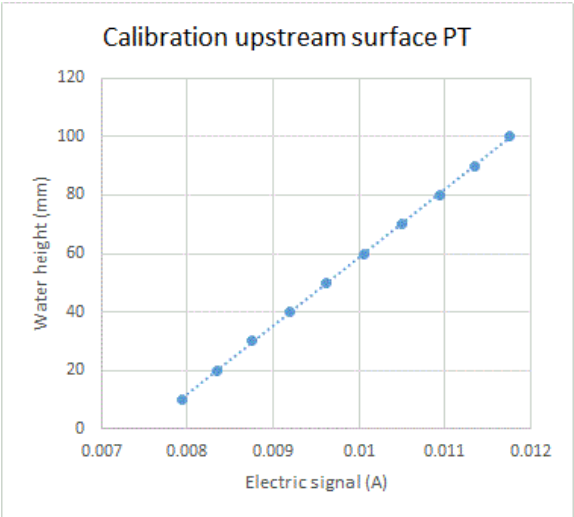

Figure 3.19: Calibration of the upstream surface pressure transducer

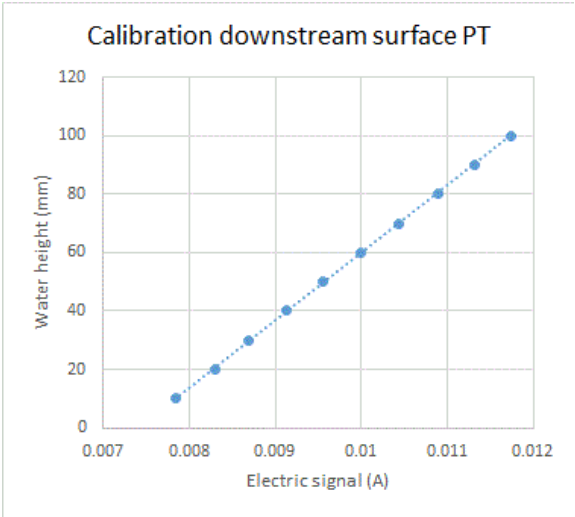

Figure 3.20: Calibration of the downstream surface pressure transducer

$$y = 55625x - 237.55 \tag{3.5}$$

for the upstream pipe pressure transducer,

$$y = 54171x - 228.98 \tag{3.6}$$

for the pressure transducer inside the manhole,

$$y = 53870x - 220.58 \tag{3.7}$$

for the downstream pipe pressure transducer,

$$y = 54393x - 232.51 \tag{3.8}$$

for the second downstream pipe pressure transducer,

$$y = (23056x - 170.74) - 3.5 \tag{3.9}$$

for the upstream surface pressure transducer and

$$y = (23334x - 174.69) - 3.5 \tag{3.10}$$

for the downstream surface pressure transducer (x being the recorded electric signal in A and y the corresponding pressure in mm).

All those equations can be implemented to the main data acquisition program in order to transform all the recorded signals into exploitable data. Figure 3.21 shows the instruments and their formula implemented to the program.

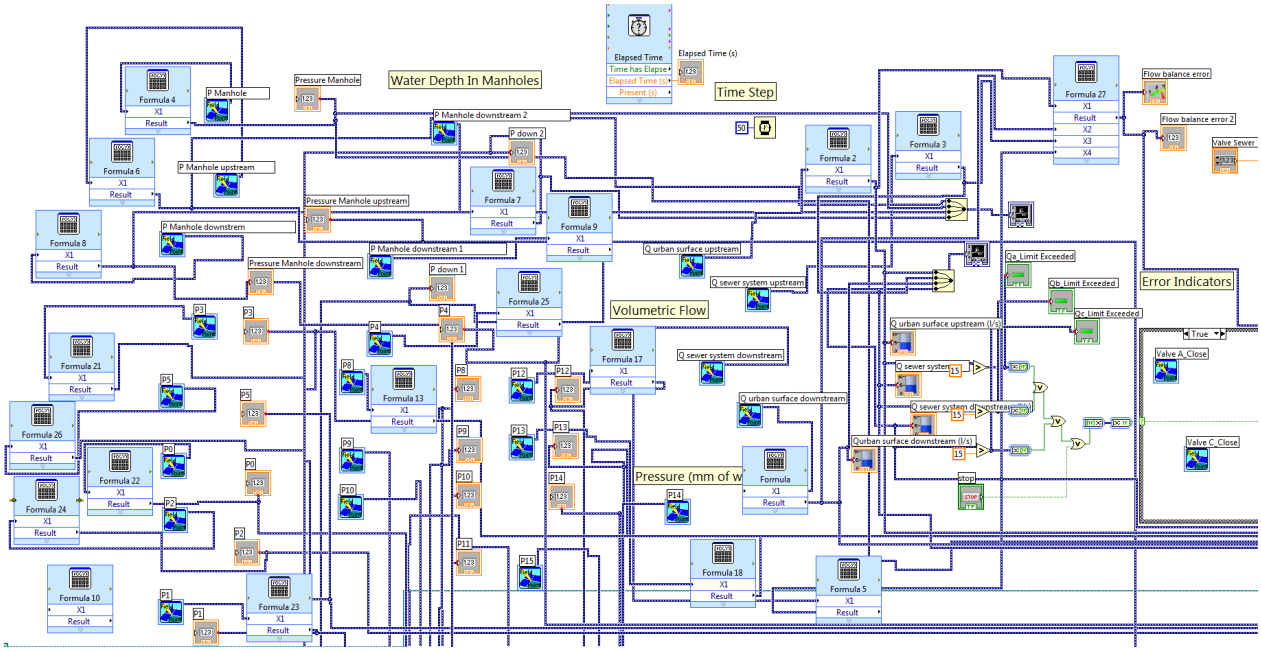

Figure 3.21: Main interface of the data collection program

3.3 Test procedure

First, 50 steady state tests are performed. After that, 48 unsteady state tests will be ran and their results are the main objective of this report.

3.3.1 Steady state tests

Several combination of flow are ran in this study. First with no flow passing through the pipes, then no flow on the surface and finally a combination of the two.

Here is a reminder of the scenarios that are carried out in this project. Those are the same than the ones performed in the previous research [12].

- Scenario 1 : Surface to sewer flow exchange with or without flow on the pipe system.
- Scenario 2 : Surface to sewer exchange with both a flow on the surface and in the sewer system.
- Scenarios 3 and 4 : The sewer system overflowing on to the surface. This configuration can happen if there is either flow on the surface (Scenario 3) or not (Scenario 4).

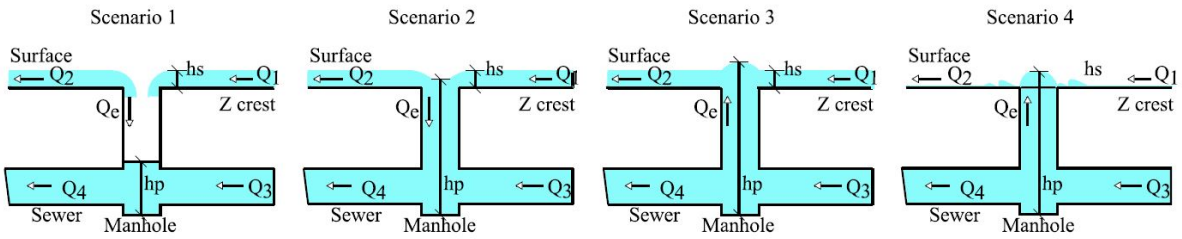

Figure 3.22: Scenarios tested in the experiments (2017) [12]

Valves A and valves C can open from 0 to 165, 165 meaning they are 100% opened. The manual valve is open at 100% after 11.5 turns. For the clarity of the report, the values of the valve openings will be expressed as percentages.

The procedure for each of those tests will consist of waiting for at least 3 minutes to obtain a steady flow, then the computer will record the data for another 3 minutes to perform the test.

No flow on the pipes (T1X)

In this first configuration, there will only be flow on the surface, nothing in the pipe system. This configuration will allow the coefficient of the weir equation to be determined. Table 3.2 shows the values of valves openings for this part of the tests.

Valve C opening = 0%	Valve A opening (%)				
	75.76	81.82	87.88	93.94	100
Manual valve opening = 100%	T11	T12	T13	T14	T15

Table 3.2: Steady state tests T1X

No flow on the surface (T2X to T4X)

The second group of tests will focus on the amount of water overflowing the manhole while the pipe system is more and more obstructed by the closure of the manual valve. Table 3.3 shows the set up of the different tests.

Valve A opening = 0%		Valve C opening (%)				
		75.76	81.82	87.88	93.94	100
Manual valve opening (%)	50	T21	T22	T23	T24	T25
	26.09	T31	T32	T33	T34	T35
	0	T41	T42	T43	T44	T45

Table 3.3: Steady state tests T2X to T4X

Combination of flows (T5X to T10X)

The last part of the steady state tests will combine the two flows, three tests with a small flow on the surface and every combination on the pipe system and three tests with a larger flow on the surface and every combination on the pipe system. As a large amount of water downstream of the surface is leading to an overflowing of the tank, it is impossible to run a test with an opening of Valve A of more than 75% (therefore this opening will be the largest flow). Tables 3.4 and 3.5 show the experimental combinations.

Valve A opening = 75.76%		Valve C opening (%)				
		75.76	81.82	87.88	93.94	100
Manual valve opening (%)	73.91	T51	T52	T53	T54	T55
	50	T61	T62	T63	T64	T65
	26.09	T71	T72	T73	T74	T75

Table 3.4: Steady state tests T5X to T7X

Valve A opening = 51.51%		Valve C opening (%)				
		75.76	81.82	87.88	93.94	100
Manual valve opening (%)	73.91	T81	T82	T83	T84	T85
	50	T91	T92	T93	T94	T95
	26.09	T101	T102	T103	T104	T105

Table 3.5: Steady state tests T8X to T10X

3.3.2 Unsteady state tests

For this part, it is crucial to run through every possible scenario, both in type of exchange flow and rain profile. A total of 60 tests will be performed, changing four parameters :

1. Duration of the event : Duration of the opening of Valve C (2 - 6 - 12 min)
2. Intensity of the peak : Maximal value of upstream sewer flow (7 - 8 - 9 - 10 l/s)
3. Magnitude of the sewer overflow : Value of the manual valve opening (26.09% - 43.48%)
4. Intensity of the upstream surface flow : Value of the opening of Valve A (51.51% - 75.76%)

In order to facilitate the methodology, the name of the tests will contain each parameter in this order. For example, a test with a duration of $2min$, a peak intensity of $7l/s$, an opening of the manual valve of 43.48% and an opening of Valve A (surface) of 51.51% will be named : T02-07-43-52. Table 3.6 shows all the possible combinations.

The procedure for each of those tests will consist on waiting for at least 3 minutes to obtain a steady flow at the upstream sewer of 4.2 to $4.8l/s$. Once the flow is steady, the recording can begin by a period of 1 to 2 minutes of steady flow. Then, it will be followed by the event, reaching the desired peak and finally go back to the former steady flow and wait for another 1 to 2 minutes.

Manual valve opening = 26% Valve A opening = 52%		Peak (l/s)			
		07	08	09	10
Event duration (min)	02				
	06				
	12				

Manual valve opening = 43% Valve A opening = 52%		Peak (l/s)			
		07	08	09	10
Event duration (min)	02				
	06				
	12				

Manual valve opening = 26% Valve A opening = 76%		Peak (l/s)			
		07	08	09	10
Event duration (min)	02				
	06				
	12				

Manual valve opening = 43% Valve A opening = 76%		Peak (l/s)			
		07	08	09	10
Event duration (min)	02				
	06				
	12				

Table 3.6: Unsteady state tests

4 Numerical models

In this chapter, the numerical models are described. The chapter mentions the equations used to link the surface water depth and the pressure head in the manhole to the exchange flow rate, in every scenario. Two numerical models are used in this report, one estimating the surface water depth as the uniform water depth and the other, more complete, solving the dynamic shallow-water equations. The first model is used in order to have quick results and a good first approximation values. The second one takes a longer time to run but generates more accurate results.

4.1 Linking equations

The equations below try to reproduce the behaviour of the four scenarios explained in Section 3.3.1. Those equations are the common equations of either a weir or an orifice.

- Scenario 1 : This scenario corresponds to the application of a free weir equation (equation 4.1). This scenario occurs when $h_p < (Z_{crest} + h_s)$ and $h_p < Z_{crest}$.

$$- Q_e = \frac{2}{3} C_i \pi D_m \sqrt{2g h_s^3} \tag{4.1}$$

- Scenario 2 : Still when $h_p < (Z_{crest} + h_s)$ but $h_p > Z_{crest}$, this scenario corresponds to the application of a submerge weir (equation 4.2) or submerge orifice equation (equation 4.3), the last one occurs when $h_s > \frac{D_m}{4}$.

$$- Q_e = C_i \pi D_m h_s \sqrt{2g(h_s + Z_{crest} - h_p)} \tag{4.2}$$

$$- Q_e = C_i A_m \sqrt{2g(h_s + Z_{crest} - h_p)} \tag{4.3}$$

- Scenarios 3 and 4 : Those scenarios correspond to the application of an orifice equation (equation 4.4) which is applicable when $h_p > (Z_{crest} + h_s)$.

$$Q_e = C_i A_m \sqrt{2g(h_p - Z_{crest} - h_s)} \tag{4.4}$$

4.2 Uniform flow model

In order to have an idea of what would be the results of the linking equations based on an uniform depth all along the surface, a first model is implemented. This simplification can be done because the geometry of the surface, specially the ratio between its width and length, would allow the flow to be uniform on the entire surface if the manhole was not present.

4.2.1 Model configuration

This model calculates the exchange flow rate based on a uniform depth : $h_s = h_u$ in equations 4.1 to 4.4. The other parameter, h_p is taken from the experimental results. Finally, two discharge coefficients C_i are tested. Appendices B.1 and B.2 contain the MATLAB code implemented for the steady and unsteady state simulations.

The uniform depth is evaluated with a Manning equation such as :

$$\frac{h_u^5}{(2h_u + L)^2} = \frac{Q^3 n^3}{L^5 s^{3/2}} \tag{4.5}$$

with $L = 4m$, $n = 0.009 s/m^{1/3}$ and $s = 1/1000$.

The Manning coefficient is chosen as the one used in Rubinato et al. [12]. This parameter is chosen by Rubinato in his PhD Thesis [11] and was determined by experiments. Those experiments observed the friction losses for several tests and compared them to friction losses obtained while using a Manning coefficient n equal to $0.009 s/m^{1/3}$. As they were similar, the coefficient was kept at a value of $0.009 s/m^{1/3}$.

4.2.2 Simulation procedure

For the steady state simulations, the code is ran for two different discharge coefficients. The first one is the coefficient found by fitting the linking equations against the observed experimental exchange flow rate to every group of tests and taking the parameter h_p, the head in the manhole, equal to the pressure head upstream in the pipe system. The second discharge coefficient is calculated the same way but so that the head in the manhole is equal to the mean value of the water pressure upstream and downstream in the pipe system.

For the unsteady state simulations, the discharge coefficients are implemented and the accuracy of the code in unsteady conditions is observed.

4.3 WOLF model

WOLF software was developed by the University of Liège and is used in this report to assess the water depth on the surface and the exchange flow happening between the surface and the sewer. Only the surface is represented by the software.

4.3.1 Program characteristics

WOLF software uses a 2D numerical model based on the solving of the fully dynamic shallow-water equations. The grid used in the model is a Cartesian, mutliblock grid meaning that different sizes of squared mesh can be implemented. The type of reconstruction can be set either to constant or linear. The time step is govern by the number of Courant which is set to 0.25.

The code of the software was modified to be able to consider every linking equation (Section 4.1). Those equations will then impose a certain flow rate that would be either added to or subtracted from an infiltration zone defined for the model.

The model presents some limitations. First, it is unable to take a parameter h_p different in time which implies that the software cannot run an unsteady surface-sewer exchange test. Secondly, the zone where the software calculates the parameter h_s in the linking equations has to be in the same block of mesh than the zone of infiltration.

4.3.2 Model configuration

This Section review all the matrices needed to run the simulations, in term of geometry, boundary conditions and initial conditions.

Geometry

The numerical model concentrates on the representation of the surface only, the interaction with the sewer system is computed with the help of linking equations (see Section 4.1). The numerical model has the same geometry as the experimental model being a surface of $8.2m$ by $4m$ with a slope of 1/1000 and a uniform friction coefficient matrix of 0.009.

A compromise between accuracy and calculation duration is made by using three different blocks with three types of mesh with the tightest being closer to the manhole. Figure 4.1 shows the geometry of the mesh. It is indicated that the larger mesh, the farthest from the manhole, has a size of $0.04m$; the second one of $0.02m$; and the last one, the closest to the manhole of $0.01m$.

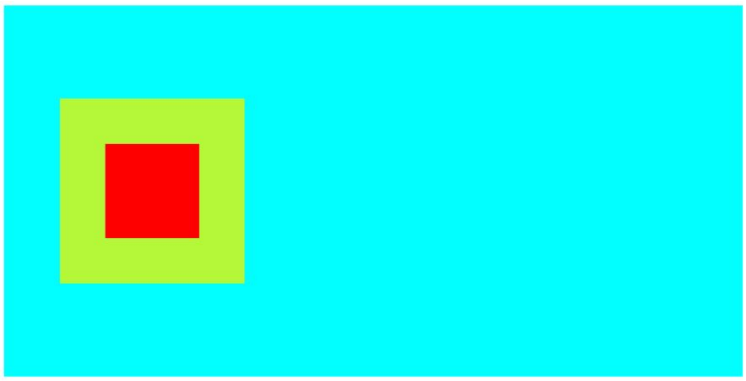

Figure 4.1: Configuration of the mesh - blue : $\Delta x = 0.04m$; green : $\Delta x = 0.02m$; red : $\Delta x = 0.01m$

A second geometry is established as well, the zone of infiltration. It represents the area were the water is collected by the manhole or escape from the sewer to the surface. In order to be accurate, this area is an arc and varies in term of thickness and angle to be able to model a full circle as well as a complete disk. Figure 4.2 shows an example of this zone of infiltration.

Figure 4.2: Zone of infiltration (angle = 180^o; thickness = $0.02m$)

This area is important for the configuration because it defines the flow exchange that occurs in the model with the help of the linking equations (Section 4.1). The chosen geometries are, for each scenario, an angle of 360^o combined with a thickness of $0.05m$ for Scenario 1 or a thickness of $0.12m$ for Scenarios 3 and 4 leading the zone to a full disk.

The last geometry represents the area were the software calculates the water depth that will be used in the linking equations. Figure 4.3 shows this zone on the left (in red) with the previous one, the zone of infiltration, on the right (in orange) this time with an angle of 360^o and a thickness of $0.05m$.

Figure 4.3: Location of the water depth used in the linking equation

The software does not allow this zone to be out of the block of mesh containing the zone of infiltration. This limitation leads to a difference between the location of the calculated surface water depth and the experimental one as seen in Figure 4.4.

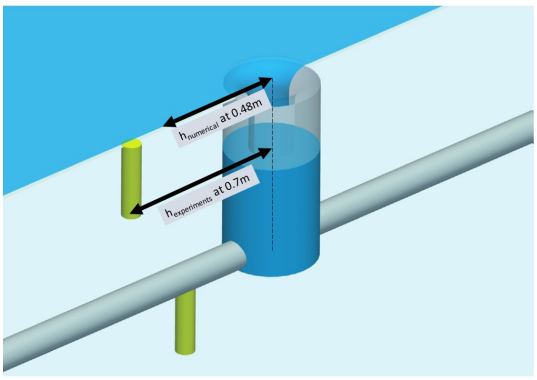

Figure 4.4: Different locations of the water depth used in the linking equation

Boundary conditions

Boundary conditions will be set at the upstream (in red) and downstream (in blue) edge of the surface. Figure 4.5 shows the location of those conditions. At the upstream edge, the condition is a certain flow rate Q_1 along the X axis corresponding to the desired test and a null flow rate along the Y axis ($Q_y = 0$). The downstream edge condition corresponds to the uniform height of the configuration, h_u.

Initial conditions

In order to start the tests in the best conditions, the initial matrices of flow and water depth will be computed by running the program and waiting for the results to stabilise (starting from matrices equal to the boundary conditions). Then, the real simulations can begin with those new initial matrices.

Figure 4.5: Location of the boundary conditions

4.3.3 Simulation procedure

It was seen in Section 4.1 that there are three input parameters that need to be assessed : h_p, h_s and C_i in order to determine the exchange flow rate. The first parameter, h_p is taken from the experiments (same than the uniform flow model). The water depth on the surface, h_s, is calculated by Wolf software for each time step and is taken at the location showed in Subsection 4.3.2. The code is ran for every test with a discharge coefficient C_i found by the observations of the experimental exchange flow rate against the linking equations.

5 Experimental results

5.1 Steady state tests

After the experimental tests were performed, the recorded data for every tests are gathered and can be found in Appendix A.1. Figures 5.1 and 5.2 show the results in term of water depth and exchange flow rate plotted in a graph. Looking at the results in term of water depth, the conclusion would be that tests T1X, T5X and T8X represent Scenario 1 (T1X with no flow on the pipe system and T5X/T8X with flow on the pipe system but not inducing surcharge of the sewer) ; T2X, T3X and T4X, Scenario 4 ; T6X, T7X, T9X and T10, Scenario 3. It appears that no result induces a Scenario 2. However, the results in term of flow rate tend to remove T53-T54-T55 and T82-T83-T84-T85 from Scenario 1 as the exchange flow rate happens from the sewer to the surface. As no real conclusion can be made from those tests, they will be removed from the analysis.

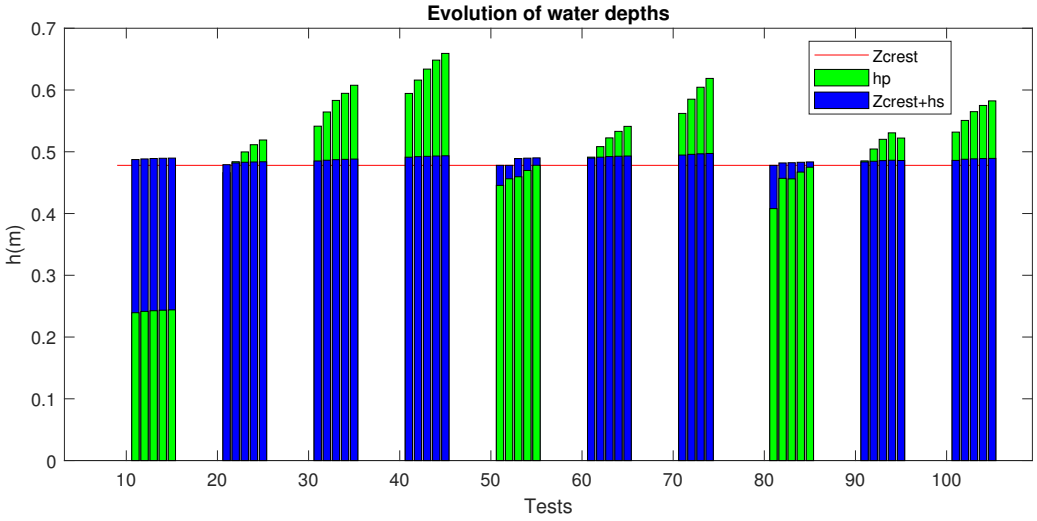

Figure 5.1: Experimental results in term of water depths

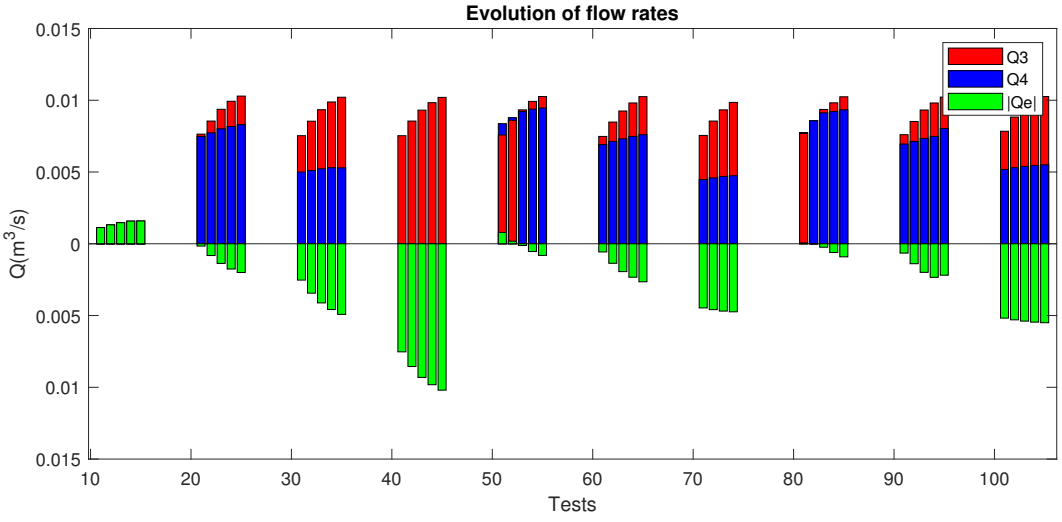

Figure 5.2: Experimental results in term of flow rates

Interesting results can be found in Table 5.2. It also shows the non-dimensional numbers : surface flow Froude number Fr_s, Reynolds number in the manhole Re_m and a scaled flow depth by the manhole diameter h_s/D_m.

5.2 Unsteady state tests

After conducting the experimental unsteady state tests, the obtained duration of them is given in Table 5.1.

Duration of unsteady period (sec)	Duration of steady period (before and after) (sec)	Total duration (sec)
120	2×40	200
350	2×100	550
$660 - 760$	2×120	$900 - 1000$

Table 5.1: Obtained duration of unsteady state tests

Moreover, other conclusions can be made after performing the experiments. If the four parameters governing the experiment are looked at again (see Section 3.3.2), the genuine values of them can be obtained.

1. Duration of the event : $200, 550$ or $1000sec$
2. Intensity of the event : from $4.2 - 4.8l/s$ to $7, 8, 9$ or $10l/s$
3. Magnitude of the sewer overflow : depending on the opening of the manual valve, the exchange flow rate can double from one opening to the next with the other parameters fixed
4. Intensity of the upstream surface flow : depending on the opening of Valve A, the upstream surface flow rate is either $0.8 - 1.0l/s$ or $6.0 - 6.2l/s$

Parameters 3 and 4 both influence the amount of surface-sewer flow exchange and can be looked at as a combination.

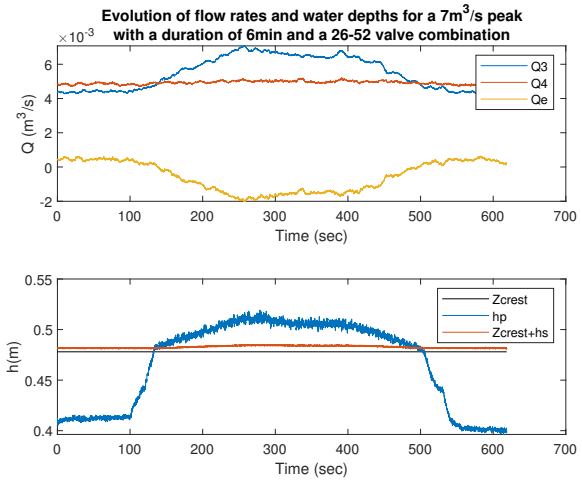

Figure 5.3: Experimental results for test 07-06-26-52

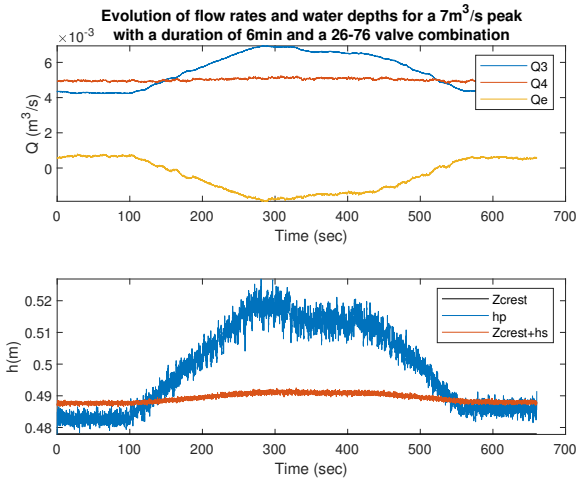

Figure 5.4: Experimental results for test 07-06-26-76

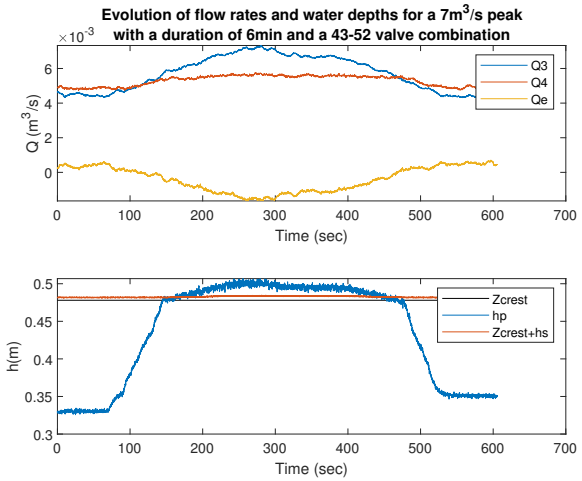

Figure 5.5: Experimental results for test 07-06-43-52

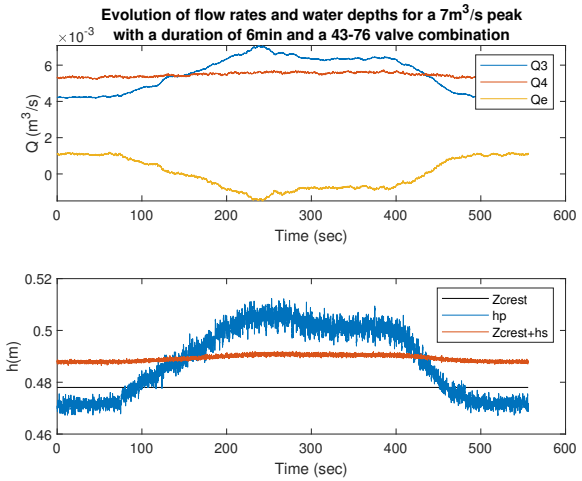

Figure 5.6: Experimental results for test 07-06-43-76

Several remarks can be taken from the results of the experimental tests. Figures 5.3 to 5.6 show the different combinations of valves openings that lead to different exchange flow rates. Those figures all show the same peak intensity of $7l/s$ with a duration of $6min$. It is seen that with a bigger flow on the surface (Valve A = 76% corresponding to a $6.0 - 6.2l/s$ flow), the beginning of the event shows a head in the manhole really close to the surface bed. However, with a smaller flow on the surface (Valve A = 52% corresponding to a $0.8 - 1.0l/s$ flow), the head in the manhole is 0.07 to $0.15m$ below the surface elevation. Another point of view can be taken by looking at the opening of the manual valve. Indeed, this valve is supposed to induce a bigger exchange flow by creating an obstruction at the end of the pipe system. By observing the exchange flow rate on the above graphs, it can be seen that a small opening of the manual valve (26%) induces a bigger exchange flow rate of about twice the amount of the bigger opening of the valve (43%).

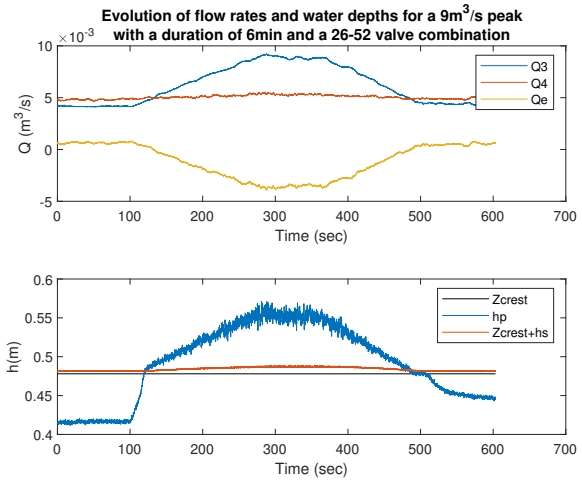

Figure 5.7: Experimental results for test 09-06-26-52

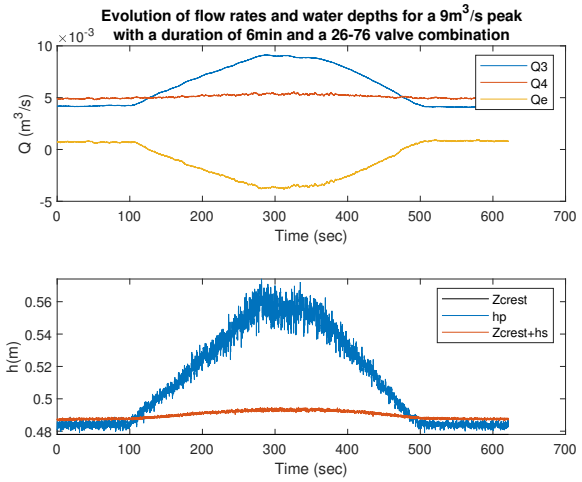

Figure 5.8: Experimental results for test 09-06-26-76

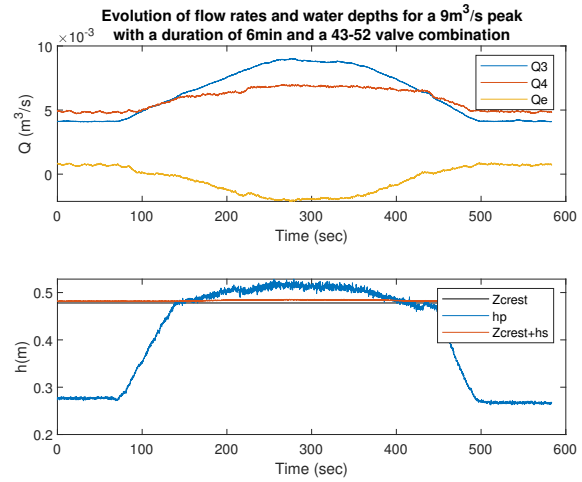

Figure 5.9: Experimental results for test 09-06-43-52

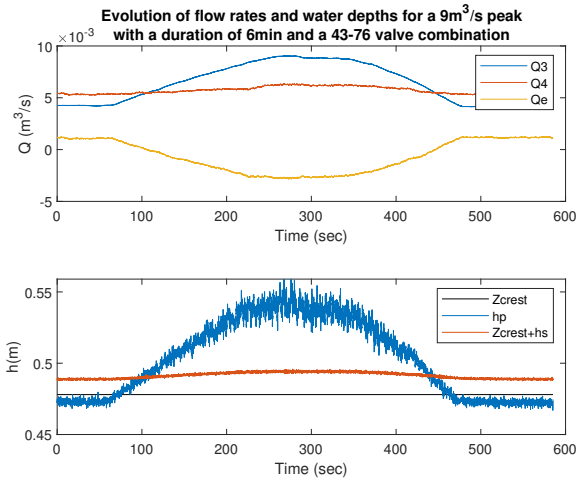

Figure 5.10: Experimental results for test 09-06-43-76

Similar observations can be made for any peak intensity as seen in Figures 5.7 to 5.10 for a $9l/s$ peak. The more intense the peak is, the more the difference is significant. One comment can be made about a difference between those graphs and the previous ones, it is about the $26-52$ valve combination. As said before, the manual valve has a small opening inducing a larger exchange flow rate. This exchange flow rate is even too big that the head in the manhole is unable to go back to the head present at the beginning. Appendix B.2 gathers all the other experimental results.

In order to see the difference in the results while changing the duration, the graphs for a $9l/s$ peak is looked at for a fixed $26-52$ valve combination.

Figures 5.11 to 5.13 show that the conclusions made in the previous paragraph can be applied to each duration.

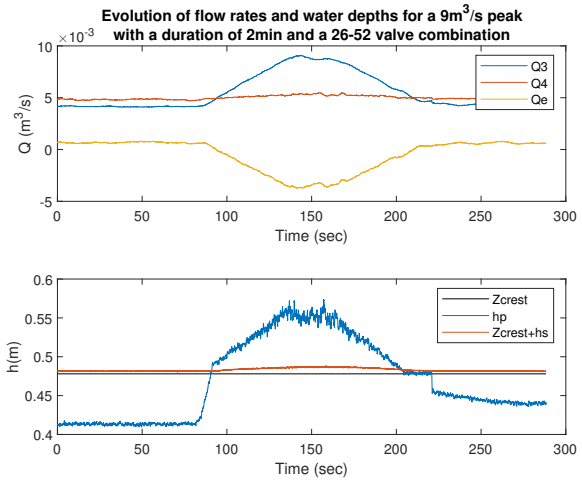

Figure 5.11: Experimental results for test 09-02-26-52

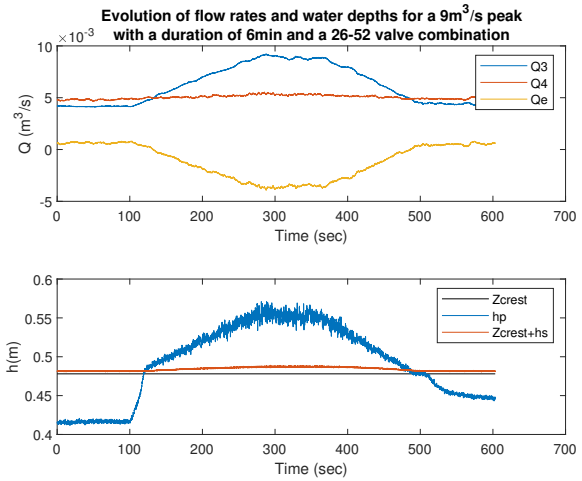

Figure 5.12: Experimental results for test 09-06-26-52

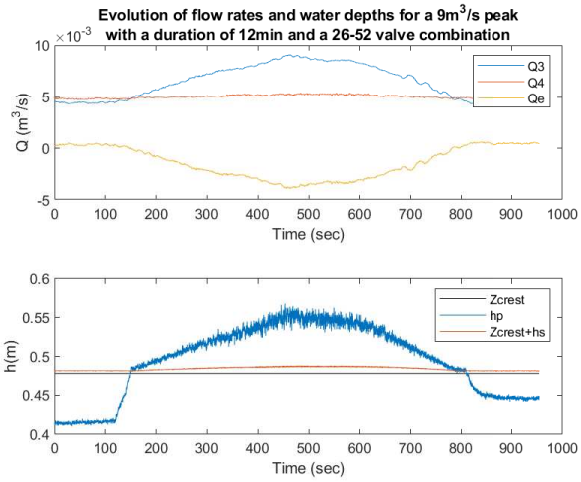

Figure 5.13: Experimental results for test 09-12-26-52

Now that comments are made about the general tendency, closer look on the values of the exchange flow rate.

Comment #1

The first group of four figures (Figures 5.14 to 5.17) show that the $43-52$ valve combination produces the smaller amount of exchange flow rate even with different peak intensities (here $9l/s$ and $10l/s$) or durations (here $2min$ and $6min$). On the other hand, the $26-52$ and $26-76$ valve combinations seem to induce the largest and same exchange flow rate.

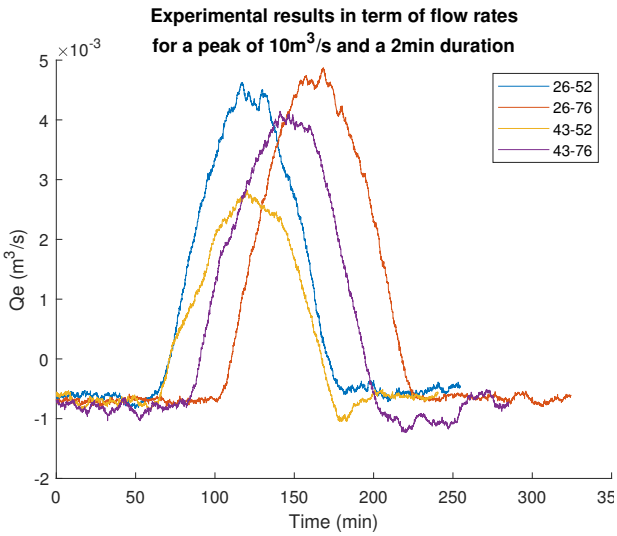

Figure 5.14: Exchange flow rate for a $9l/s$ peak and $2min$ duration

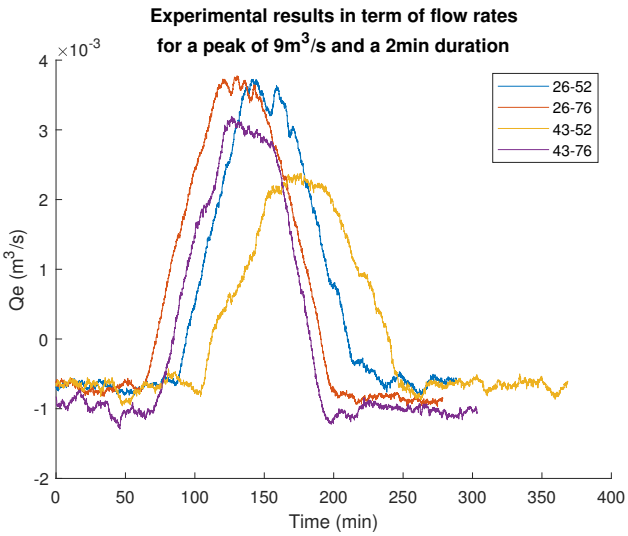

Figure 5.15: Exchange flow rate for a $10l/s$ peak and $2min$ duration

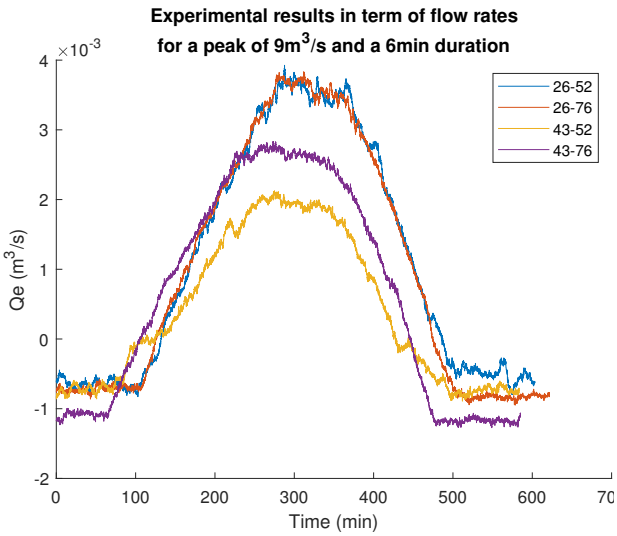

Figure 5.16: Exchange flow rate for a $9l/s$ peak and $6min$ duration

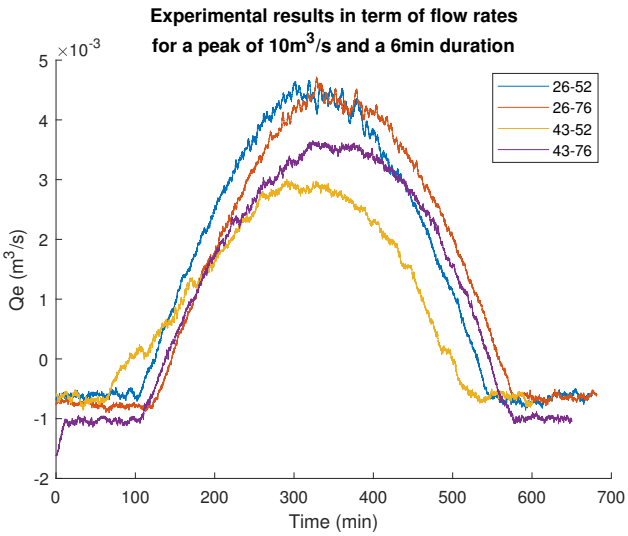

Figure 5.17: Exchange flow rate for a $10l/s$ peak and $6min$ duration

Comment #2

Figures 5.18 to 5.20 allow the peak intensities to be analysed at every duration. In order to do that, the valve combination is set to $26 - 52$. It is seen that, as expected, the higher the peak intensity, the larger the exchange flow rate. The graphs also show that this increase of exchange flow rate is uniform with the increase in the peak intensity.

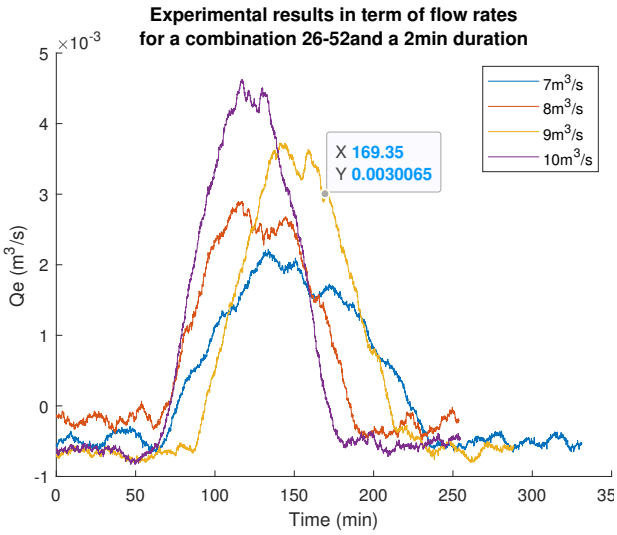

Figure 5.18: Exchange flow rate for a $2min$ duration and a $26 - 52$ valve combination[1]

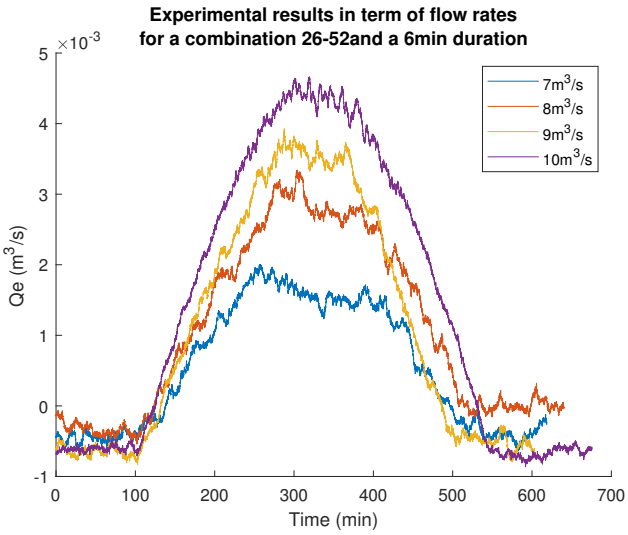

Figure 5.19: Exchange flow rate for a $6min$ duration and a $26 - 52$ valve combination[1]

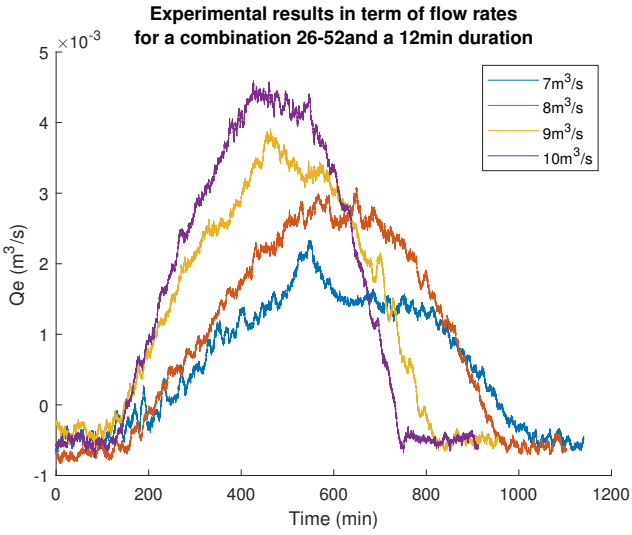

Figure 5.20: Exchange flow rate for a $12min$ duration and a $26 - 52$ valve combination[1]

[1] The legend of Figures 5.18 to 5.20 contains a mistake, the unit for the flow rates is l/s and not m^3/s

Comment #3

Last comment is about to see if the uniform increase of exchange flow rate with the increase of the peak is present for each valve combination. Figures 5.21 to 5.24 show every valve combination for a $6min$ duration event. It is seen that the increase in exchange flow rate is present for each valve combination except for the $43-52$ combination. It is now usual that the $43-52$ valve combination is different than the other combinations. This is observed due to the combination having the lowest upstream surface flow rate, the largest manual valve opening and a small peak intensity. This results in the flow being too small to provide the same pattern as the other combinations.

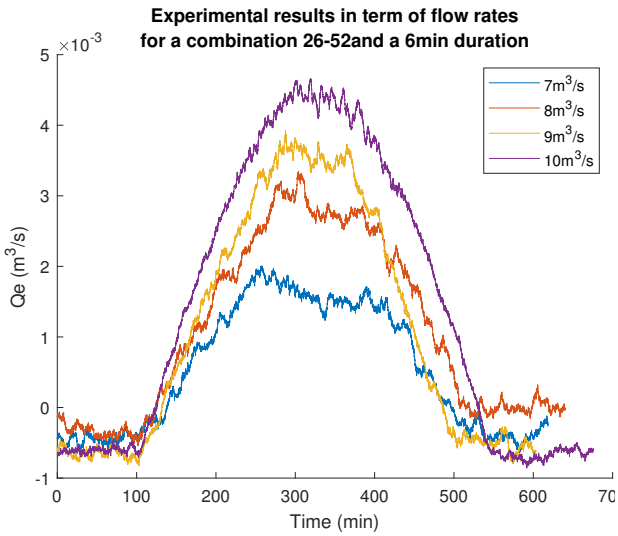

Figure 5.21: Exchange flow rate for a $26-52$ valve combination and $6min$ duration[2]

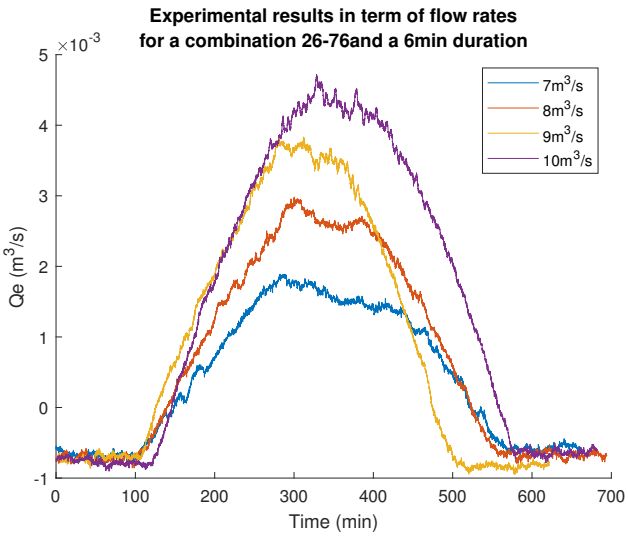

Figure 5.22: Exchange flow rate for a $26-76$ valve combination and $6min$ duration[2]

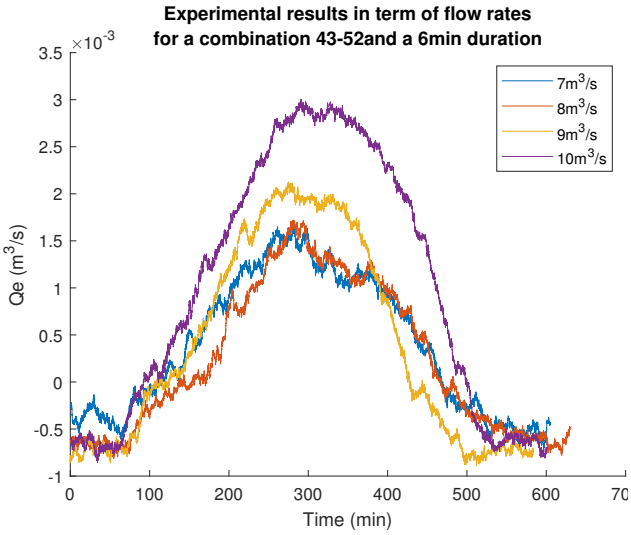

Figure 5.23: Exchange flow rate for a $43-52$ valve combination and $6min$ duration[2]

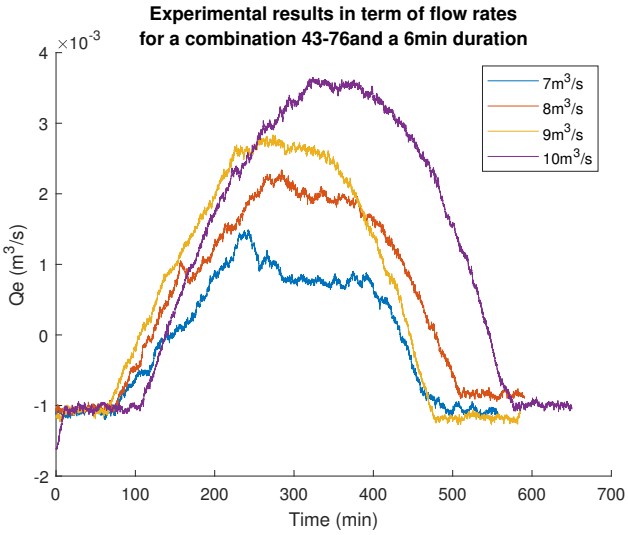

Figure 5.24: Exchange flow rate for a $43-76$ valve combination and $6min$ duration[2]

[2] The legend of Figures 5.21 to 5.24 contains a mistake, the unit for the flow rates is l/s and not m^3/s

Scenario	Test	$Q_e(m^3/s)$	$h_{s,exp}(m)$	$Fr_s(-)$	$Re_m(-)$	$h_s/D_m(-)$
	T11	-0.00113	0.00937	0.610	6066	0.039
	T12	-0.00132	0.01039	0.627	7047	0.043
	T13	-0.00147	0.01107	0.645	7834	0.046
	T14	-0.00158	0.01148	0.663	8431	0.048
	T15	-0.00159	0.01176	0.674	8494	0.049
	T51	-0.00079	0.00983	0.572	4199	0.041
	T52	-0.00018	0.01071	0.503	969	0.045
S1	T53	0.00012	0.01115	0.473	361	0.046
	T54	0.00054	0.01168	0.442	2846	0.049
	T55	0.00081	0.01211	0.418	4284	0.050
	T81	-0.00006	0.00384	0.365	313	0.016
	T82	0.00001	0.00389	0.351	36	0.016
	T83	0.00024	0.00425	0.306	1255	0.018
	T84	0.00061	0.00497	0.233	3222	0.021
	T85	0.00091	0.00555	0.198	4817	0.023
	T61	0.00057	0.01186	0.426	3045	0.049
	T62	0.00136	0.01325	0.361	7204	0.055
	T63	0.00194	0.01420	0.326	10286	0.059
	T64	0.00233	0.01476	0.308	12386	0.062
	T65	0.00265	0.01512	0.298	14051	0.063
	T71	0.00447	0.01667	0.258	16318	0.069
	T72	0.00459	0.01784	0.233	21007	0.074
	T73	0.00469	0.01868	0.218	24609	0.078
	T74	0.00474	0.01922	0.208	27124	0.080
S3	T91	0.00065	0.00516	0.223	3455	0.021
	T92	0.00139	0.00664	0.146	7382	0.028
	T93	0.00199	0.00766	0.116	10550	0.032
	T94	0.00234	0.00827	0.103	12390	0.034
	T95	0.00219	0.00785	0.111	11634	0.033
	T101	0.00518	0.00800	0.095	14149	0.033
	T102	0.00530	0.00989	0.115	18721	0.029
	T103	0.00539	0.01053	0.0112	22158	0.030
	T104	0.00546	0.01100	0.105	23483	0.031
	T105	0.00550	0.01126	0.103	25249	0.032
	T21	0.00016	0.00107	0.003	861	0.004
	T22	0.00082	0.00393	0.000	4331	0.016
	T23	0.00137	0.00501	0.000	7263	0.021
	T24	0.00176	0.00544	0.000	9349	0.023
	T25	0.00200	0.00579	0.000	10584	0.024
	T31	0.00253	0.00710	0.000	13429	0.030
	T32	0.00344	0.00828	0.000	18252	0.034
S4	T33	0.00412	0.00919	0.000	21849	0.038
	T34	0.00458	0.00972	0.000	24322	0.041
	T35	0.00492	0.01018	0.000	26108	0.042
	T41	0.00753	0.01350	0.000	39950	0.056
	T42	0.00855	0.01456	0.000	45338	0.061
	T43	0.00931	0.01532	0.000	49403	0.064
	T44	0.00982	0.01587	0.000	52122	0.066
	T45	0.01020	0.01625	0.000	54100	0.068

Table 5.2: Experimental results for every tests for Scenarios 1, 3 and 4

6 Analysis of experimental tests

This chapter will analyse the results of the experimental tests conducted following the procedure explained in Section 3.3. The goal of the analysis is to try to find the discharge coefficient for each scenario.

6.1 Steady state tests

The initial method follows the same procedure as Rubinato et al. [12] for the value of the head in the manhole (h_p) measured upstream of the manhole. A second method is conducted with the value of h_p as the mean between the measured head upstream and downstream of the manhole.

6.1.1 Method 1 : h_p = upstream pipe pressure

This first method implements the parameter h_p of the linking equations (Section 4.1) as the recorded upstream pipe pressure head. Graph 6.1 compares results obtained by Rubinato et al. [12] and this experiment after method 1 has been used on both sets of data.

Discharge coefficient C_i

Once all the experiments are done and all the data collected for the flow rates and water depths, a discharge coefficient C_i can be fitted using the linking equations given in Section 4.1.

In order to find the discharge coefficients corresponding to the different tests, the exchange flow rate is compared to the other half of the linking equations (Section 4.1). For this method, the water depth in the manhole (h_p) is taken as the one upstream in the pipe system. Figures 6.1, 6.2 and 6.3 show the exchange flow rate against its linking equation for the three scenarios.

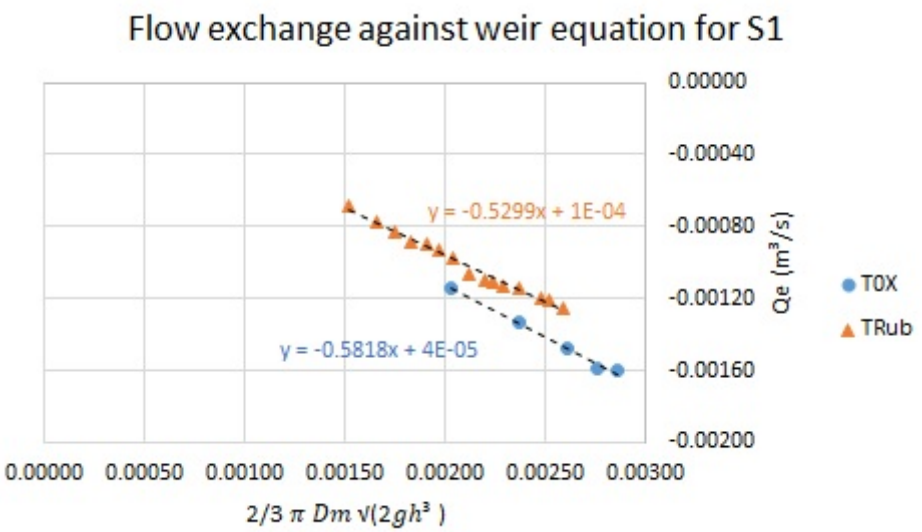

Figure 6.1: Flow exchange against weir equation for Scenario S1

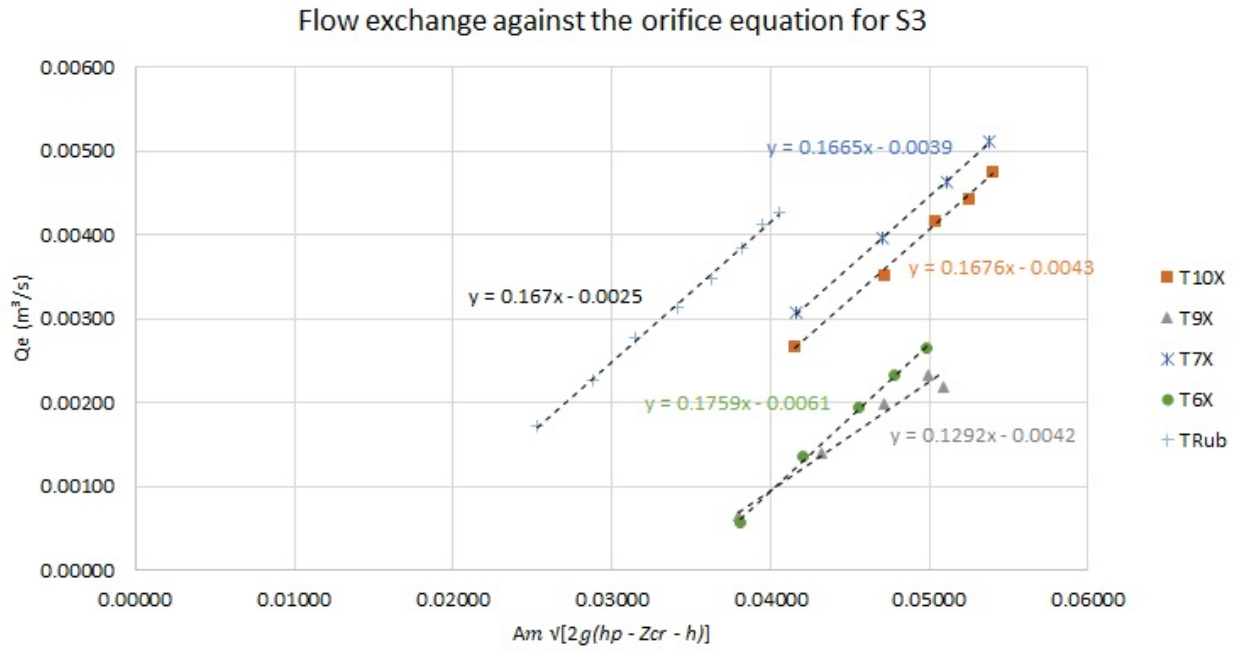

Figure 6.2: Flow exchange against orifice equation for Scenario S3 - Method 1

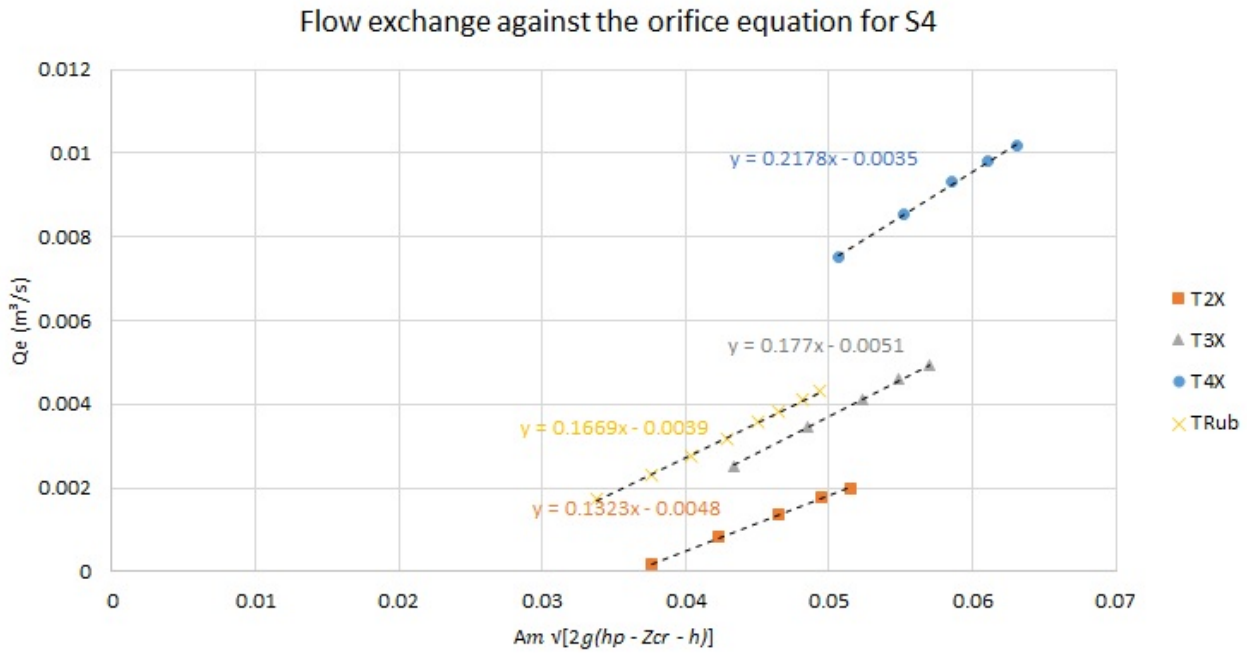

Figure 6.3: Flow exchange against orifice equation for Scenario S4 - Method 1

Table 6.1 gathers all the discharge coefficient C_i fitted from the previous graphs for every group of tests, this represents the slope of every tendency curve. In order to follow this method the independent term of the fitted equation is neglected.

The results gathered by Rubinato et al. [12] are similar to the ones obtained in this study. The error between the new results and Rubinato et al. ones could come from an error during the calibration of the instruments, the flow rates and water depths are recorded as an electrical signal that is modified by an equation found by calibration. Those equations were different than the equations used previously by Rubinato et al. [12]. However, no improvement is seen by using the old equation to the new recorded signals, they are even further apart. The error does not come from the calibrations.

As the error of the flow meter is 0.5% of the maximal flow rate ($11l/s$) meaning a $0.055l/s$ error and the exchange flow rate is calculated based on two different flow rates (Q_3 and Q_4), the error of the estimation of the exchange flow rate is about $0.11l/s$. This value is not negligible and could allow a better connection between the two sets of results. Furthermore, the error of the pressure transducers is 0.2% of the maximal water depth ($100mm$ for the surface pressure transducer and $500mm$ for the pipe pressure transducers) meaning a $0.2mm$ error for the surface water depth and $1mm$ for the pipe pressure head. Those errors are presented in Figures 6.4 and 6.5

Scenario	Tests	$C_i(-)$	$C_{i,Rub}(-)$ [12]
S1	T1X	0.5819	0.5299
S2	-	-	0.056
S3	T6X	0.1759	0.167
	T7X	0.1665	
	T9X	0.1292	
	T10X	0.1676	
S4	T2X	0.1323	0.1699
	T3X	0.1770	
	T4X	0.2178	

Table 6.1: Discharge coefficient - Method 1

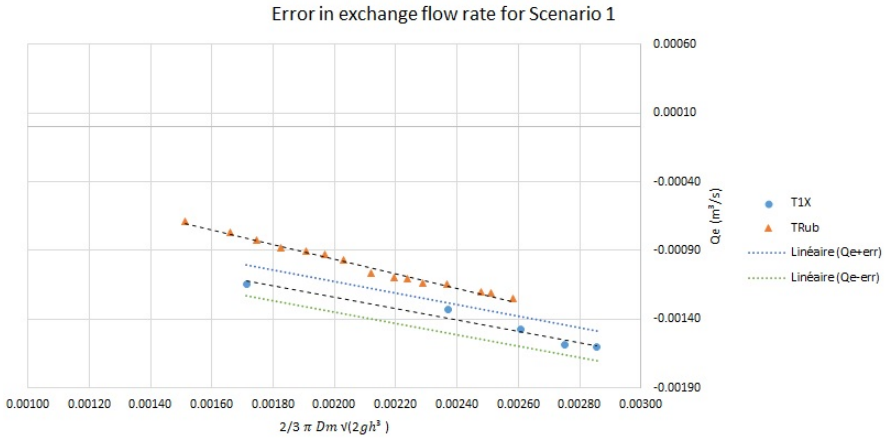

Figure 6.4: Error coming from flow rates measurements for Scenario 1

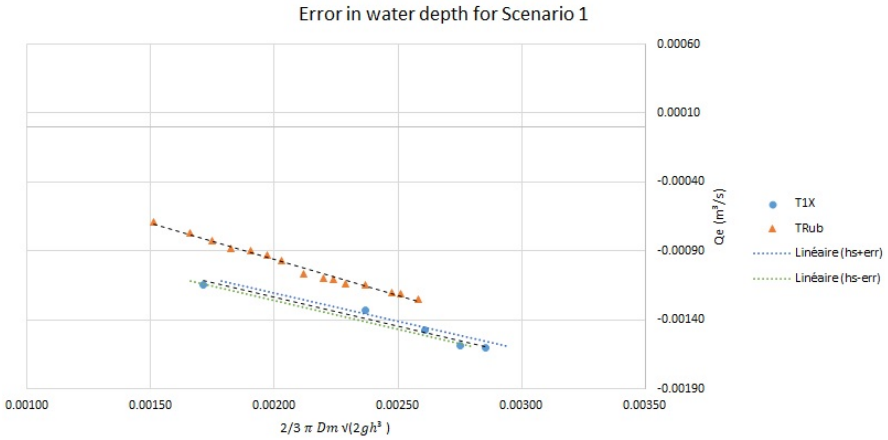

Figure 6.5: Error coming from water depths measurements for Scenario 1

From now on, it is chosen to continue with only the groups of tests T1X (for Scenario 1), T6X (for Scenario 3) and T3X (for Scenario 4) in order to lighten the report knowing that the other tests are showing similar analysis results. However, all the results for the other tests are available in Appendix A.1.

Exchange flow rate

The exchange flow rate calculated from the experimental flow rates and the ones calculated based on the linking equations (computed with the experimental surface depth and the coefficient fitted before) are compared in Figures 6.6, 6.7 and 6.8.

The two exchange flow rates can be defined as : $Q_e(Q_{exp}) = Q_4 - Q_3$ and $Q_e(h_{exp}, C_i) =$ eq. 4.1 to eq. 4.4 depending on the scenario.

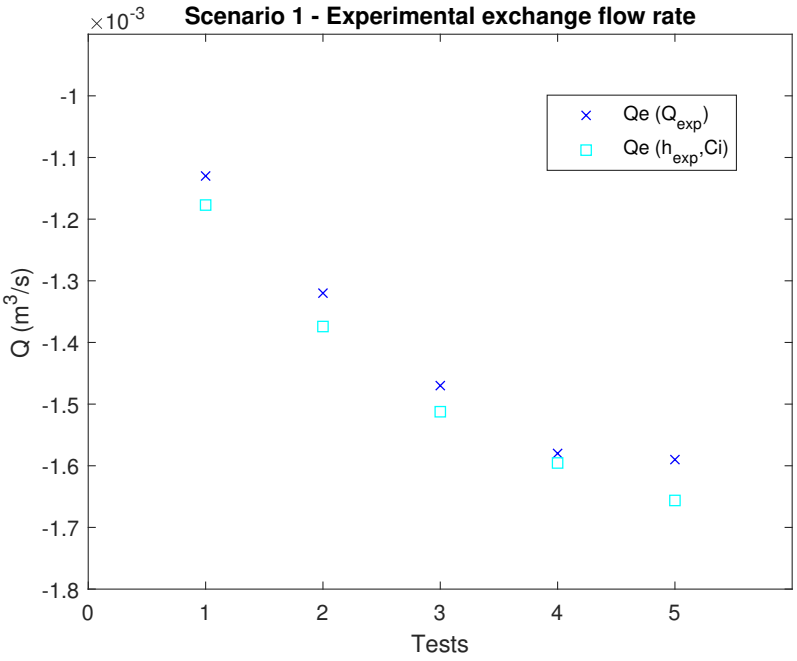

Figure 6.6: Results of experimental tests for Scenario 1 configurations

It is shown on Figure 6.6 that taking a coefficient C_i equal to 0.5819 and calculating the exchange flow rate results in a good approximation of the flow rate with a maximal error of 4%. This error is calculated based on Equation 6.1.

$$Error\ (\%) = \frac{Q_e(Q_{exp}) - Q_e(h_{exp}, C_i)}{Q_e(h_{exp}, C_i)} \times 100 \tag{6.1}$$

Figures 6.7 and 6.8 show that the approximation of the exchange flow rate using the coefficients $C_i = 0.1759$ for Scenario 3 and $C_i = 0.1770$ for Scenario 4 is not as accurate as for Scenario 1. Indeed, the error rises to 85% for Scenario 3 and 65% for Scenario 4. The choice of neglecting the independent term of the fitted equations for C_i might not be the best solution. This method can be improved.

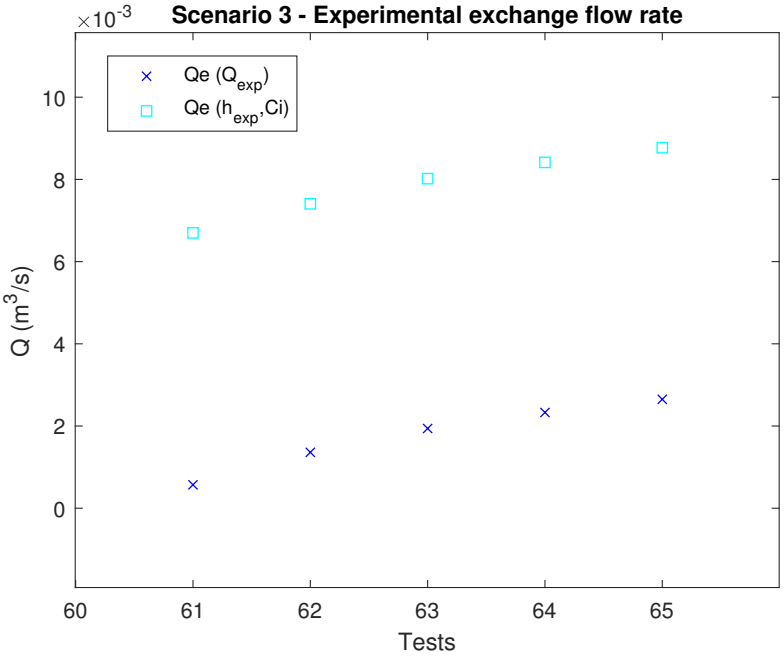

Figure 6.7: Results of experimental tests for Scenario 3 configurations

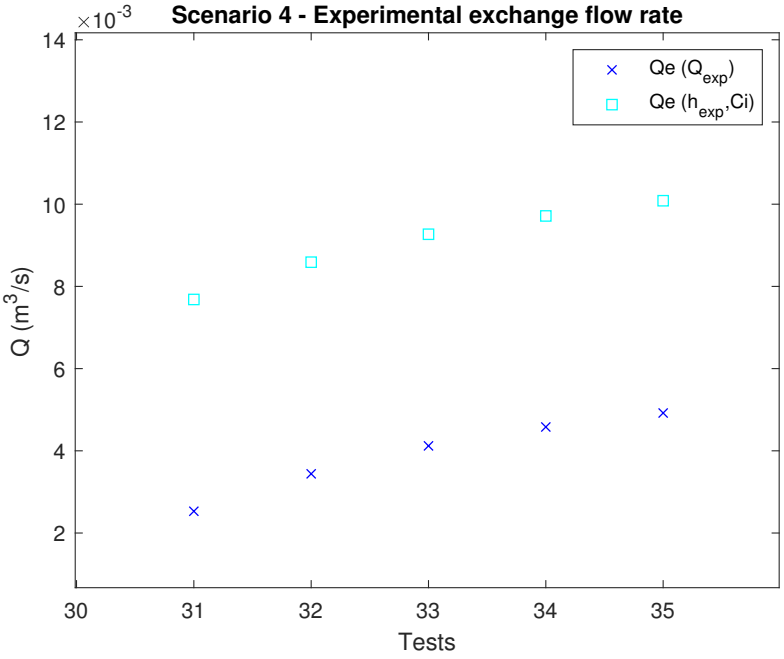

Figure 6.8: Results of experimental tests for Scenario 4 configurations

6.1.2 Method 1 : Improvement

This section gathers and comments the observations made by an internal report of the University of Liège [9] about the results of Rubinato et al. [12]. As concluded before, the first method has some limitations, the independent terms of the fitted equations for the discharge coefficient are neglected but the order of those terms can be as much as 2.5 to $5l/s$ for Scenarios 3 and 4 which cannot be considered negligible as the order of magnitude of the executed upstream flow rates (on the surface or in the pipe) is about $10l/s$. The internal report of the University of Liège shows that, taking the independent term into account in the calculations results in a better estimation of the exchange flow rate. Figures 6.9 and 6.10 show the differences. On the other hand, the results for Scenarios 1 and 2

are already good with a independent term of about $0.1l/s$ which can be neglected.

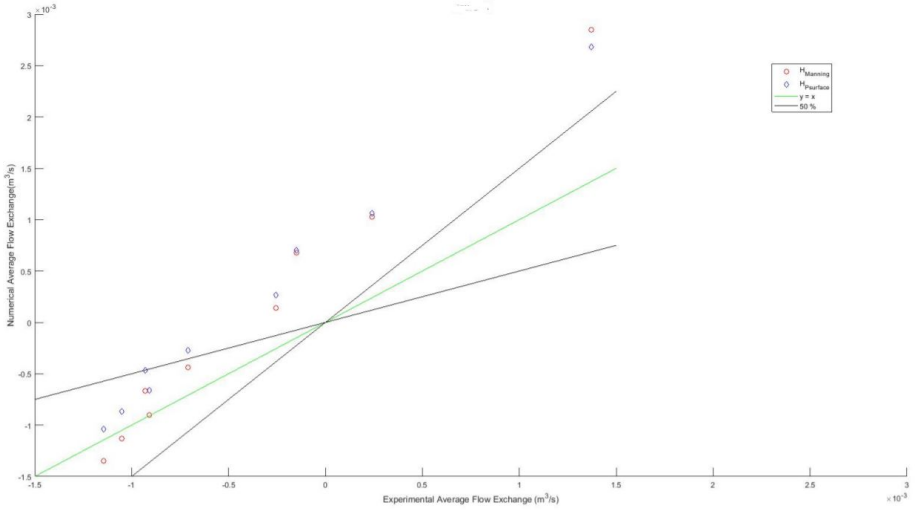

Figure 6.9: Results of experimental tests without the independent term of the fitted equation for C_i

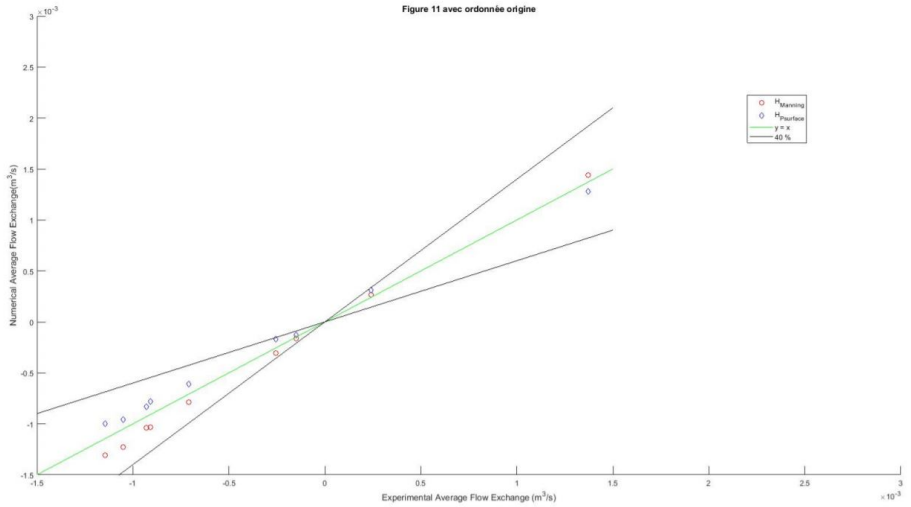

Figure 6.10: Results of experimental tests with the independent term of the fitted equation for C_i

Unfortunately, this independent term makes no physical meaning. Indeed, the tendency curves should go through the origin as we expect the equation to be null with a null exchange flow rate. The second method will try to make that happen.

6.1.3 Method 2 : h_p = mean of upstream and downstream pipe pressure

The second method follows the same procedure as the first but the parameter h_p, head in he manhole, is now calculated with the mean value between the water pressure upstream and downstream of the manhole, in the pipe system. The results for Scenario 1 stay the same as the linking equation is independent of h_p.

Discharge coefficient C_i

The discharge coefficient for Scenario 1 is kept as the linking equation for Scenario 1 does not involve the value of the head in the manhole.

With this second method, it is seen in Figure 6.11 that one tendency curve can now be fitted for all the tests belonging to the same Scenario. Moreover, the curve intercepts the y-axis closer to the origin with an independent term of $0.1l/s$. This can be considered negligible as the order of magnitude of the flow rates is still $10l/s$.

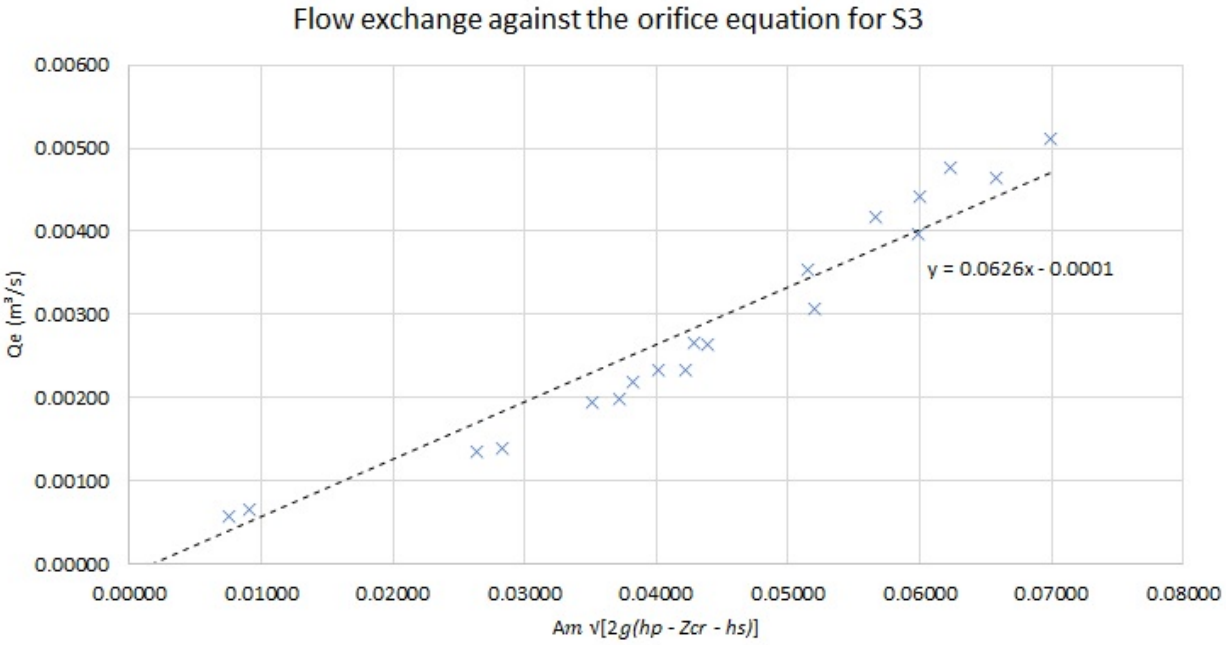

Figure 6.11: Flow exchange against orifice equation for Scenario S3 - Method 2

For Scenario 4, Figure 6.12, two groups has to be made. The first one is the group of tests with the valve down stream of the pipe system completely closed (T4X). Indeed, this group of tests induces all the flow from the pipe system to go to the surface. The other group consists of the other tests (T2X and T3X). Two different equations can be fitted. The equation for the first group (triangles in the Figure) still keep an independent term that can be considered not negligible ($2.6l/s$). The equation fitted from the second group almost goes trough the origin with an independent term of $0.2l/s$.

Scenario	$C_i(-)$
S1	0.5819
S3	0.0626
S4	0.0670

Table 6.2: Discharge coefficient - Method 2

Table 6.2 gathers the new discharge coefficients for each scenario. In this method, only one discharge coefficient is found for its scenario and the independent term is about 1% of the maximal flow rate.

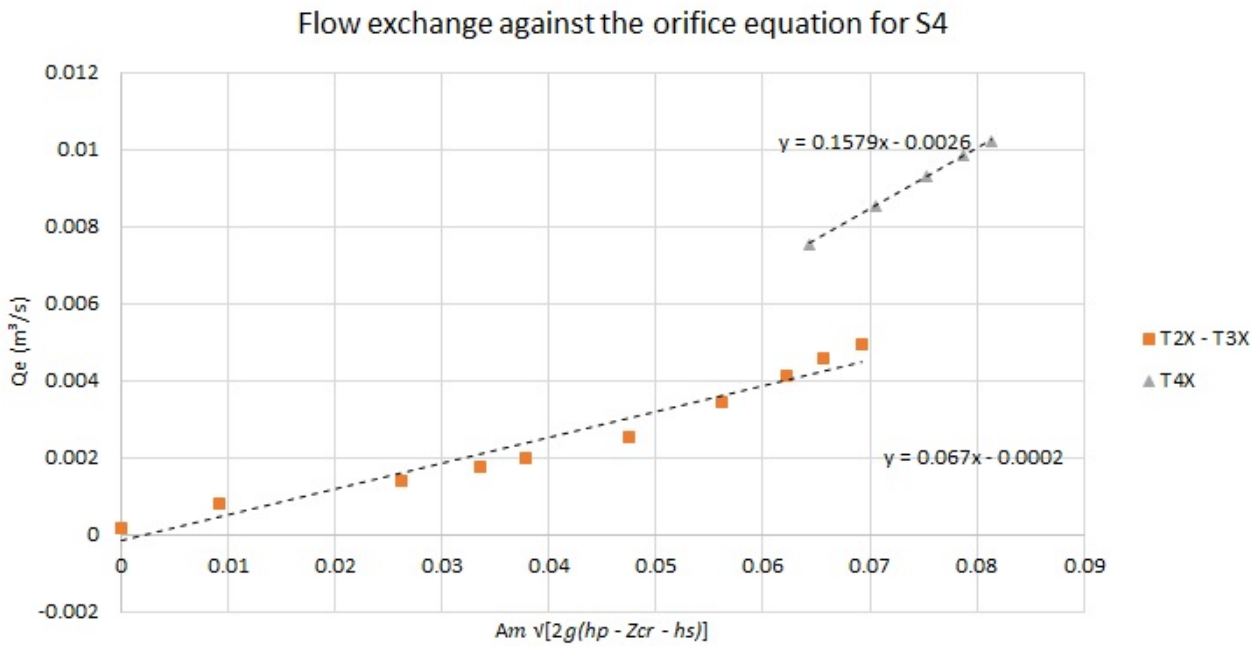

Figure 6.12: Flow exchange against orifice equation for Scenario S4 - Method 2

Exchange flow rate

Applying the new coefficients to the linking equations of Scenario 3 and 4, Figures 6.13 and 6.14 are drawn.

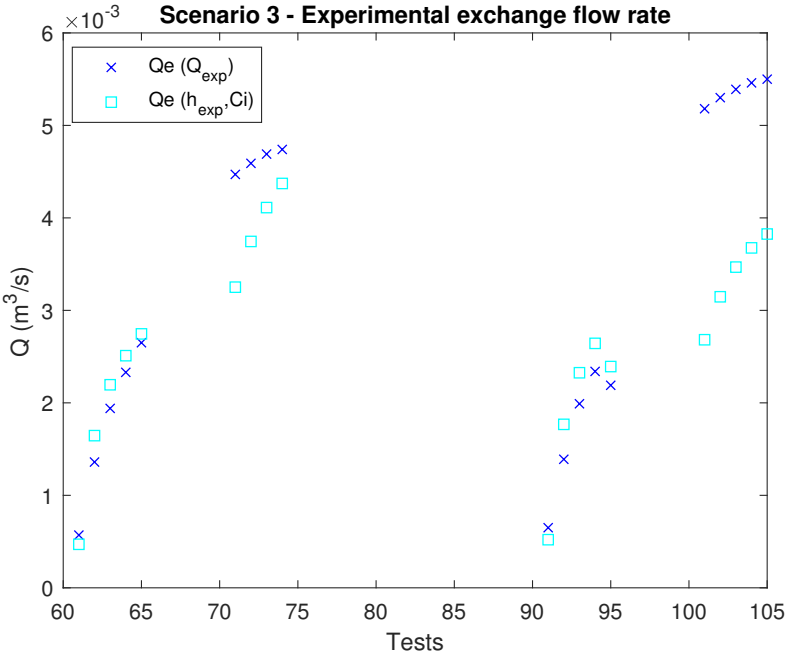

Figure 6.13: Results of experimental tests for Scenario 3 configurations

This new version leads to a better approximation of the exchange flow rate for intermediate values. Indeed, the error found for Scenario 3 for the intermediate values goes from 3% to a maximum of 20%. However, the model tends to underestimate the exchange flow rate for values higher than $5l/s$ and the errors for this range are still sometimes up to 90%.

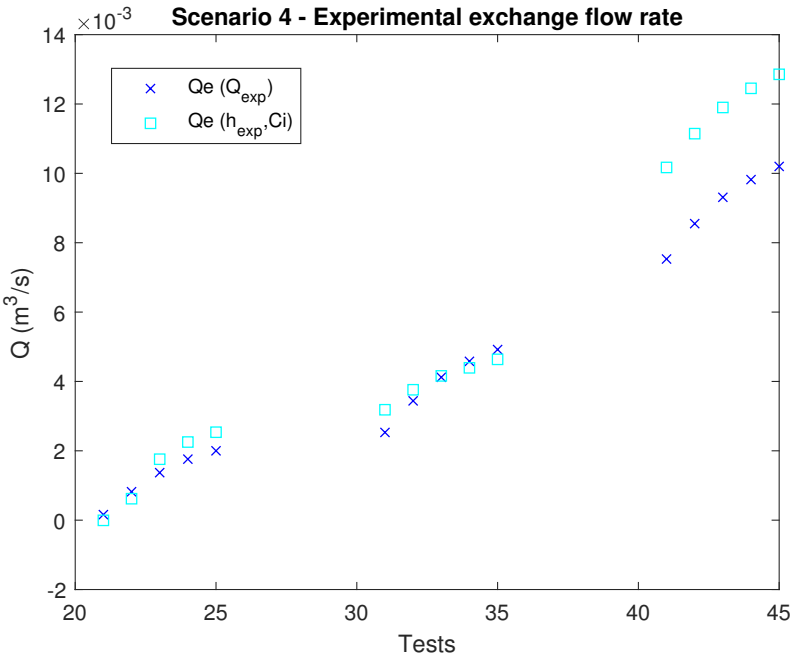

Figure 6.14: Results of experimental tests for Scenario 4 configurations

For Scenario 4, the percentage of error is similar (from 1% to 24%) and even appropriate for the whole range of exchange flow rates.

A conclusion can be made saying that the calibration of the discharge coefficient is really dependent of the head in the manhole, h_p. Also, the independent term of the tendency curves cannot be disregarded even if is considered small. Indeed, the independent term of the first method is of the order of $5l/s$ which is 50% of the current maximal flow rates observed for this project.

6.2 Unsteady state tests

Figure 6.15 shows the general mass exchange in a certain period given by Table 5.1 and compares the actual exchange flow rate to the one calculated with the linking equations and a discharge coefficient based on the previous conclusions.

Some tendencies can be seen in this graph. The general mass exchange is always positive meaning that it mainly develop a sewer to surface exchange. The general mass exchange also increases with the duration of the event. It appears to be really dependent of the opening of the manual valve downstream of the pipe system (26% or 43%), this is logical because the aim of the closure of this valve is to induce more exchange flow. The surface flow rate (regulated by Valve A, 52% or 76%), however, does not influence as much the general mass exchange.

The estimation of the exchange flow rate is globally overestimated by the linking equations. However, the error is not good as most of the tests are within a 25% margin of error, but can be acceptable (see Figure 6.16).

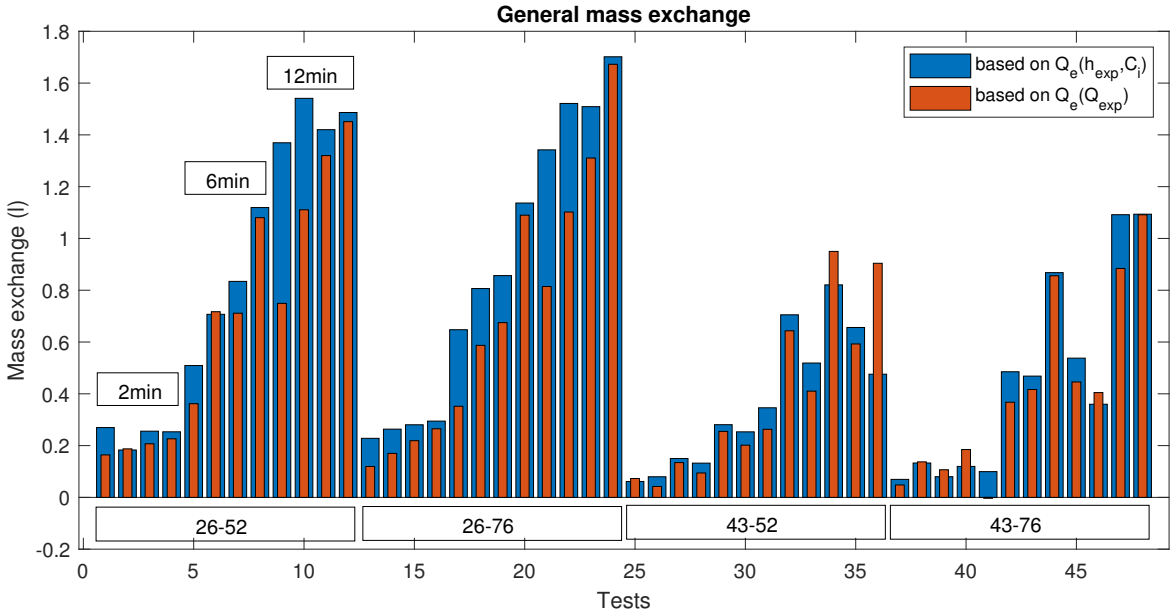

Figure 6.15: General mass exchange for all tests

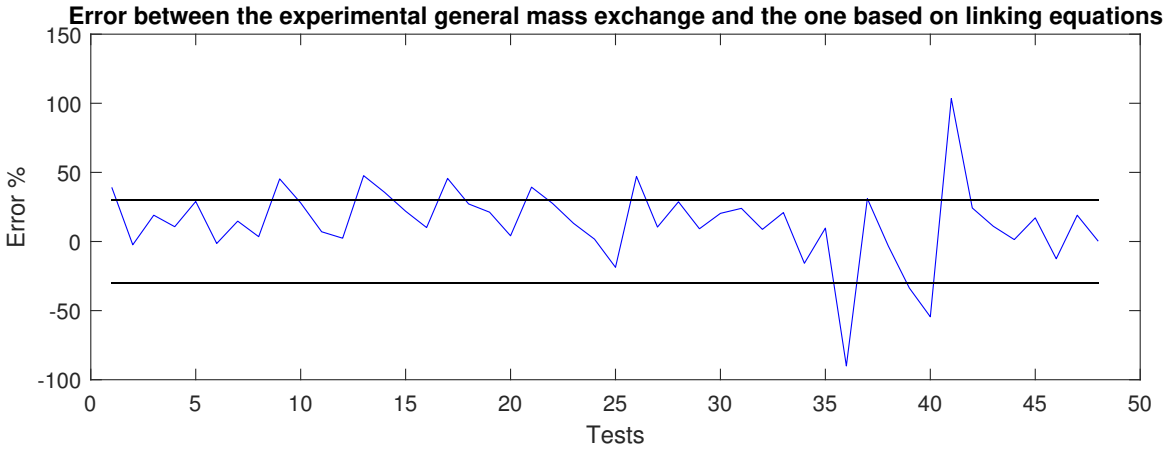

Figure 6.16: Error in the general mass exchange for all tests

Figures 6.17 to 6.20 show the general mass exchange for each peak intensity. The tendency to rise with the duration of the event is clearer on those graphs.

The actual graphs representing the flow rates and water depths will be analysed in the next chapter with numerical simulations.

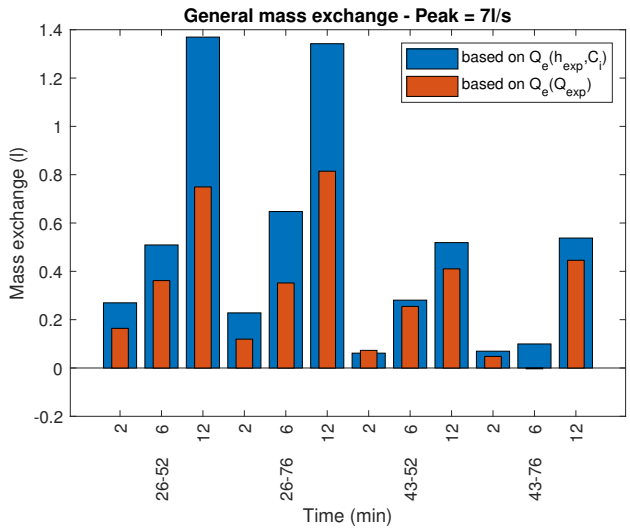

Figure 6.17: General mass exchange for a peak intensity of $7l/s$

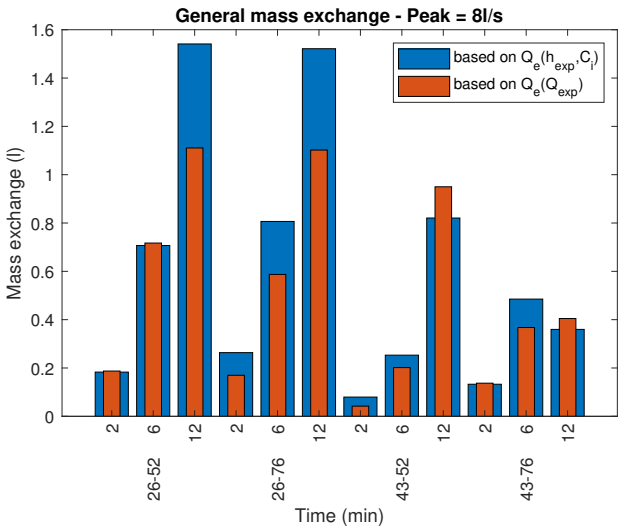

Figure 6.18: General mass exchange for a peak intensity of $8l/s$

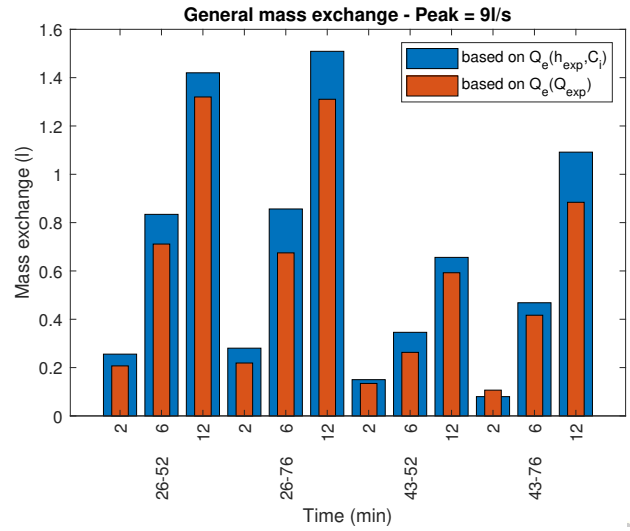

Figure 6.19: General mass exchange for a peak intensity of $9l/s$

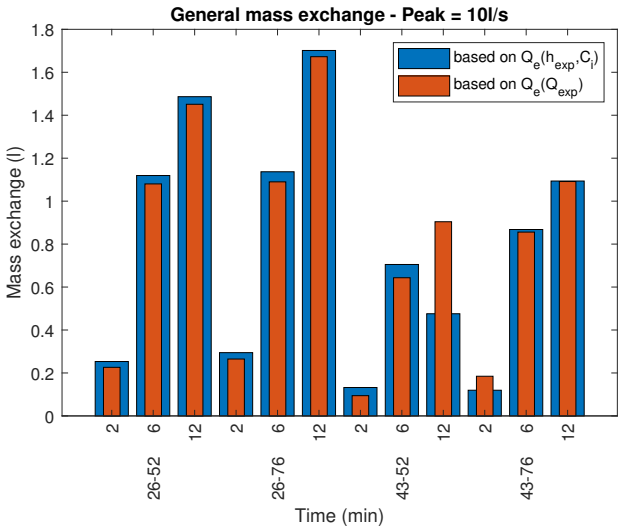

Figure 6.20: General mass exchange for a peak intensity of $10l/s$

7 Comparison with numerical simulations

The experimental results will be compared with the two numerical models described in Chapter 4. The first one is a 1D uniform flow and the other, more complex, is a 2D numerical model using shallow-water equations, called Wolf. Wolf software is not used to compute the unsteady state tests because it is not yet capable to input a parameter h_p variable in time.

7.1 Steady state tests

7.1.1 Method 1 : h_p = upstream pipe pressure

Water depths

Three different surface water depths (h_s) are observed in the next graphs. The experimental water depth ($h_s(h_{exp})$), the uniform water depth ($h_s(h_u)$) and the one calculated by Wolf software ($h_s(h_{wolf})$). As seen in Section 4.3.1, the experimental and the Wolf water depths are not considered at the same location due to limitations of the software.

Figures 7.1, 7.2 and 7.3 contain those three water depths for each Scenario.

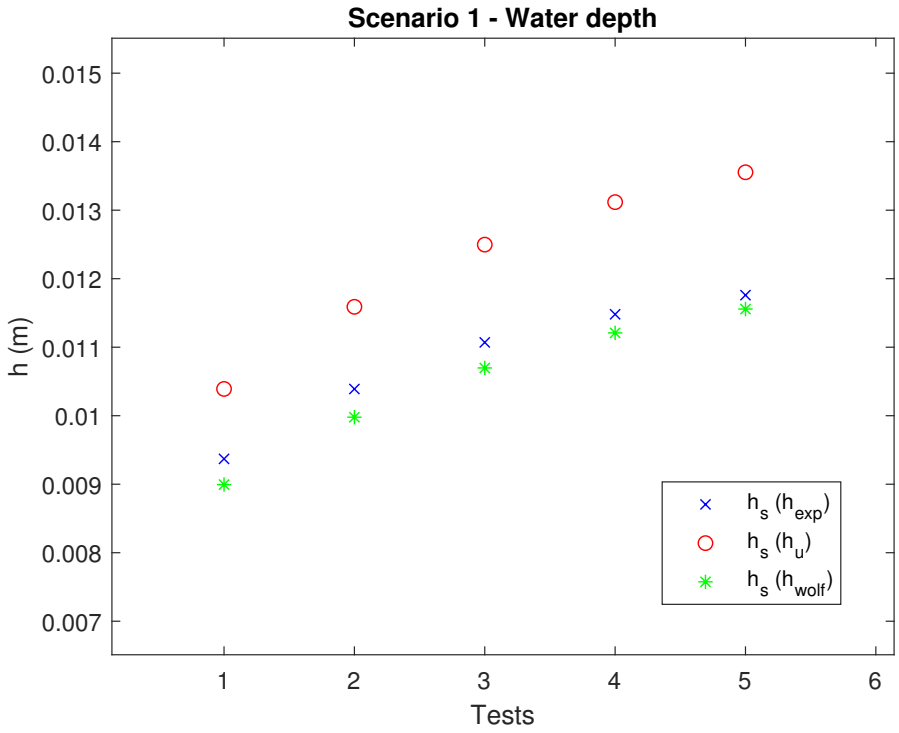

Figure 7.1: Results of numerical simulations for Scenario 1 in term of water depth

It is shown in Figure 7.1 (Scenario 1) that Wolf software calculates a better approximation of h_s than the uniform flow model for the surface water depth. The maximal errors between the experimental and the calculated water depths are 12.5% for the uniform water depth and 4% for Wolf water depth. Those errors are acceptable. The uniform flow calculation tends to overestimate the water depth while Wolf software tends to underestimate it. However, the trend of each curve seems

to be the same which can relate to a good evolution of the calculations with the surface upstream flow rate.

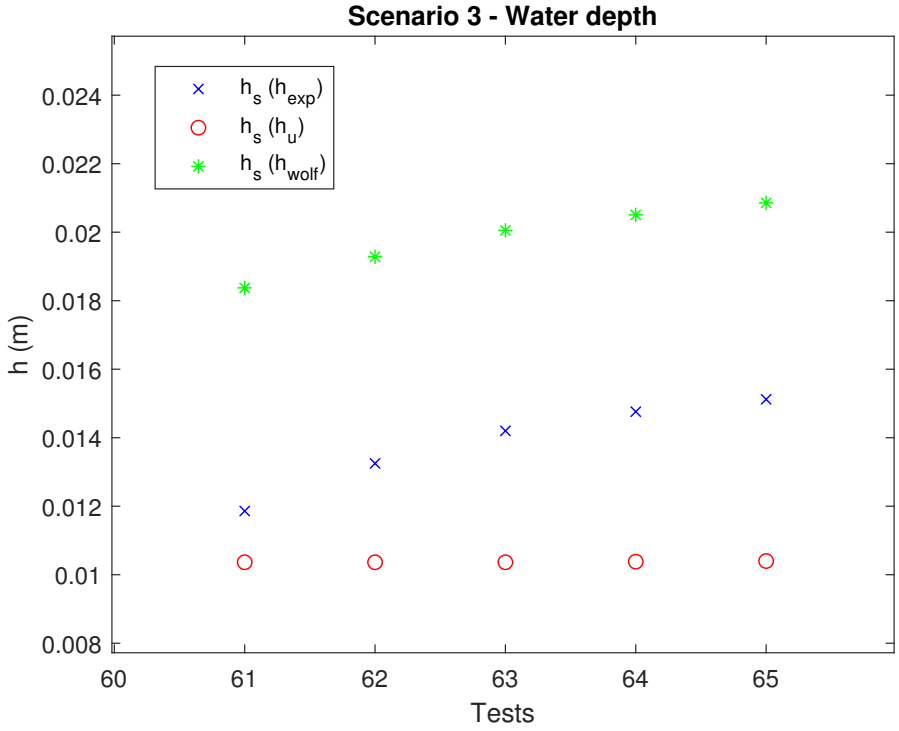

Figure 7.2: Results of numerical simulations for Scenario 3 in term of water depth - Method 1

The error between the uniform water depth and the experimental one is 40% and with Wolf software is 35% as seen in Figure 7.2 for Scenario 3. The observations are reversed for this Scenario compared to Scenario 1. The error is of the same magnitude for each model but the software is now overestimating the water depth while the uniform flow model underestimates it. It makes sense for the uniform flow model to underestimate the experimental water depth as it does not take into account the additional flow coming from the manhole which increases the water depth around it. As for Wolf software, the overestimation comes from the additional exchange flow ,itself also overestimated as can be seen in Section 7.1.1, as they are interdependent in the software.

Figure 7.3 shows the results for Scenario 4. The same conclusions as the ones for Scenario 3 can be made in term of uniform flow. However, in this case, h_s is now underestimated by Wolf software to a maximal error of almost 100%.

Exchange flow rate

After the observations about the results in water depths, results in terms of exchange flow rate can be examined. Figures 7.4, 7.5 and 7.6 display those results. First, the differences between the exchange flow rate calculated with experimental data (either with experimental flow rates, $Q_e(Q_{exp})$, or the experimental water depth and a discharge coefficient, $Q_e(h_{exp}, C_{i,1})$ and the ones calculated with a discharge coefficient and either a uniform water depth, $Q_e(h_u, C_{i,1})$ or one calculated with Wolf software, $Q_e(h_{wolf}, C_{i,1})$).

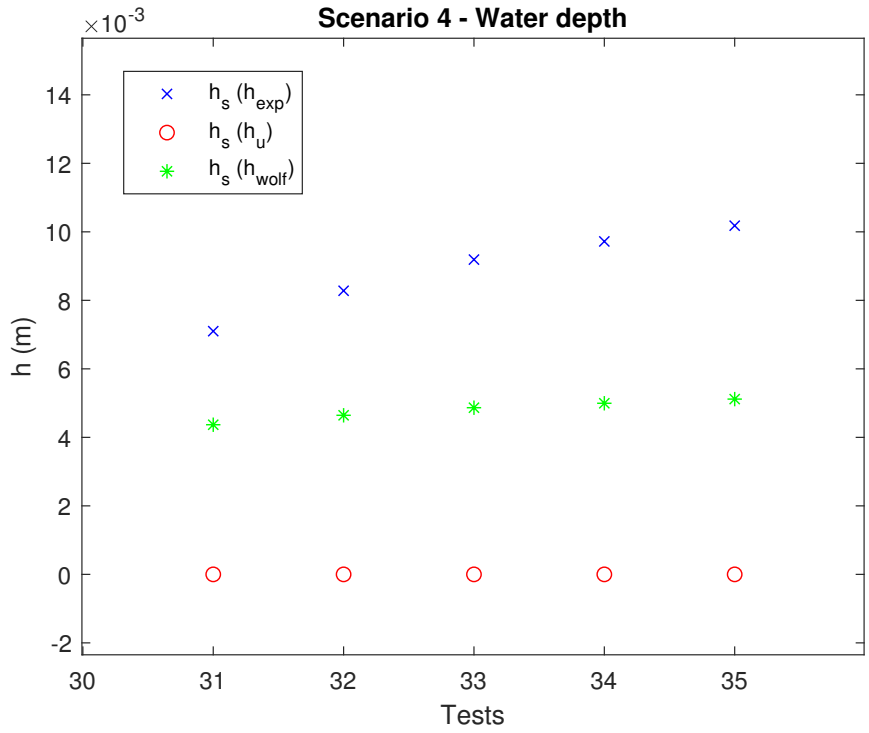

Figure 7.3: Results of numerical simulations for Scenario 4 in term of water depth - Method 1

In Figure 7.4 it is seen that the value of Q_e with a uniform water depth is, in absolute value, overestimated up to 20%. As the error in the estimation of the water depth was only 12.5%, it is increased by the error coming from the estimated value of the discharge coefficient which was a maximum of 4%. In the WOLF simulations, the value is closer from the experimental one with a maximal error of 13.5% which is still bigger than the value coming from the estimation of the water depth which was 4%.

Scenario 3 results observed in Figure 7.5 show that both calculations are far from the experimental flow results but are still very close to the exchange flow rate calculated with the experimental water depth and the discharge coefficient. Table 7.1 displays the values of the different errors. A conclusion can be made from those results, the discharge coefficient might not be appropriate to match the experimental flow rates.

Similar observations are made for Scenario 4 (Figure 7.6), the errors are given in Table 7.2.

Test	Error with $Q_e(Q_{exp})$ (%)		Error with $Q_e(h_{exp}, C_i)$ (%)	
	$Q_e(h_u, C_i)$	$Q_e(h_{wolf}, C_i)$	$Q_e(h_u, C_i)$	$Q_e(h_{wolf}, C_i)$
T61	91.6	89.3	1.9	26.0
T62	82.1	78.0	2.6	19.7
T63	76.4	72.1	2.5	15.1
T64	73.34	68.7	3.7	13.0
T65	70.84	66.1	3.5	12.2

Table 7.1: Evolution of the error of $Q_e(Q_{exp})$ or $Q_e(h_{exp}, C_i)$ to $Q_e(h_u, C_i)$ or $Q_e(h_{wolf}, C_i)$ for Scenario 3

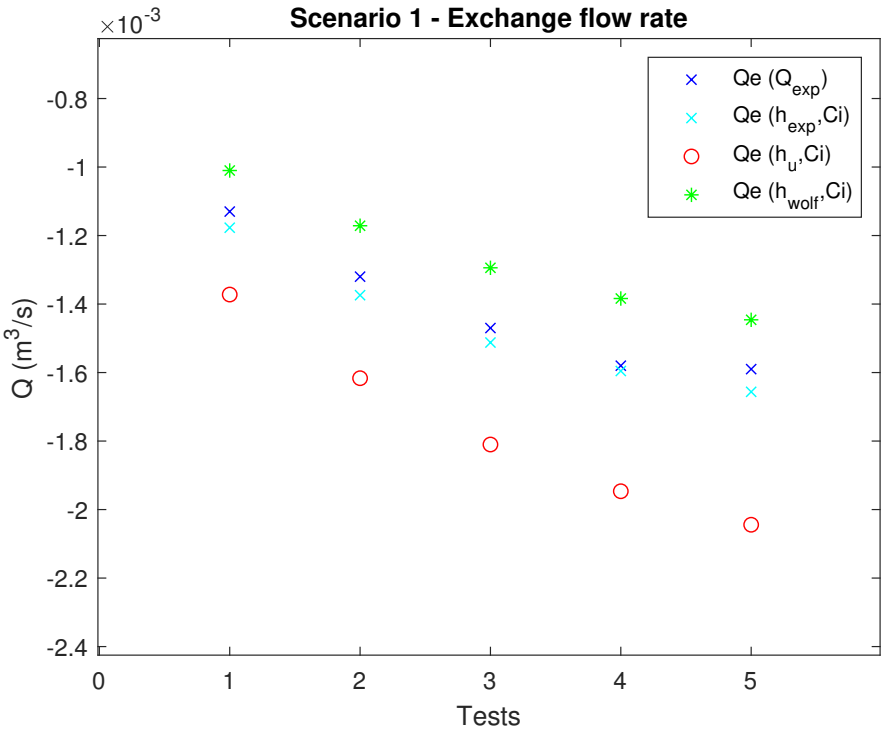

Figure 7.4: Results of numerical simulations for Scenario 1 in term of exchange flow rate

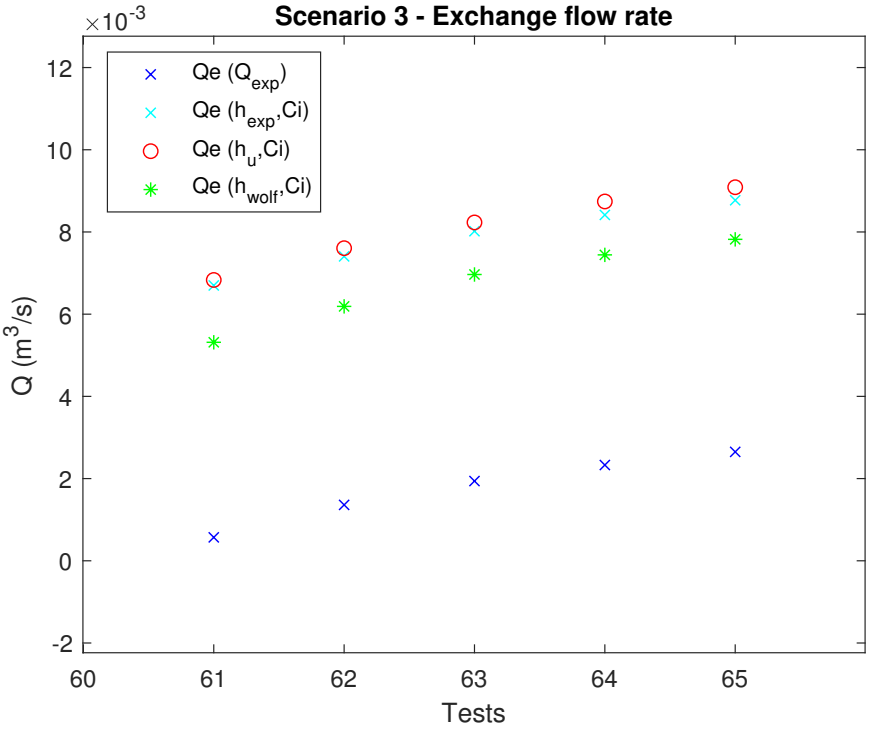

Figure 7.5: Results of numerical simulations for Scenario 3 in term of exchange flow rate - Method 1

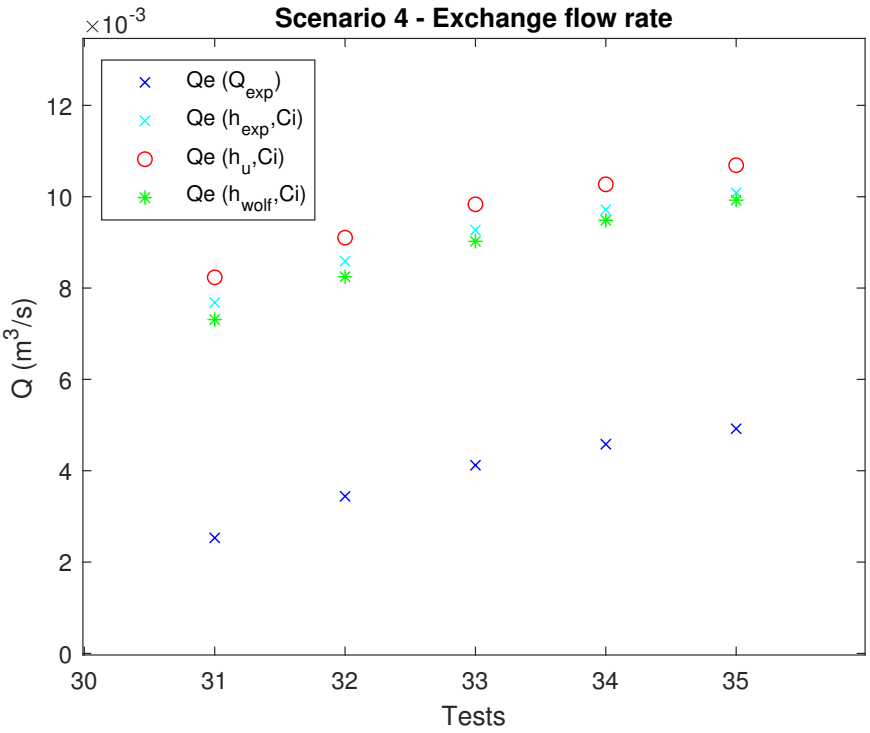

Figure 7.6: Results of numerical simulations for Scenario 4 in term of exchange flow rate - Method 1

Test	Error with $Q_e(Q_{exp})$ (%)		Error with $Q_e(h_{exp}, C_i)$ (%)	
	$Q_e(h_u, C_i)$	$Q_e(h_{wolf}, C_i)$	$Q_e(h_u, C_i)$	$Q_e(h_{wolf}, C_i)$
T31	69.3	65.4	6.7	5.1
T32	62.2	58.3	5.6	4.1
T33	58.1	54.3	5.7	2.7
T34	55.4	51.7	5.4	2.4
T35	54.0	50.4	5.7	1.6

Table 7.2: Evolution of the error of $Q_e(Q_{exp})$ or $Q_e(h_{exp}, C_i)$ to $Q_e(h_u, C_i)$ or $Q_e(h_{wolf}, C_i)$ for Scenario 4

7.1.2 Method 2 : h_p = mean of upstream and downstream pipe pressure

Water depths

The results in water depth will not change compared to the results for the first method because the value of the uniform surface water depth does not change in relation to the head in the manhole. However, the surface water depth would change in Wolf software as every parameter is interdependent. For this method, Wolf software is unfortunately not used. Figures 7.7 and 7.8 gather the previous results for Scenarios 3 and 4.

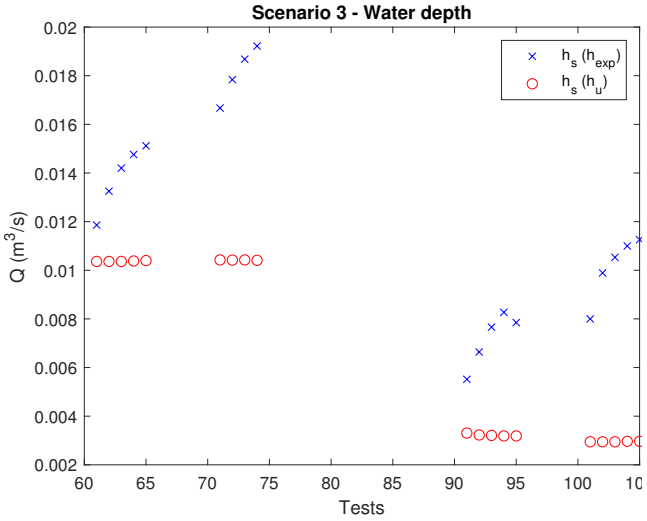

Figure 7.7: Results of numerical simulations for Scenario 3 in term of water depth - all methods

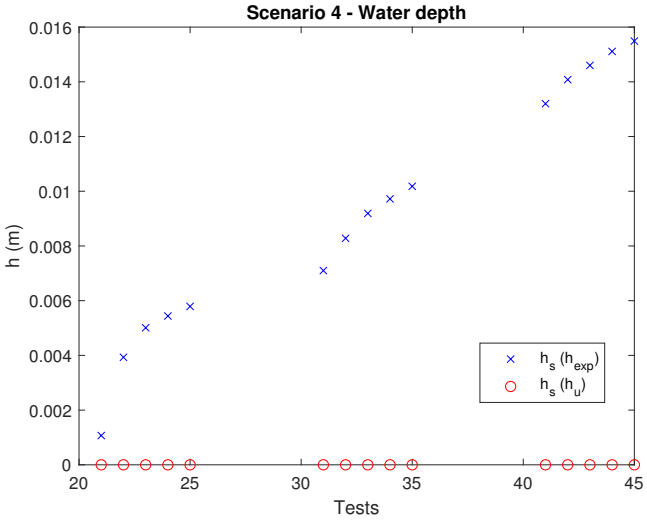

Figure 7.8: Results of numerical simulations for Scenario 4 in term of water depth - all methods

Exchange flow rate

With the implementation of the coefficients found with the second method, the results are more accurate. Indeed, the error of those tests is maximum 20% for exchange flow rates under $5l/s$ compared to 90% with the first method. However, the error can reach 85% for exchange flow rates above that limit. As the exchange flow rate calculated with the linking equations and the experimental water depth stays really close to the other calculated flow rate (calculated with the uniform flow model) even over the limit of $5l/s$, a conclusion would be that the discharge coefficient is not appropriate for exchange flow rates bigger than $5l/s$.

The error is even lower for Scenario 4. The better estimation is made for intermediate exchange flow rates with an error from 0 to 20%. The lower and higher exchange flow rates reach a 30% maximal error which is significantly reduced compared to the 70% of the first method.

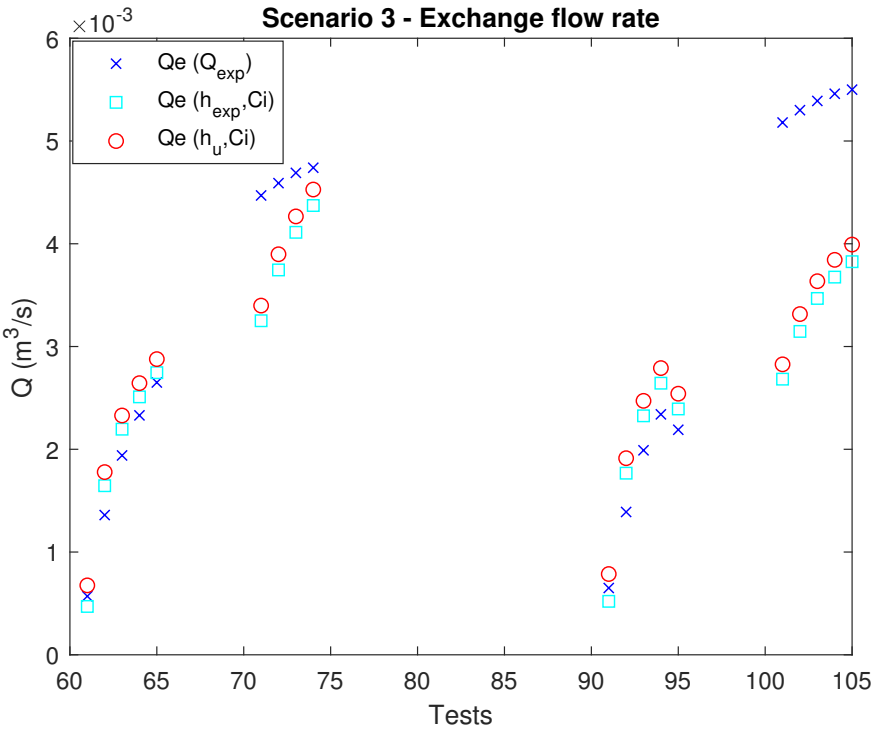

Figure 7.9: Results of numerical simulations for Scenario 3 in term of exchange flow rate - Method 2

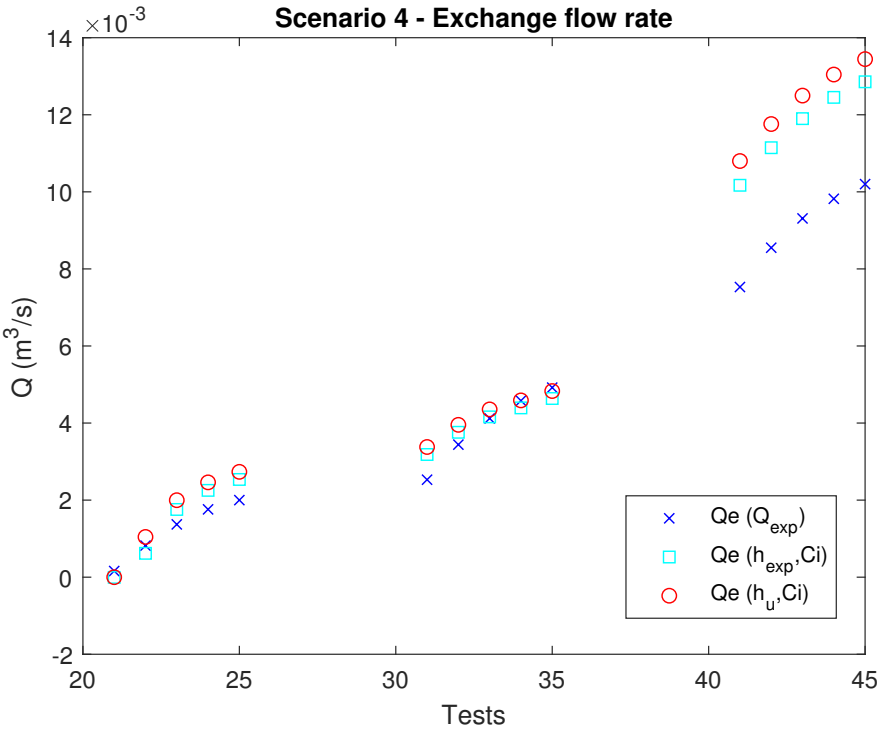

Figure 7.10: Results of numerical simulations for Scenario 4 in term of exchange flow rate - Method 2

7.2 Unsteady state tests

There are 48 unsteady state tests that were conducted in the facility. Only the uniform flow model is used due to a limitation of WOLF software, being unable to run some parameters that vary in time. General tendencies can be expressed from the graphs. In order to illustrate the tendency observed,

two sets of data are presented. The two sets are composed of events with a duration of 6 minutes, a peak intensity of either $7l/s$ or $9l/s$ and all ranges of surface flow rate ($0.8 - 1.0l/s$, 52% opening of Valve A or $6.0 - 6.2l/s$, 76% opening) and exchange flow rate (govern by the manual valve at the end of the pipe system). The comparison is made by looking at some of the results but knowing that the tendency of the other results is similar. The 48 results are gathered in Appendix B.2. Figures 7.11 to 7.18 show the considered simulations.

A general comment that can be made that is the evaluation of the exchange flow rate with the experimental water depth implemented in the linking equation ($Q_e(h_{exp}, Ci)$) matches the evaluation of the uniform flow model ($Q_e(h_u, Ci)$).

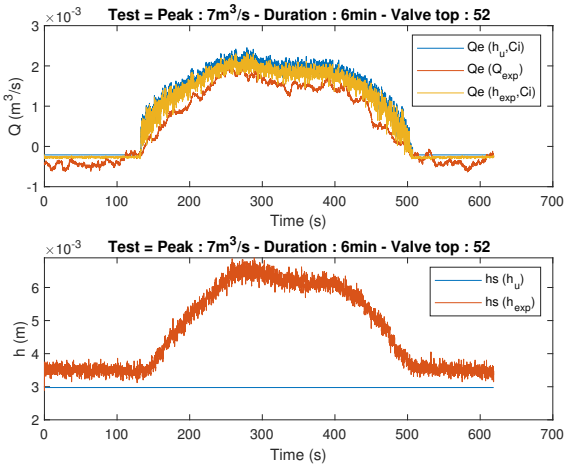

Figure 7.11: Numerical simulation for test 07-06-26-52

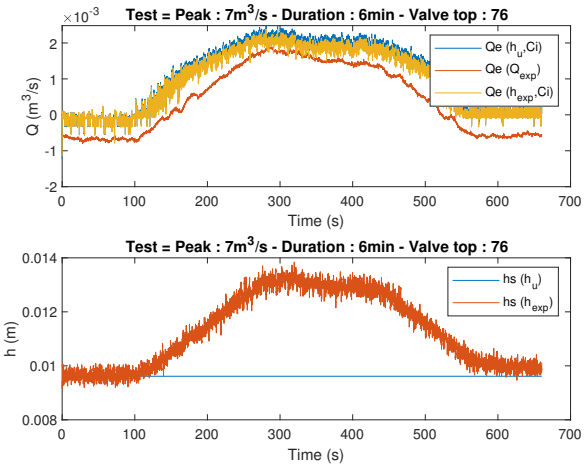

Figure 7.12: Numerical simulation for test 07-06-26-76

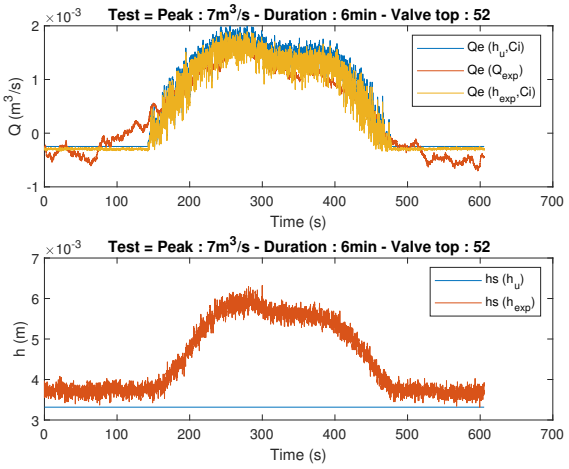

Figure 7.13: Numerical simulation for test 07-06-43-52

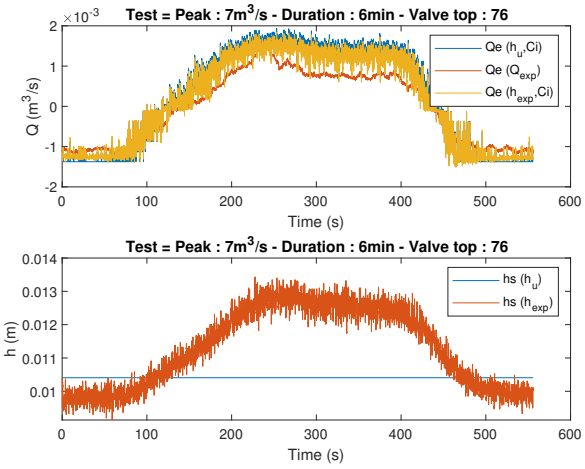

Figure 7.14: Numerical simulation for test 07-06-43-76

Surface-to-sewer

The modelization of the water depth as a uniform water depth in the first scenario (kind of a steady state at the beginning and the end of the event) matches the experimental results. For bigger upstream surface flow rates (Figures 7.12 and 7.14 or 7.16 and 7.18), the water depth is well represented by a uniform flow with a tendency to overestimate the actual surface water depth. For the

smaller upstream surface flow rates, on the other hand, the uniform flow model underestimates the real surface water depth. The modelled exchange flow rate is close to the experimental one but for each combination, it is overestimated.

Intermediate state

Between Scenario 1 and Scenario 3 phases, the event goes trough an intermediate phase with Scenario 2. This step is really short and the link between the equations is not imposed which leads to a discontinuity in the graphs. It is even more noticeable for the bigger peak events (Figures 7.15 to 7.18).

Sewer-to-surface exchange

Scenario 3 appears during the unsteady part of the event. The model completely underestimates the actual water depth. It is due to the fact that the uniform flow model only takes into consideration the upstream surface flow and not the additional exchange flow rate.

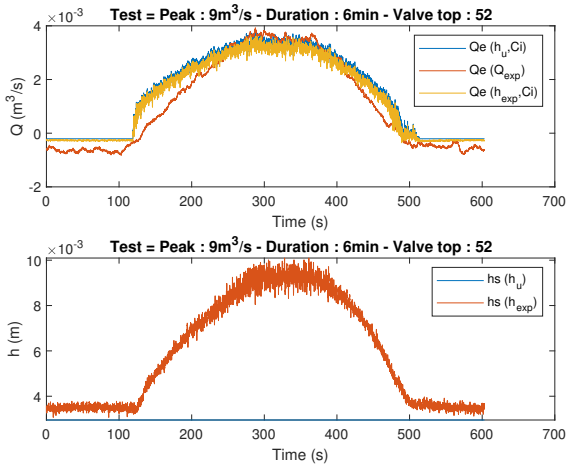

Figure 7.15: Numerical simulation for test 09-06-26-52

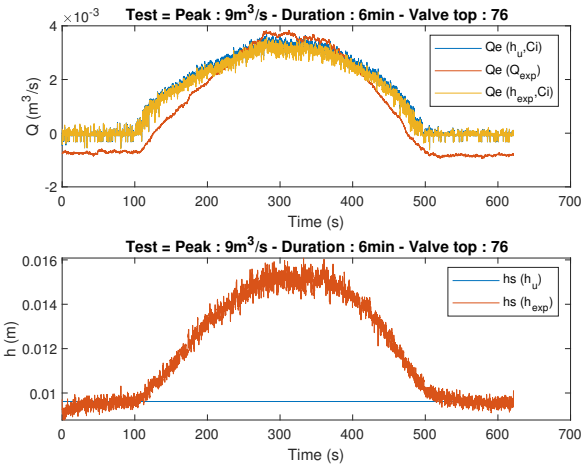

Figure 7.16: Numerical simulation for test 09-06-26-76

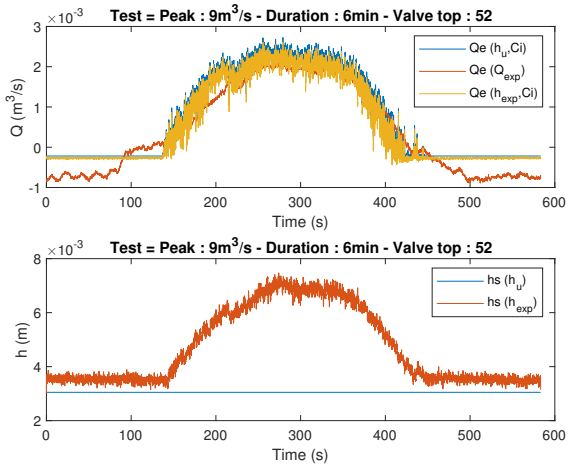

Figure 7.17: Numerical simulation for test 09-06-43-52

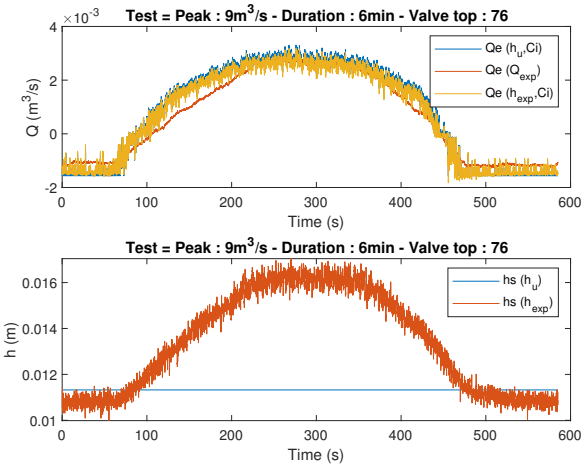

Figure 7.18: Numerical simulation for test 09-06-43-76

The comparison between the exchange flow rate calculated with the experimental depth and the linking equations to the uniform flow model shows that even if the water depth is underestimated in the uniform flow model, the flow exchange is very similar. The conclusion that can be made is that the model is not very sensitive to the evaluation of the water depth compared to the evaluation of the discharge coefficient.

Looking at the exchange flow rate, in general, the model overestimates the actual exchange flow rate. However, two comments can be made. First, in the cases of a peak intensity bigger than $7l/s$, see Figures 7.15 and 7.16 for example, the peak part of the graph is underestimated compared to the experimental flow rate. Secondly, the $43 - 52$ valve combination (Figures 7.13 and 7.17) tends to stay too long in the first scenario leading to an underestimation of the exchange flow rate at the beginning and the end of Scenario 3.

It is possible also to find some differences in similar tests but with different total durations. Figures 7.19 to 7.21 show that the the shorter the event, the worse it is represented. It is logical because a long unsteady event tends to be a combination of several small steady events at the end.

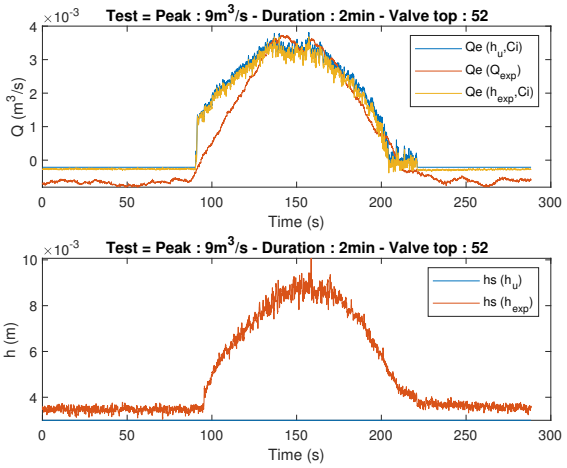

Figure 7.19: Numerical simulation for test 09-02-26-52

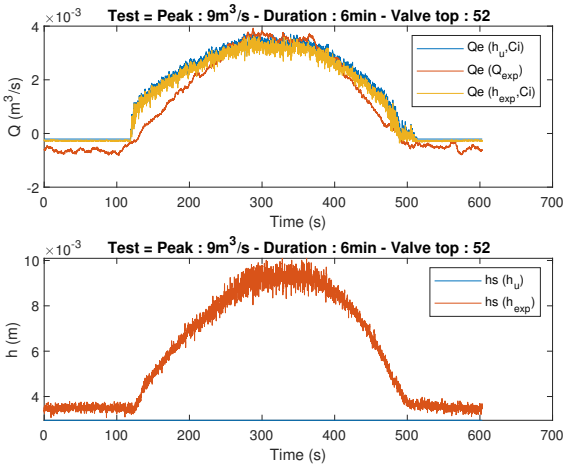

Figure 7.20: Numerical simulation for test 09-06-26-52

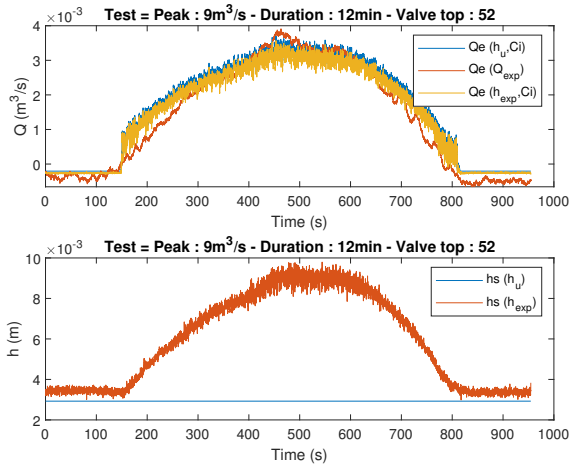

Figure 7.21: Numerical simulation for test 09-12-26-52

7.3 Discussion and perspectives

As stated before the main issue formulated by Rubinato et al. [12] about the overestimation of the exchange flow rate was significantly reduced by the application of the second method (using an average between the upstream and downstream pipe pressure instead of only the upstream one). However, a second problem that is not covered in this report is the discontinuity between the different scenarios. Indeed, the linking equations (Section 4.1) are not designed to provide a continuity between them. Figure 7.22 show the zone for each scenarios based on their area of application with the implementation of Rubinato et al. [12] results. Further work should focus on the issue to connect all the parts without discontinuities.

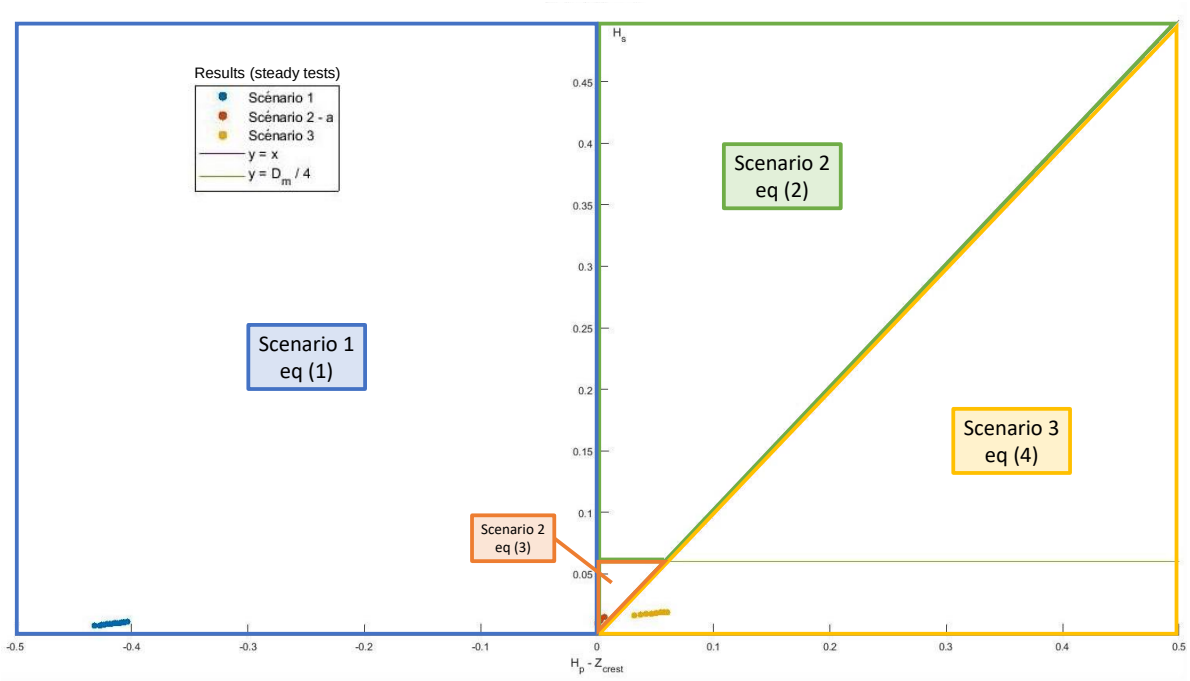

Figure 7.22: Area of application for each Scenario with the implementation of Rubinato et al. [12] results

8 Conclusion

In this present work, experimental testing was important in order to observe several configurations leading to a surface-to-sewer or sewer-to-surface exchange flow. Fifty steady and forty-eight unsteady state tests were performed.

The steady state tests were performed and analysed first. Each test was categorised to a certain scenario depending on the measured surface water depth and pressure in the manhole. From the equation corresponding to the scenario (illustrated by the weir or orifice flow exchange equations) and the measured parameters in the facility, one coefficient was obtained : the discharge coefficient. Two methods were used to find this coefficient. The first one followed the same procedure as Rubinato et al. [12] by estimating the pressure in the manhole with the recorded upstream pressure in the pipe system. The other procedure, estimated the pressure in the manhole by averaging the upstream and downstream pressure in the pipe system. Both of the methods consisted of comparing the exchange flow rate against the weir or orifice equations.

The results of the first method were adequate for the weir scenarios. However, the fitting of the discharge coefficient for the orifice scenarios were not accurate enough for the method to have a physical meaning, it had to neglect some terms with an order of magnitude similar to the experimental input parameters. The second method resulted to a better evaluation of the discharge coefficient. The value of the discharge coefficient for the weir scenario was 0.5819 and for the orifice scenarios, 0.0626 for configurations with a flow on the surface and 0.0670 with no flow on the surface.

Numerical results using the two different discharge coefficients were observed. At first, the results with the first discharge coefficient were gathered comparing the differences between the exchange flow rate, calculated with experimental data (either with experimental flow rates or the experimental water depth and the discharge coefficient) and the ones calculated with the discharge coefficient and either a uniform water depth or one calculated with Wolf software. The errors between the exchange flow rate from experimental flow rates and any other exchange flow rate were up to 100% even with the one calculated with the experimental water depth. The conclusion is that the coefficient is not adapted for the scenarios. The second discharge coefficient was then observed. The results were much better with an maximal error of 20%.

As well as assessing the model's capability to find the discharge coefficient of steady state tests, this report also implemented this discharge coefficient to the unsteady state model. It was observed that the uniform flow model matches the experimental model even if it tends to globally overestimate the exchange flow rate. However, the results have significantly improved compared to the ones obtained by Rubinato et al. [12]. The conclusions of the analysis of the unsteady state tests were that the model has a better performance when the event is longer or when the exchange flow rate is higher.

Further work should focus on removing the discontinuities existing in the transition between one scenario to another. This reflects the transition from a surface-to-sewer exchange configuration to a sewer-to-surface.

List of Figures

List of Tables

A Appendix : Experimental results

A.1 Steady state results

A.1.1 Experimental results

Tests	Valve C	Valve A	Q surf	Q sew	Q surf	Q sew	P mh	P sew	P sew	P sew	P surf	P surf
	-	-	UP (l/s)	UP (l/s)	DN (l/s)	DN (l/s)	mm	UP (mm)	DN (mm)	DN2 (mm)	UP (mm)	DN (mm)
T11	0.00	125.00	6.93	-0.01	5.74	1.13	55.27	51.53	78.77	66.57	8.37	12.01
T12	0.00	135.00	8.31	-0.01	6.89	1.32	62.02	58.75	83.12	68.93	10.39	13.19
T13	0.00	145.00	9.42	-0.01	7.91	1.47	65.73	64.22	85.19	71.50	11.07	14.10
T14	0.00	155.00	10.21	-0.01	8.60	1.58	70.35	69.08	86.91	73.27	11.48	14.70
T15	0.00	165.00	10.78	-0.01	9.15	1.59	73.25	71.90	87.93	74.52	11.76	15.21
T21	125.00	0.00	0.00	7.64	-0.04	7.48	467.16	514.39	418.23	303.56	1.07	2.95
T22	135.00	0.00	0.00	8.55	0.68	7.73	470.29	526.44	441.69	321.15	3.93	4.87
T23	145.00	0.00	0.00	9.37	1.26	8.01	472.22	536.90	463.47	333.10	5.01	5.61
T24	155.00	0.00	0.00	9.93	1.63	8.17	473.28	544.47	478.82	342.93	5.44	6.14
T25	165.00	0.00	0.00	10.29	1.94	8.30	474.47	549.97	489.11	352.17	5.79	6.43
T31	125.00	0.00	0.00	7.53	2.94	5.00	483.52	532.01	550.87	506.22	7.10	7.58
T32	135.00	0.00	0.00	8.54	4.01	5.10	485.67	544.92	584.80	535.94	8.28	8.88
T33	145.00	0.00	0.00	9.34	4.42	5.22	487.64	555.48	611.25	559.26	9.19	9.80
T34	155.00	0.00	0.00	9.88	4.70	5.30	489.10	562.74	627.20	574.42	9.72	10.38
T35	165.00	0.00	0.00	10.21	5.28	5.29	489.78	569.02	646.33	591.39	10.18	10.81
T41	125.00	0.00	0.00	7.53	7.40	0.00	493.40	555.52	633.87	639.28	13.50	13.24
T42	135.00	0.00	0.00	8.55	8.40	0.00	493.05	568.61	664.13	669.66	14.56	14.08
T43	145.00	0.00	0.00	9.31	9.24	0.00	492.00	578.87	689.71	695.19	15.32	14.69
T44	155.00	0.00	0.00	9.83	9.43	0.00	490.82	586.76	709.74	714.56	15.87	15.11
T45	165.00	0.00	0.00	10.20	10.43	0.00	490.37	593.23	724.49	728.84	16.25	15.49
T51	125.00	125.00	6.99	7.58	6.24	8.37	474.00	520.76	371.16	236.25	9.83	12.56
T52	135.00	125.00	6.99	8.60	6.84	8.79	474.00	530.87	381.49	232.03	10.71	13.11
T53	145.00	125.00	6.97	9.33	7.04	9.21	474.06	538.52	381.05	214.86	11.15	13.34
T54	155.00	125.00	6.99	9.92	7.43	9.38	474.03	544.28	395.40	222.01	11.68	13.66
T55	165.00	125.00	6.98	10.26	7.68	9.46	473.66	548.63	407.21	231.79	12.11	13.88
T61	125.00	125.00	6.90	7.48	7.50	6.91	478.23	525.93	456.60	358.65	11.86	13.81
T62	135.00	125.00	6.90	8.48	8.27	7.13	477.89	535.35	481.63	382.21	13.25	14.45
T63	145.00	125.00	6.90	9.25	8.87	7.31	477.38	543.89	501.89	388.91	14.20	14.87
T64	155.00	125.00	6.92	9.81	9.42	7.48	477.72	549.68	516.06	400.48	14.76	15.17
T65	165.00	125.00	6.94	10.25	9.32	7.60	477.90	554.97	527.24	409.88	15.12	15.47
T71	125.00	125.00	6.97	7.55	11.08	4.47	487.42	537.71	586.19	555.19	16.67	16.50
T72	135.00	125.00	6.96	8.55	11.70	4.59	489.75	551.04	619.24	585.97	17.84	17.10
T73	145.00	125.00	6.97	9.33	12.23	4.69	491.55	561.62	646.96	612.07	18.68	17.57
T74	155.00	125.00	6.95	9.85	12.31	4.74	492.71	569.31	668.52	631.96	19.22	17.86
T81	125.00	85.00	1.09	7.69	0.97	7.75	399.00	446.09	337.90	222.13	3.84	5.10
T82	135.00	85.00	1.07	8.57	1.05	8.57	467.33	523.64	389.94	241.52	3.89	5.26
T83	145.00	85.00	1.06	9.36	1.34	9.12	466.39	531.24	381.25	215.54	4.25	5.61
T84	155.00	85.00	1.03	9.82	1.63	9.21	466.54	537.36	397.20	225.10	4.97	6.11
T85	165.00	85.00	1.02	10.24	1.89	9.33	466.75	542.18	407.98	231.06	5.55	6.46
T91	125.00	85.00	1.03	7.60	1.71	6.95	471.57	519.02	451.46	347.10	5.16	6.23
T92	135.00	85.00	0.99	8.52	2.23	7.13	473.46	531.14	477.91	366.86	6.64	7.21
T93	145.00	85.00	0.98	9.32	2.83	7.34	474.92	540.91	499.28	382.34	7.66	7.98
T94	155.00	85.00	0.97	9.81	3.32	7.48	476.42	548.28	513.21	393.97	8.27	8.48
T95	165.00	85.00	0.97	10.22	2.79	8.03	474.14	550.21	494.37	356.95	7.85	8.14
T101	125.00	85.00	0.85	7.84	3.28	5.18	480.09	528.96	534.66	486.45	8.00	8.66
T102	135.00	85.00	0.85	8.83	4.00	5.30	482.05	540.40	561.48	507.40	7.05	9.89
T103	145.00	85.00	0.85	9.57	4.31	5.39	483.17	548.31	581.86	528.90	7.13	10.53
T104	155.00	85.00	0.86	9.89	4.83	5.46	484.01	554.04	595.98	550.54	7.52	11.00
T105	165.00	85.00	0.86	10.26	5.23	5.50	483.85	558.12	606.74	564.60	7.59	11.26

Figure A.1: Recorded data for every experimental test

A.1.2 Experimental analysis

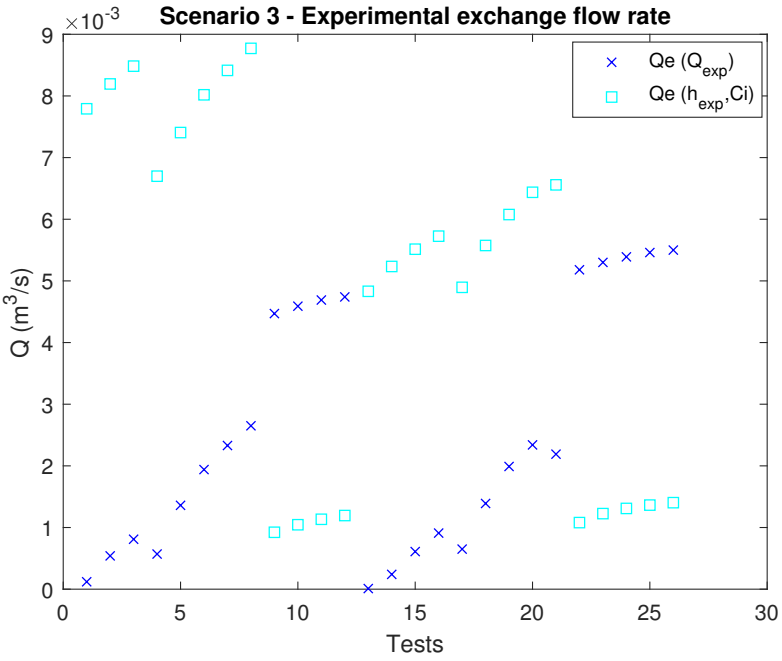

Figure A.2: Results of experimental tests for Scenario 3 configurations - Qe

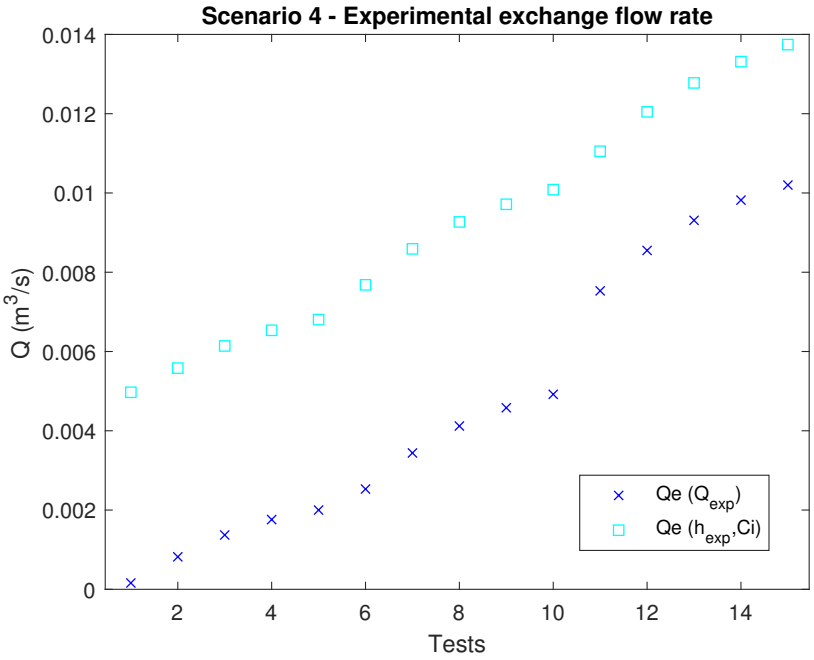

Figure A.3: Results of experimental tests for Scenario 4 configurations - Qe

A.2 Unsteady state results

A.2.1 Experimental results

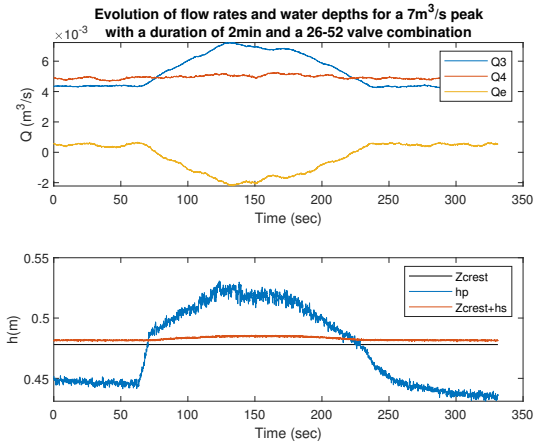

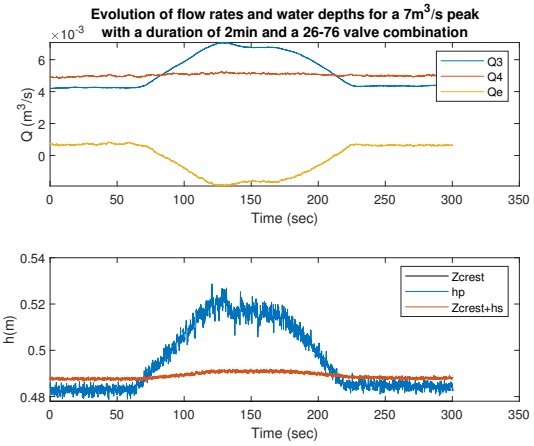

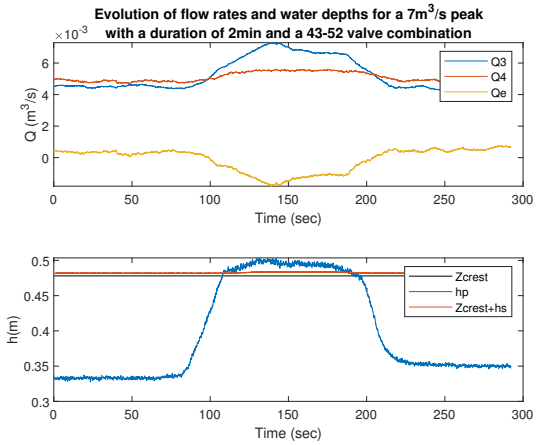

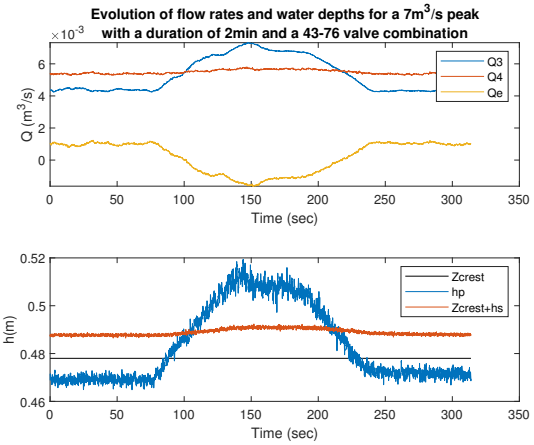

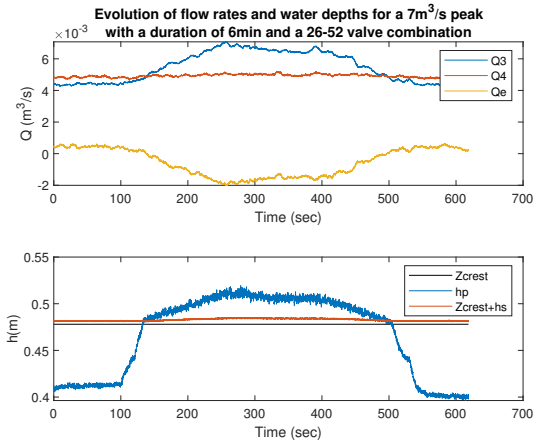

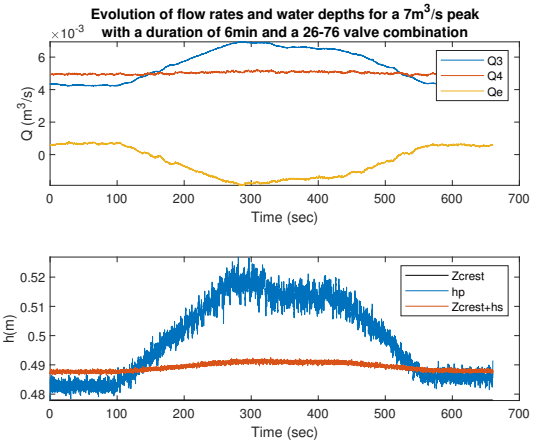

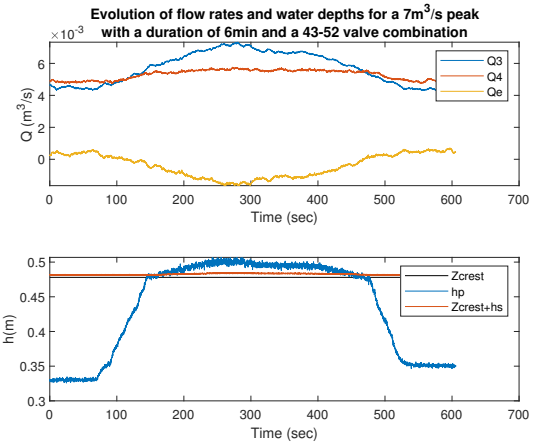
Evolution of flow rates and water depths for a 7m3/s peak with a duration of 6min and a 43-52 valve combination
Q (m3/s)
Q3
Q4
Qe
Time (sec)
h(m)
Zcrest
hp
Zcrest+hs
Time (sec)

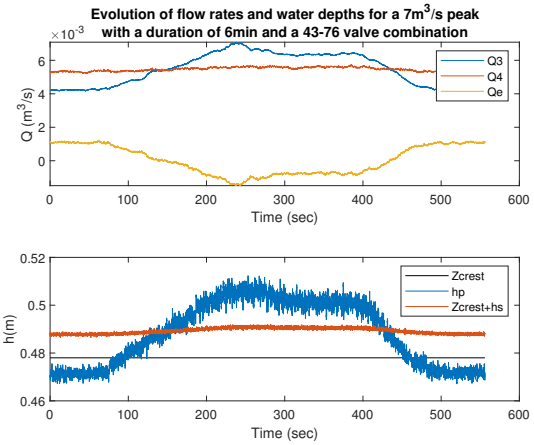
Evolution of flow rates and water depths for a 7m3/s peak with a duration of 6min and a 43-76 valve combination
Q (m3/s)
Q3
Q4
Qe
Time (sec)
h(m)
Zcrest
hp
Zcrest+hs
Time (sec)

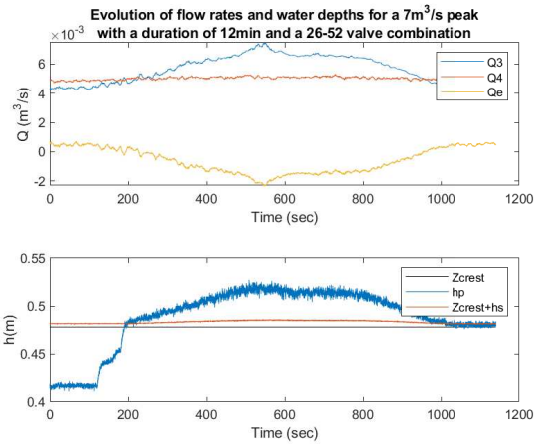
Evolution of flow rates and water depths for a 7m3/s peak with a duration of 12min and a 26-52 valve combination
Q (m3/s)
Q3
Q4
Qe
Time (sec)
h(m)
Zcrest
hp
Zcrest+hs
Time (sec)

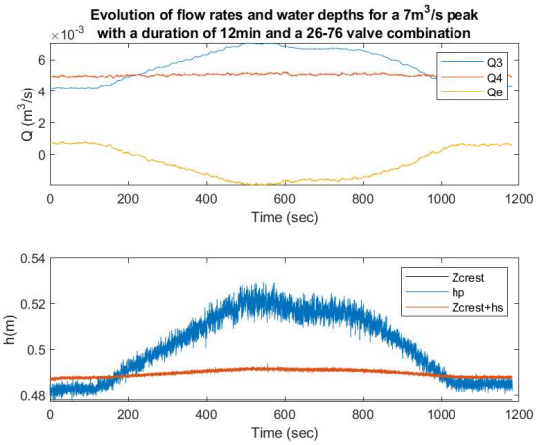
Evolution of flow rates and water depths for a 7m3/s peak with a duration of 12min and a 26-76 valve combination
Q (m3/s)
Q3
Q4
Qe
Time (sec)
h(m)
Zcrest
hp
Zcrest+hs
Time (sec)

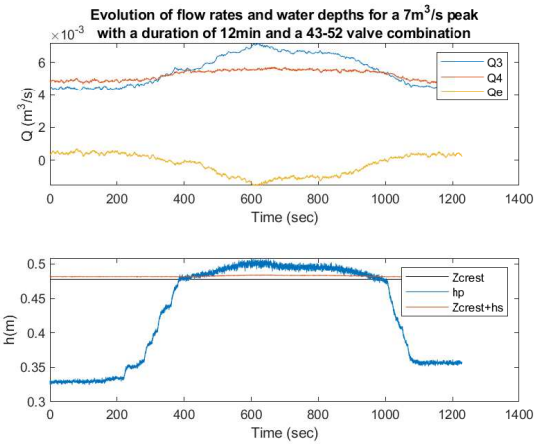
Evolution of flow rates and water depths for a 7m3/s peak with a duration of 12min and a 43-52 valve combination
Q (m3/s)
Q3
Q4
Qe
Time (sec)
h(m)
Zcrest
hp
Zcrest+hs
Time (sec)

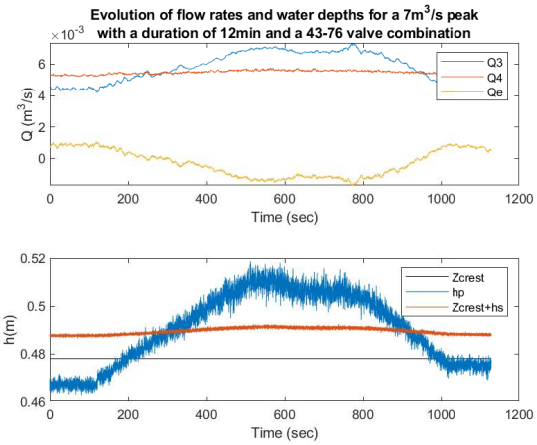
Evolution of flow rates and water depths for a 7m3/s peak with a duration of 12min and a 43-76 valve combination
Q (m3/s)
Q3
Q4
Qe
Time (sec)
h(m)
Zcrest
hp
Zcrest+hs
Time (sec)

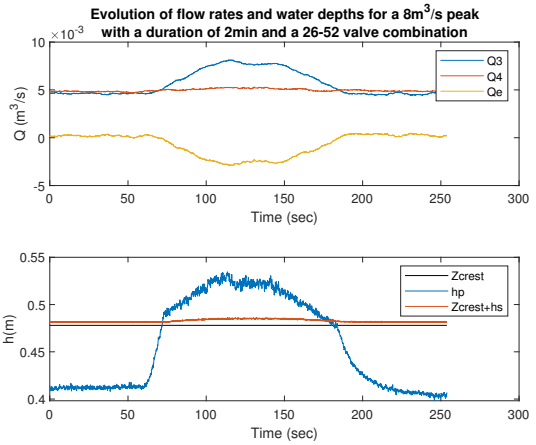
Evolution of flow rates and water depths for a 8m3/s peak with a duration of 2min and a 26-52 valve combination
Q (m3/s)
Q3
Q4
Qe
Time (sec)
h(m)
Zcrest
hp
Zcrest+hs
Time (sec)

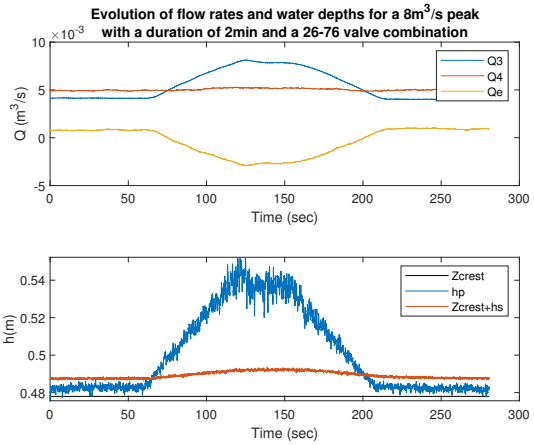
Evolution of flow rates and water depths for a 8m3/s peak with a duration of 2min and a 26-76 valve combination
Q (m3/s)
Q3
Q4
Qe
Time (sec)
h(m)
Zcrest
hp
Zcrest+hs
Time (sec)

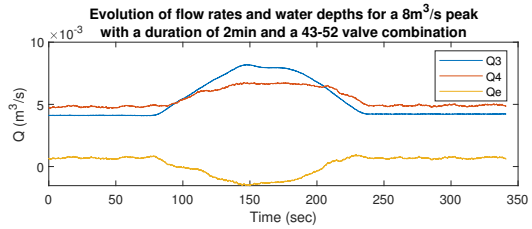
Evolution of flow rates and water depths for a 8m3/s peak with a duration of 2min and a 43-52 valve combination
Q (m3/s)
Q3
Q4
Qe
Time (sec)

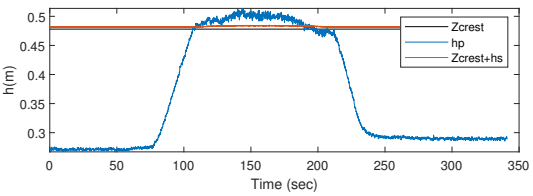
h(m)
Zcrest
hp
Zcrest+hs
Time (sec)

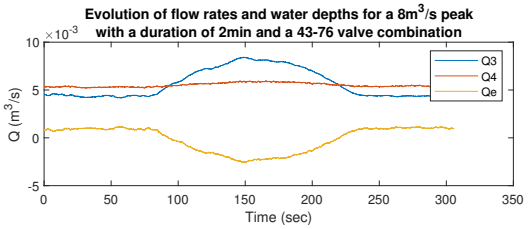
Evolution of flow rates and water depths for a 8m3/s peak with a duration of 2min and a 43-76 valve combination
Q (m3/s)
Q3
Q4
Qe
Time (sec)

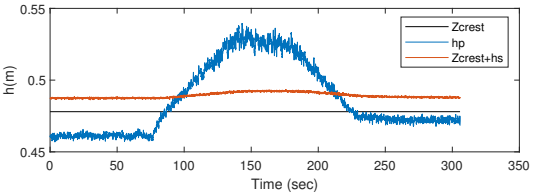
h(m)
Zcrest
hp
Zcrest+hs
Time (sec)

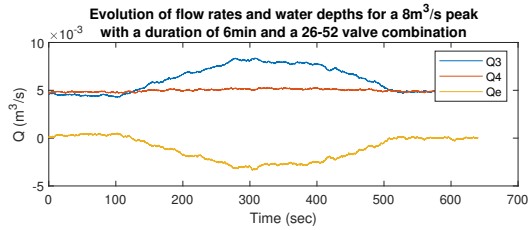
Evolution of flow rates and water depths for a 8m3/s peak with a duration of 6min and a 26-52 valve combination
Q (m3/s)
Q3
Q4
Qe
Time (sec)

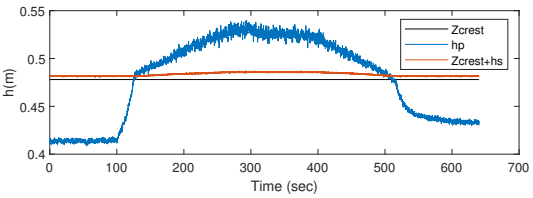
h(m)
Zcrest
hp
Zcrest+hs
Time (sec)

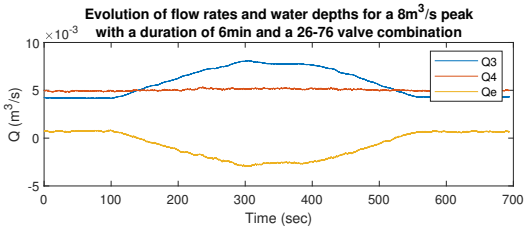
Evolution of flow rates and water depths for a 8m3/s peak with a duration of 6min and a 26-76 valve combination
Q (m3/s)
Q3
Q4
Qe
Time (sec)

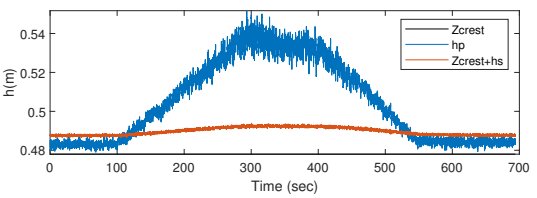
h(m)
Zcrest
hp
Zcrest+hs
Time (sec)

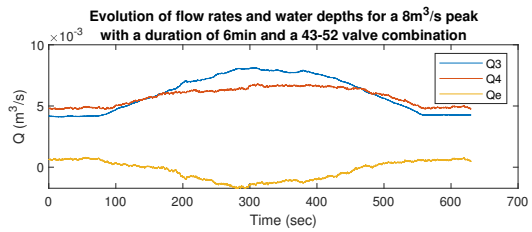
Evolution of flow rates and water depths for a 8m3/s peak with a duration of 6min and a 43-52 valve combination
Q (m3/s)
Q3
Q4
Qe
Time (sec)

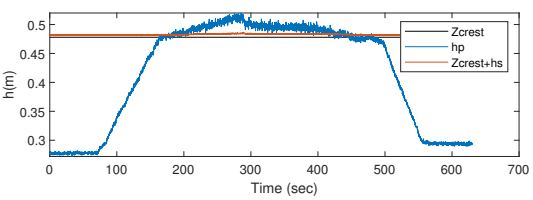
h(m)
Zcrest
hp
Zcrest+hs
Time (sec)

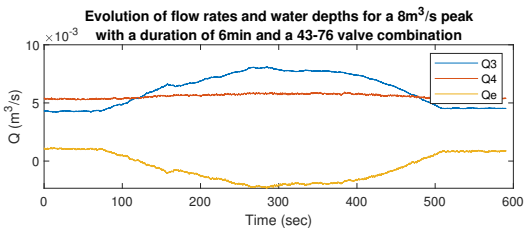
Evolution of flow rates and water depths for a 8m3/s peak with a duration of 6min and a 43-76 valve combination
Q (m3/s)
Q3
Q4
Qe
Time (sec)

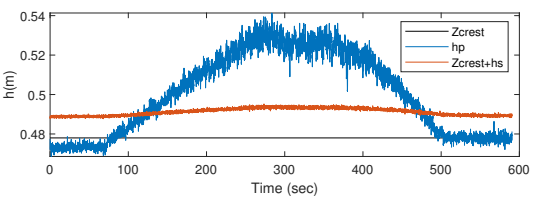
h(m)
Zcrest
hp
Zcrest+hs
Time (sec)

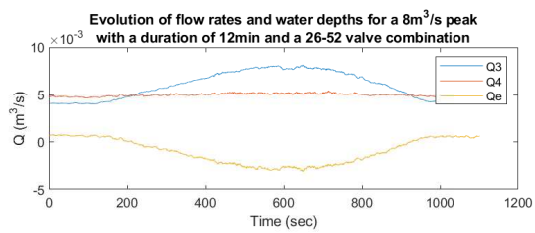
Evolution of flow rates and water depths for a 8m3/s peak with a duration of 12min and a 26-52 valve combination
Q (m3/s)
Q3
Q4
Qe
Time (sec)

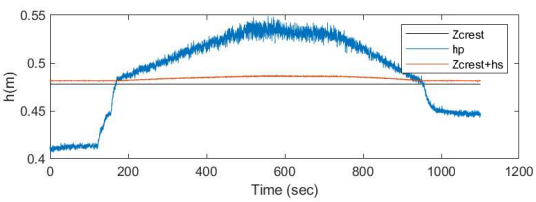
h(m)
Zcrest
hp
Zcrest+hs
Time (sec)

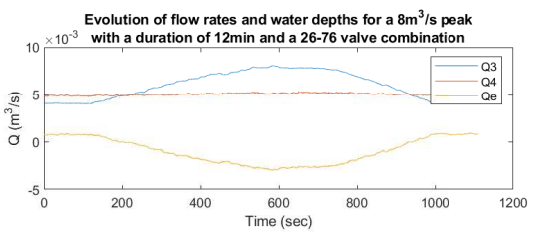
Evolution of flow rates and water depths for a 8m3/s peak with a duration of 12min and a 26-76 valve combination
Q (m3/s)
Q3
Q4
Qe
Time (sec)

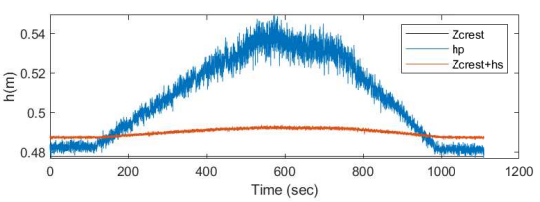
h(m)
Zcrest
hp
Zcrest+hs
Time (sec)

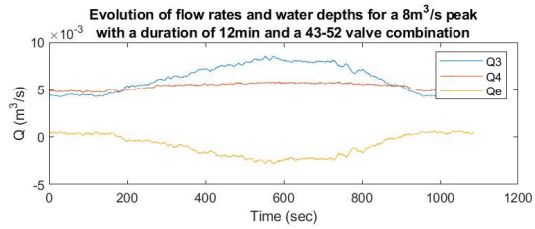
Evolution of flow rates and water depths for a 8m3/s peak with a duration of 12min and a 43-52 valve combination
Q (m3/s)
Time (sec)
Q3
Q4
Qe

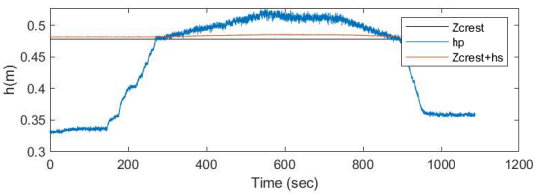
h(m)
Time (sec)
Zcrest
hp
Zcrest+hs

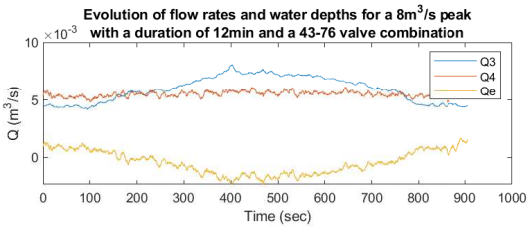
Evolution of flow rates and water depths for a 8m3/s peak with a duration of 12min and a 43-76 valve combination
Q (m3/s)
Time (sec)
Q3
Q4
Qe

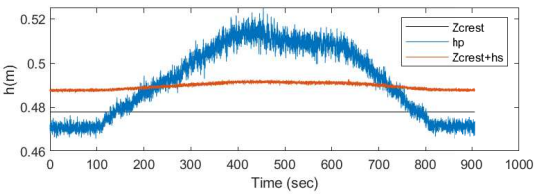
h(m)
Time (sec)
Zcrest
hp
Zcrest+hs

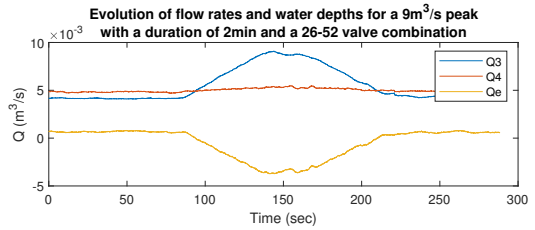
Evolution of flow rates and water depths for a 9m3/s peak with a duration of 2min and a 26-52 valve combination
Q (m3/s)
Time (sec)
Q3
Q4
Qe

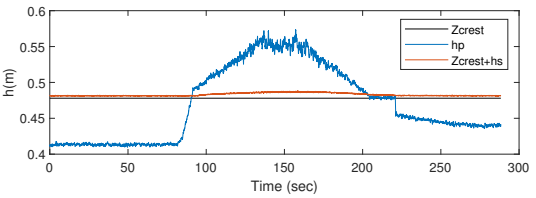
h(m)
Time (sec)
Zcrest
hp
Zcrest+hs

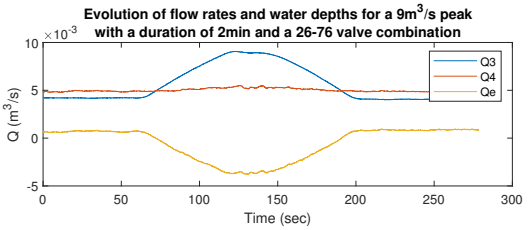
Evolution of flow rates and water depths for a 9m3/s peak with a duration of 2min and a 26-76 valve combination
Q (m3/s)
Time (sec)
Q3
Q4
Qe

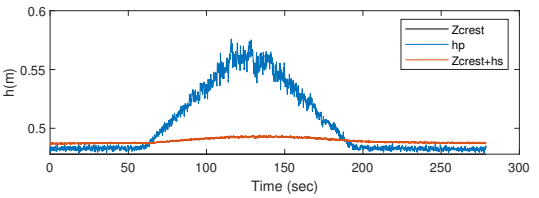
h(m)
Time (sec)
Zcrest
hp
Zcrest+hs

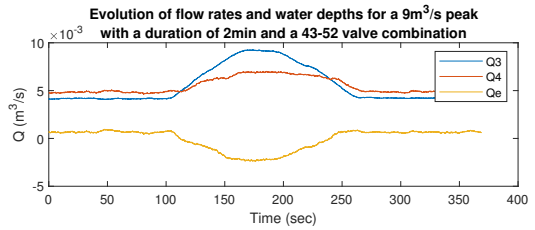
Evolution of flow rates and water depths for a 9m3/s peak with a duration of 2min and a 43-52 valve combination
Q (m3/s)
Time (sec)
Q3
Q4
Qe

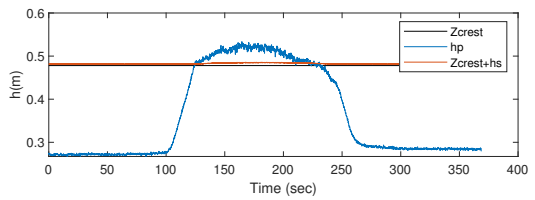
h(m)
Time (sec)
Zcrest
hp
Zcrest+hs

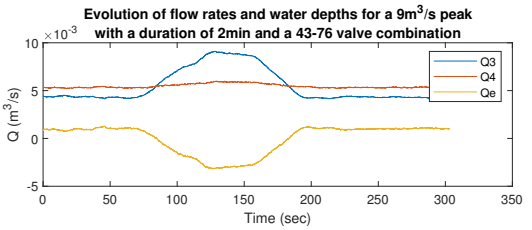
Evolution of flow rates and water depths for a 9m3/s peak with a duration of 2min and a 43-76 valve combination
Q (m3/s)
Time (sec)
Q3
Q4
Qe

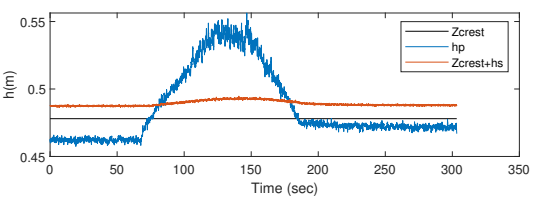
h(m)
Time (sec)
Zcrest
hp
Zcrest+hs

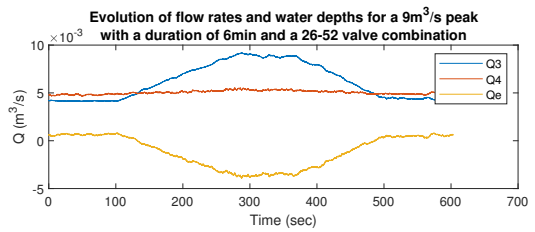
Evolution of flow rates and water depths for a 9m3/s peak with a duration of 6min and a 26-52 valve combination
Q (m3/s)
Time (sec)
Q3
Q4
Qe

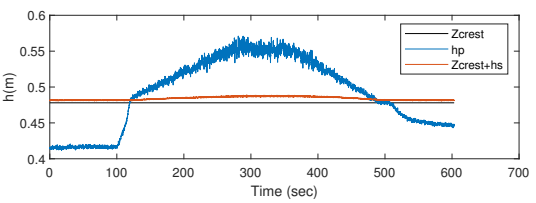
h(m)
Time (sec)
Zcrest
hp
Zcrest+hs

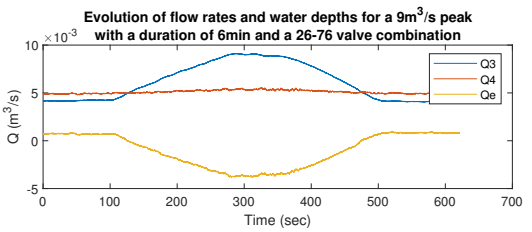
Evolution of flow rates and water depths for a 9m3/s peak with a duration of 6min and a 26-76 valve combination
Q (m3/s)
Time (sec)
Q3
Q4
Qe

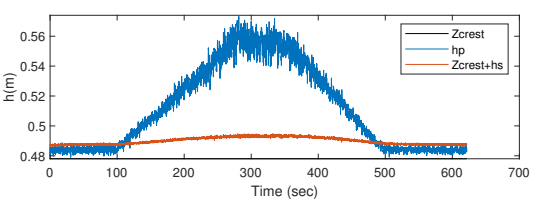
h(m)
Time (sec)
Zcrest
hp
Zcrest+hs

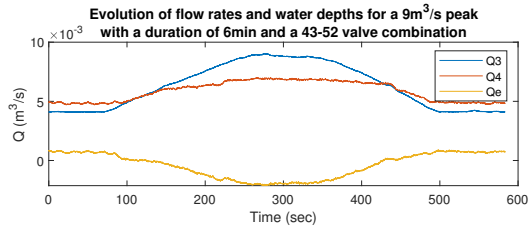
Evolution of flow rates and water depths for a 9m3/s peak with a duration of 6min and a 43-52 valve combination
Q (m3/s)
Time (sec)
Q3
Q4
Qe

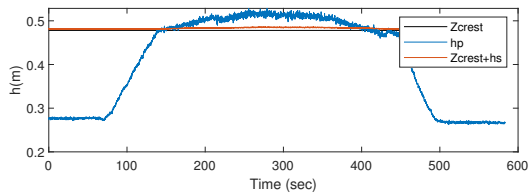
h(m)
Time (sec)
Zcrest
hp
Zcrest+hs

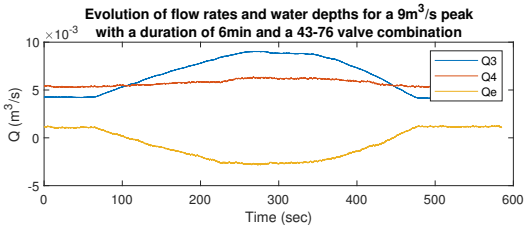
Evolution of flow rates and water depths for a 9m3/s peak with a duration of 6min and a 43-76 valve combination
Q (m3/s)
Time (sec)
Q3
Q4
Qe

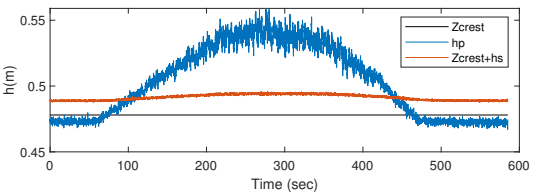
h(m)
Time (sec)
Zcrest
hp
Zcrest+hs

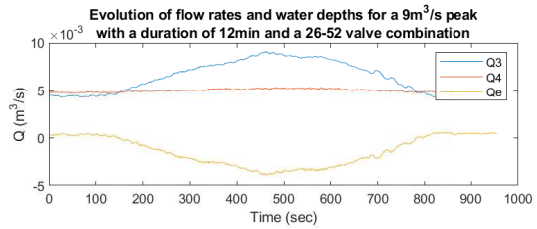
Evolution of flow rates and water depths for a 9m3/s peak with a duration of 12min and a 26-52 valve combination
Q (m3/s)
Time (sec)
Q3
Q4
Qe

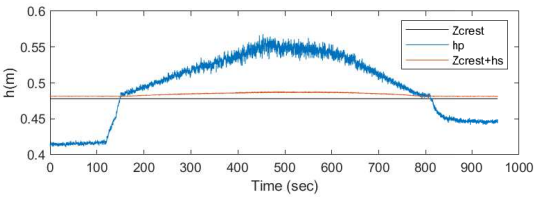
h(m)
Time (sec)
Zcrest
hp
Zcrest+hs

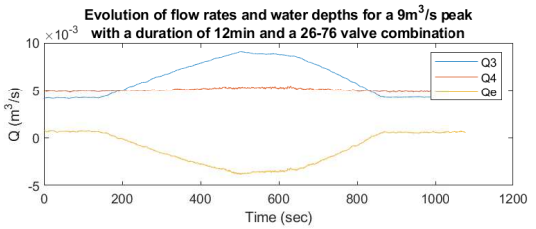
Evolution of flow rates and water depths for a 9m3/s peak with a duration of 12min and a 26-76 valve combination
Q (m3/s)
Time (sec)
Q3
Q4
Qe

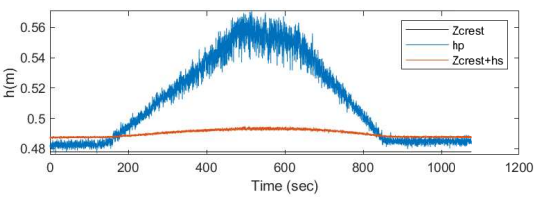
h(m)
Time (sec)
Zcrest
hp
Zcrest+hs

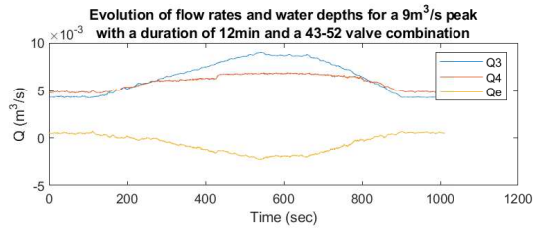
Evolution of flow rates and water depths for a 9m3/s peak with a duration of 12min and a 43-52 valve combination
Q (m3/s)
Time (sec)
Q3
Q4
Qe

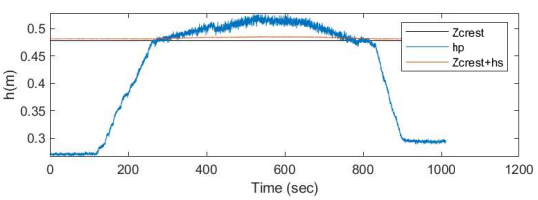
h(m)
Time (sec)
Zcrest
hp
Zcrest+hs

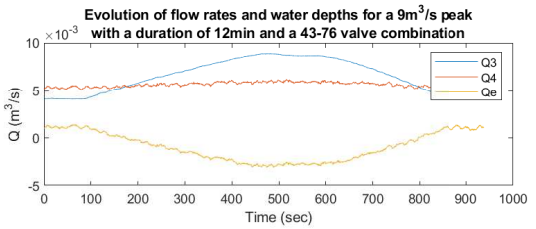
Evolution of flow rates and water depths for a 9m3/s peak with a duration of 12min and a 43-76 valve combination
Q (m3/s)
Time (sec)
Q3
Q4
Qe

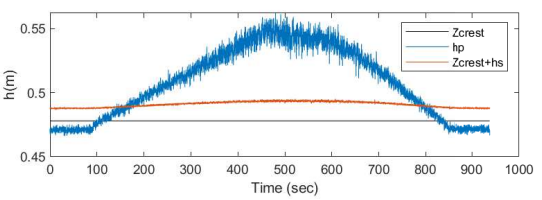
h(m)
Time (sec)
Zcrest
hp
Zcrest+hs

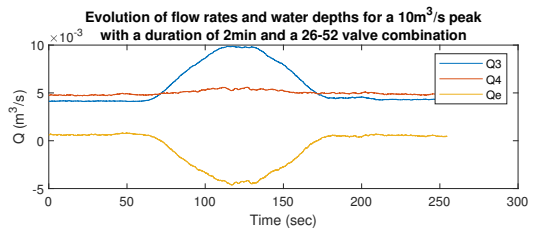
Evolution of flow rates and water depths for a 10m3/s peak with a duration of 2min and a 26-52 valve combination
Q (m3/s)
Time (sec)
Q3
Q4
Qe

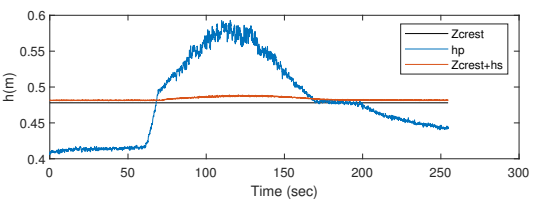
h(m)
Time (sec)
Zcrest
hp
Zcrest+hs

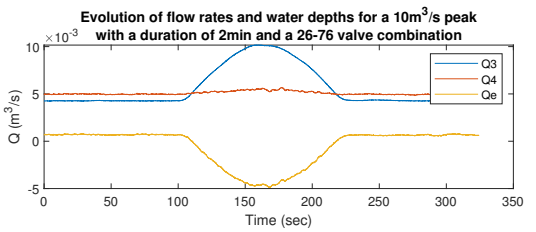
Evolution of flow rates and water depths for a 10m3/s peak with a duration of 2min and a 26-76 valve combination
Q (m3/s)
Time (sec)
Q3
Q4
Qe

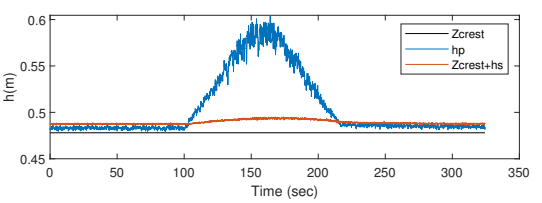
h(m)
Time (sec)
Zcrest
hp
Zcrest+hs

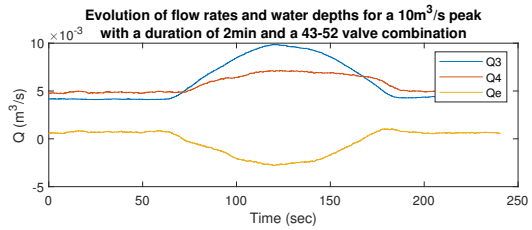
Evolution of flow rates and water depths for a 10m3/s peak with a duration of 2min and a 43-52 valve combination
Q (m3/s)
Time (sec)
Q3
Q4
Qe

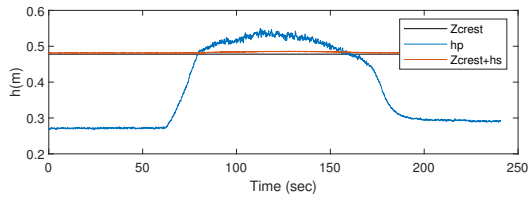
h(m)
Time (sec)
Zcrest
hp
Zcrest+hs

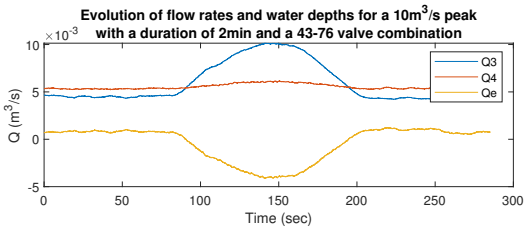
Evolution of flow rates and water depths for a 10m3/s peak with a duration of 2min and a 43-76 valve combination
Q (m3/s)
Time (sec)
Q3
Q4
Qe

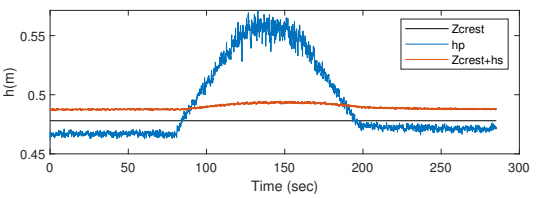
h(m)
Time (sec)
Zcrest
hp
Zcrest+hs

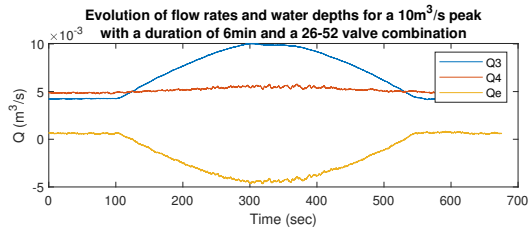
Evolution of flow rates and water depths for a 10m3/s peak with a duration of 6min and a 26-52 valve combination
Q (m3/s)
Time (sec)
Q3
Q4
Qe

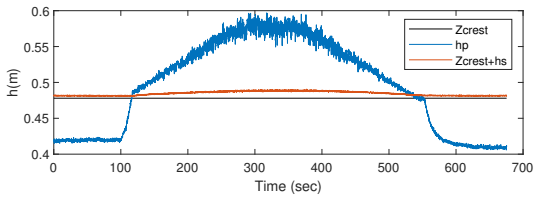
h(m)
Time (sec)
Zcrest
hp
Zcrest+hs

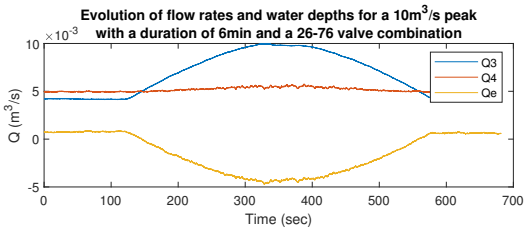
Evolution of flow rates and water depths for a 10m3/s peak with a duration of 6min and a 26-76 valve combination
Q (m3/s)
Time (sec)
Q3
Q4
Qe

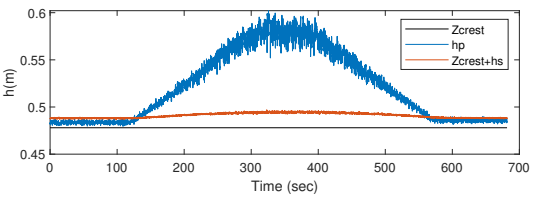
h(m)
Time (sec)
Zcrest
hp
Zcrest+hs

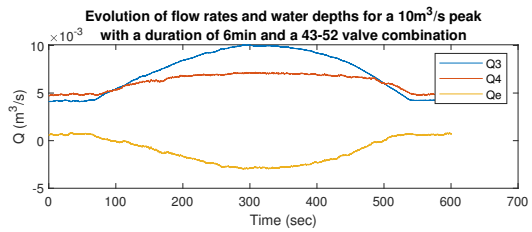
Evolution of flow rates and water depths for a 10m3/s peak with a duration of 6min and a 43-52 valve combination
Q (m3/s)
Time (sec)
Q3
Q4
Qe

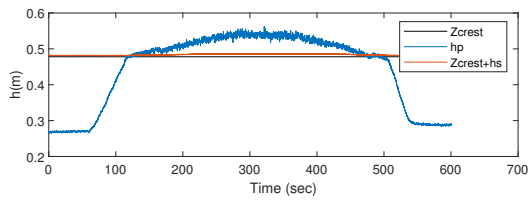
h(m)
Time (sec)
Zcrest
hp
Zcrest+hs

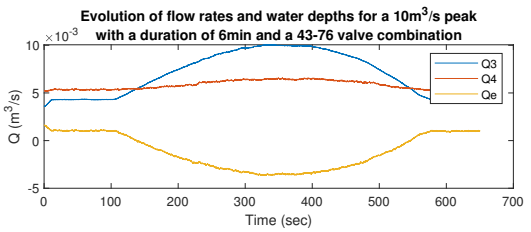
Evolution of flow rates and water depths for a 10m3/s peak with a duration of 6min and a 43-76 valve combination
Q (m3/s)
Time (sec)
Q3
Q4
Qe

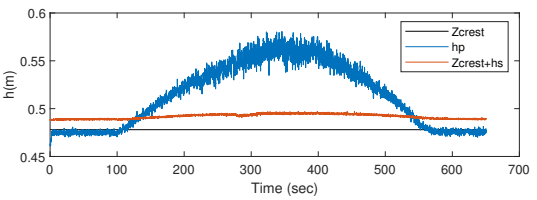
h(m)
Time (sec)
Zcrest
hp
Zcrest+hs

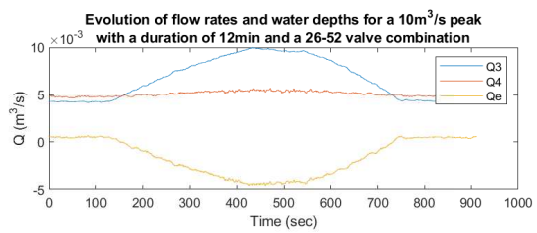
Evolution of flow rates and water depths for a 10m3/s peak with a duration of 12min and a 26-52 valve combination
Q (m3/s)
Time (sec)
Q3
Q4
Qe

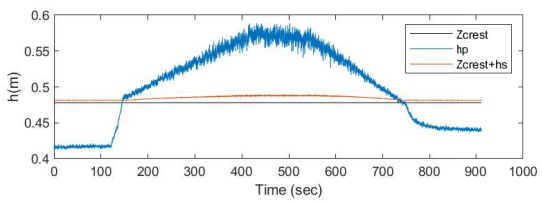
h(m)
Time (sec)
Zcrest
hp
Zcrest+hs

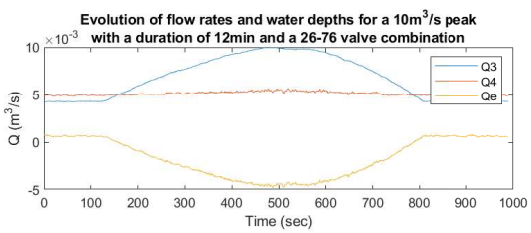
Evolution of flow rates and water depths for a 10m3/s peak with a duration of 12min and a 26-76 valve combination
Q (m3/s)
Time (sec)
Q3
Q4
Qe

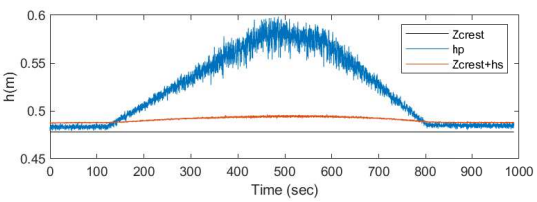
h(m)
Time (sec)
Zcrest
hp
Zcrest+hs

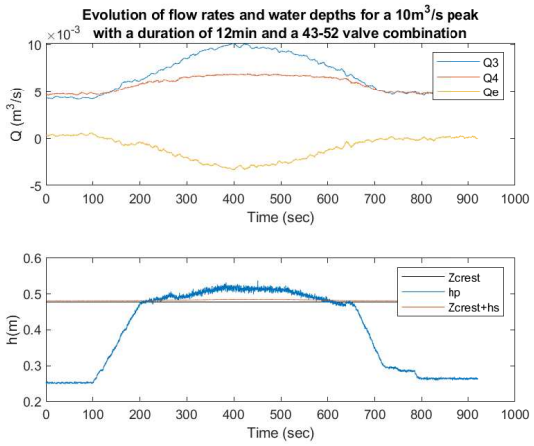
Evolution of flow rates and water depths for a 10m3/s peak
with a duration of 12min and a 43-52 valve combination
×10-3
Q (m3/s)
Q3
Q4
Qe
Time (sec)
h(m)
Zcrest
hp
Zcrest+hs
Time (sec)

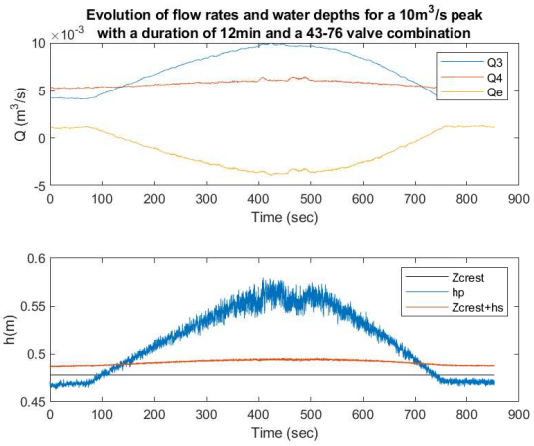
Evolution of flow rates and water depths for a 10m3/s peak
with a duration of 12min and a 43-76 valve combination
×10-3
Q (m3/s)
Q3
Q4
Qe
Time (sec)
h(m)
Zcrest
hp
Zcrest+hs
Time (sec)

B Appendix : Numerical simulations

B.1 Steady state simulations

B.1.1 Matlab code

```
%Author : Fantine Fontaine
%Date : May–June 2019
%Subject : Calculation of surface uniform depth that will be implemented in
%the calculation of exchange sewer–surface flow rate in steady state
%conditions

close all;
clear all;
clc

%% Data

Test = [01 02 03 04 05 ...
    21 22 23 24 25 ...
    31 32 33 34 35 ...
    41 42 43 44 45 ...
    51 52 53 54 55 ...
    61 62 63 64 65 ...
    71 72 73 74 ...
    81 82 83 84 85 ...
    91 92 93 94 95 ...
    101 102 103 104 105];
Ci = [0.5819 0.5819 0.5819 0.5819 0.5819 ...
    0.1323 0.1323 0.1323 0.1323 0.1323 ...
    0.177 0.177 0.177 0.177 0.177 ...
    0.2178 0.2178 0.2178 0.2178 0.2178 ...
    0.1 0.1 0.1747 0.1747 0.1747 ...
    0.1759 0.1759 0.1759 0.1759 0.1759 ...
    0.0222 0.0222 0.0222 0.0222 ...
    0.016 0.1189 0.1189 0.1189 0.1189 ...
    0.1292 0.1292 0.1292 0.1292 0.1292 ...
    0.026 0.026 0.026 0.026 0.026]; %fitted from experimental data
Ci2 = [0.48 0.475 0.47 0.47 0.45 ...
    0.0043 0.0193 0.0294 0.0355 0.0387 ...
    0.056 0.066 0.073 0.078 0.081 ...
    0.136 0.141 0.147 0.148 0.15 ...
    0.206 0.043 0.0027 0.01145 0.01665 ...
    0.015 0.032 0.043 0.049 0.053 ...
    0.1 0.09 0.085 0.083 ...
    0.016 0.0001 0.005 0.013 0.019 ...
```

```
    0.017 0.032 0.042 0.047 0.043 ...
    0.118 0.108 0.102 0.099 0.097]; %calibrated so that Qe(hexp) correspond
hp = [0.4 0.4 0.4 0.4 0.4 ...
    0.514 0.526 0.536 0.544 0.549 ...
    0.532 0.544 0.555 0.562 0.569 ...
    0.555 0.568 0.578 0.587 0.594 ...
    0.520 0.531 0.538 0.544 0.549 ...
    0.526 0.535 0.543 0.550 0.555 ...
    0.538 0.551 0.562 0.569 ...
    0.478 0.524 0.531 0.537 0.542 ...
    0.519 0.531 0.541 0.548 0.550 ...
    0.529 0.540 0.548 0.554 0.558]; %m head in the manhole
Qin = [0.00693 0.00831 0.00942 0.01021 0.01078 ...
    0 0 0 0 0 ...
    0 0 0 0 0 ...
    0 0 0 0 0 ...
    0.00699 0.00699 0.00697 0.00699 0.00698 ...
    0.0069 0.0069 0.0069 0.00692 0.00694 ...
    0.00697 0.00696 0.00697 0.00695 ...
    0.00109 0.00107 0.00106 0.00103 0.00102 ...
    0.00103 0.00099 0.00098 0.00097 0.00097 ...
    0.00085 0.00085 0.00085 0.00086 0.00086]; %m^3/s flow rate from the sur

g = 9.81;
L = 4; %m
K = 1/0.009; %Manning
s = 1/1000; %slope
Dm = 0.24; %m manhole diameter
Am = 0.0452; %m^2 manhole area
Zcrest = 0.478; %m

%% Calculation of Qe(hu,Ci1) and Qe(hu,Ci2)

hu = zeros(1,length(Qin));
Qexch = zeros(1,length(Qin)); %Qe(hu,Ci1)
Qexch2 = zeros(1,length(Qin)); %Qe(hu,Ci2)
SC = zeros(1,length(Qin)); %scenario

for i = 1:length(Qin)
    syms x
    eq = x^5/(2*x+L)^2 == Qin(i)^3/(L^5*K^3*s^(3/2)); %Manning equation for
    solx = solve(eq,x);
    h = vpa(solx);
    hu(i) = double(h(5,1));


    if hp(i) < (Zcrest+hu(i))
        if hp(i) < Zcrest %free weir eq
            Qexch(i) = -2/3*Ci(i)*pi*Dm*sqrt(2*g*hu(i)^3);
            SC(i) = 1;
```

```
            Qexch2(i) = -2/3*Ci2(i)*pi*Dm*sqrt(2*g*hu(i)^3);
        else
            if hu(i) < (Am/(pi*Dm)) %Submerge weir eq
                Qexch(i) = -Ci(i)*pi*Dm*hu(i)*sqrt(2*g*(Zcrest+hu(i)-hp(i))
                SC(i) = 2;
                Qexch2(i) = -Ci2(i)*pi*Dm*hu(i)*sqrt(2*g*(Zcrest+hu(i)-hp(i
            else   %Submerge orifice eq
                Qexch(i) = -Ci(i)*Am*sqrt(2*g*(Zcrest+hu(i)-hp(i)));
                SC(i) = 2;
                Qexch2(i) = -Ci2(i)*Am*sqrt(2*g*(Zcrest+hu(i)-hp(i)));
            end
        end
    else   %Orifice eq
        Qexch(i) = Ci(i)*Am*sqrt(2*g*(-hu(i)-Zcrest+hp(i)));
        if Qin(i) == 0
            SC(i) = 4;
        else
            SC(i) = 3;
        end
        Qexch2(i) = Ci2(i)*Am*sqrt(2*g*(-hu(i)-Zcrest+hp(i)));
    end

end

%% Experimental results

Qexp = [-0.00113 -0.00132 -0.00147 -0.00158 -0.00159 ...
    0.00016 0.00082 0.00137 0.00176 0.002 ...
    0.00253 0.00344 0.00412 0.00458 0.00492 ...
    0.00753 0.00855 0.00931 0.00982 0.01020 ...
    -0.00079 -0.00018 0.00012 0.00054 0.00081 ...
    0.00057 0.00136 0.00194 0.00233 0.00265 ...
    0.00447 0.00459 0.00469 0.00474 ...
    -0.00006 0.00001 0.00024 0.00061 0.00091 ...
    0.00065 0.00139 0.00199 0.00234 0.00219 ...
    0.00518 0.00530 0.00539 0.00546 0.00550]; %m^3/s calculated from Q4-Q3

hexp = [0.00937 0.01039 0.01107 0.01148 0.01176...
    0.00107 0.00393 0.00501 0.00544 0.00579 ...
    0.0071 0.00828 0.00919 0.00972 0.01018 ...
    0.0132 0.01408 0.0146 0.01511 0.01549 ...
    0 0 0.011 0.01168 0.01211 ...
    0.01186 0.01325 0.0142 0.01476 0.01512 ...
    0.01667 0.01784 0.01868 0.01922 ...
    0 0.00389 0.00425 0.00497 0.00555 ...
    0.005516 0.00664 0.00766 0.00827 0.00785 ...
    0.008 0.00989 0.01053 0.011 0.01126]; %m experimental water depth upstre

Qexpcalc = [-0.001177125 -0.001374153 -0.001512344 -0.001595474 -0.00165626
    0.004971209 0.005580509 0.00614015 0.006534964 0.006804972 ...
```

```
    0.007682332 0.008589511 0.009269038 0.009714252 0.01008453 ...
    0.011052908 0.012047065 0.012776975 0.013314646 0.013743425 ...
    0 0 0.007791729 0.00819435 0.008483335 ...
    0.006698514 0.007406279 0.00801855 0.008414443 0.008771539 ...
    0.000922954 0.001045186 0.00113367 0.001194384 ...
    0 0.004831373 0.005234015 0.005514396 0.005725632 ...
    0.004895728 0.005574519 0.006076175 0.006437365 0.006557971 ...
    0.001079952 0.001225762 0.001309645 0.001363813 0.001403171 ];%m^3/s ca

%% Wolf results

Qwolf = [0.00101013 0.001171375 0.001294176 0.001383845 0.001446002 ...
    -0.003967854 -0.005086775 -0.005793072 -0.006187892 -0.006507459 ...
    -0.007310261 -0.008247104 -0.009023021 -0.009484432 -0.009924885 ...
    -0.01106781 -0.012102952 -0.012915368 -0.013475407 -0.013880845 ...
    0 0 -0.006417841 -0.006923468 -0.00724297 ...
    -0.005315813 -0.006189337 -0.006965448 -0.007442622 -0.007820342 ...
    -0.000879422 -0.001019913 -0.001109645 -0.001192 ...
    0 -0.003952417 -0.004447472 -0.004788237 -0.005056151 ...
    -0.004002123 -0.004838897 -0.005447828 -0.005839894 -0.005947752 ...
    -0.001006729 -0.00115438 -0.00124331 -0.001306117 -0.001346395]; %m^3/s

Qwolf = -Qwolf;

hs_wolf = [0.008994833 0.009978163 0.010697395 0.011208902 0.011557345 ...
    0.003343079 0.003674127 0.00390133 0.004025677 0.004124915 ...
    0.004368762 0.004643977 0.004865774 0.004995148 0.005117031 ...
    0.005426786 0.005699279 0.005908467 0.006050574 0.006152369 ...
    0 0 0.019583046 0.020084195 0.020391559 ...
    0.01837429 0.019282615 0.020052249 0.020506211 0.020855077 ...
    0.012415078 0.012691477 0.012862504 0.012986728 ...
    0 0.009903864 0.010289767 0.010157596 0.009310492 ...
    0.009847922 0.009566658 0.005809943 0.00441442 0.004271971 ...
    0.005786256 0.006023507 0.006163203 0.006260403 0.006321948]; %m

%% Summary

ERR = (Qexch-Qexp)./Qexch*100;
ERR2 = (Qexch2-Qexp)./Qexch2*100;

Results = [Test' SC' hexp' hu' hs_wolf' Qexp' Qexpcalc' Qexch' Qexch2' Qwol

%% Plot : Experimental results

figure()
plot(1:5,Qexp(1:5),'bx');
hold on
plot(1:5,Qexpcalc(1:5),'cs');
hold off
legend('Qe (Q_{exp})','Qe (h_{exp},Ci)');
```

```
title('Scenario 1 - Experimental exchange flow rate');
ylabel('Q (m^3/s)');
xlabel('Tests');

figure()
plot(1:26,Qexp([23:34,36:end]),'bx');
hold on
plot(1:26,Qexpcalc([23:34,36:end]),'cs');
hold off
legend('Qe (Q_{exp})','Qe (h_{exp},Ci)');
title('Scenario 3 - Experimental exchange flow rate');
ylabel('Q (m^3/s)');
xlabel('Tests');

figure()
plot(1:15,Qexp(6:20),'bx');
hold on
plot(1:15,Qexpcalc(6:20),'cs');
hold off
legend('Qe (Q_{exp})','Qe (h_{exp},Ci)');
title('Scenario 4 - Experimental exchange flow rate');
ylabel('Q (m^3/s)');
xlabel('Tests');

%% Plot : Comparison with numerical models

figure()
plot(1:5,hexp(1:5),'bx');
hold on
plot(1:5,hu(1:5),'ro');
plot(1:5,hs_wolf(1:5),'g*');
hold off
legend('h_s (h_{exp})','h_s (h_u)','h_s (h_{wolf})');
title('Scenario 1 - Water depth');
ylabel('h (m)');
xlabel('Tests');

figure()
plot(1:5,Qexp(1:5),'bx');
hold on
plot(1:5,Qexpcalc(1:5),'cx');
plot(1:5,Qexch(1:5),'ro');
plot(1:5,Qexch2(1:5),'mo');
plot(1:5,Qwolf(1:5),'g*');
hold off
legend('Qe (Q_{exp})','Qe (h_{exp},Ci1)','Qe (h_u,Ci1)','Qe (h_u,Ci2)','Qe
title('Scenario 1 - Exchange flow rate');
ylabel('Q (m^3/s)');
xlabel('Tests');
```

```
figure()
plot(1:26,hexp([23:34,36:end]),'bx');
hold on
plot(1:26,hu([23:34,36:end]),'ro');
plot(1:26,hs_wolf([23:34,36:end]),'g*');
hold off
legend('h_s (h_{exp})','h_s (h_u)','h_s (h_{wolf})');
title('Scenario 3 - Water depth');
ylabel('Q (m^3/s)');
xlabel('Tests');

figure()
plot(1:26,Qexp([23:34,36:end]),'bx');
hold on
plot(1:26,Qexpcalc([23:34,36:end]),'cx');
plot(1:26,Qexch([23:34,36:end]),'ro');
plot(1:26,Qexch2([23:34,36:end]),'mo');
plot(1:26,Qwolf([23:34,36:end]),'g*');
hold off
legend('Qe (Q_{exp})','Qe (h_{exp},Ci1)','Qe (h_u,Ci1)','Qe (h_u,Ci2)','Qe
title('Scenario 3 - Exchange flow rate');
ylabel('Q (m^3/s)');
xlabel('Tests');

figure()
plot(1:15,hexp(6:20),'bx');
hold on
plot(1:15,hu(6:20),'ro');
plot(1:15,hs_wolf(6:20),'g*');
hold off
legend('h_s (h_{exp})','h_s (h_u)','h_s (h_{wolf})');
title('Scenario 4 - Water depth');
ylabel('h (m)');
xlabel('Tests');

figure()
plot(1:15,Qexp(6:20),'bx');
hold on
plot(1:15,Qexpcalc(6:20),'cx');
plot(1:15,Qexch(6:20),'ro');
plot(1:15,Qexch2(6:20),'mo');
plot(1:15,Qwolf(6:20),'g*');
hold off
legend('Qe (Q_{exp})','Qe (h_{exp},Ci1)','Qe (h_u,Ci1)','Qe (h_u,Ci2)','Qe
title('Scenario 4 - Exchange flow rate');
ylabel('Q (m^3/s)');
xlabel('Tests');

figure()
plot(1:length(Ci),Ci,'r+');
```

```
hold on
plot(1:length(Ci),Ci2,'mo');
hold off
title('Value of Ci');
legend('Ci1 : fitted','Ci2 : calibrated');
ylabel('Ci (-)');
xlabel('Tests');
```

B.1.2 Numerical results for Method 1

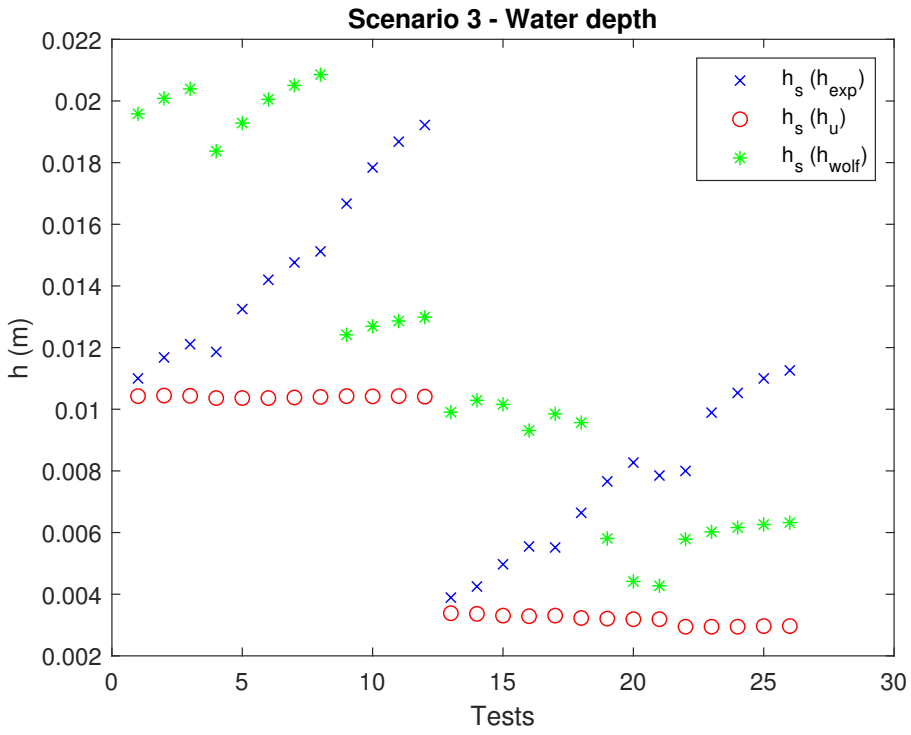

Figure B.1: Results of numerical simulations for Scenario 3 in term of water depth

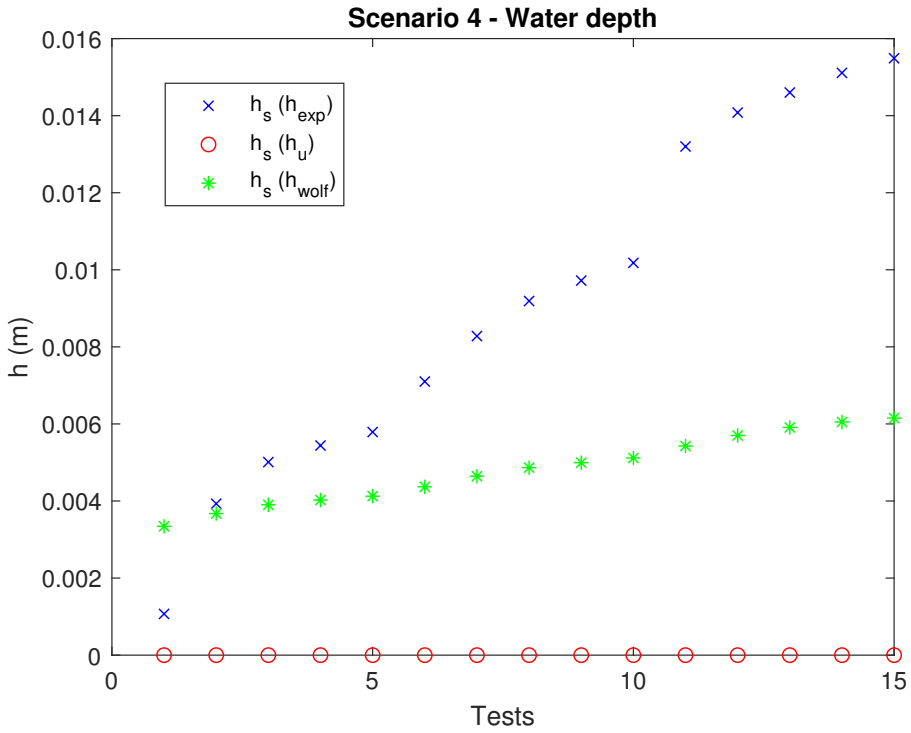

Figure B.2: Results of numerical simulations for Scenario 4 in term of water depth

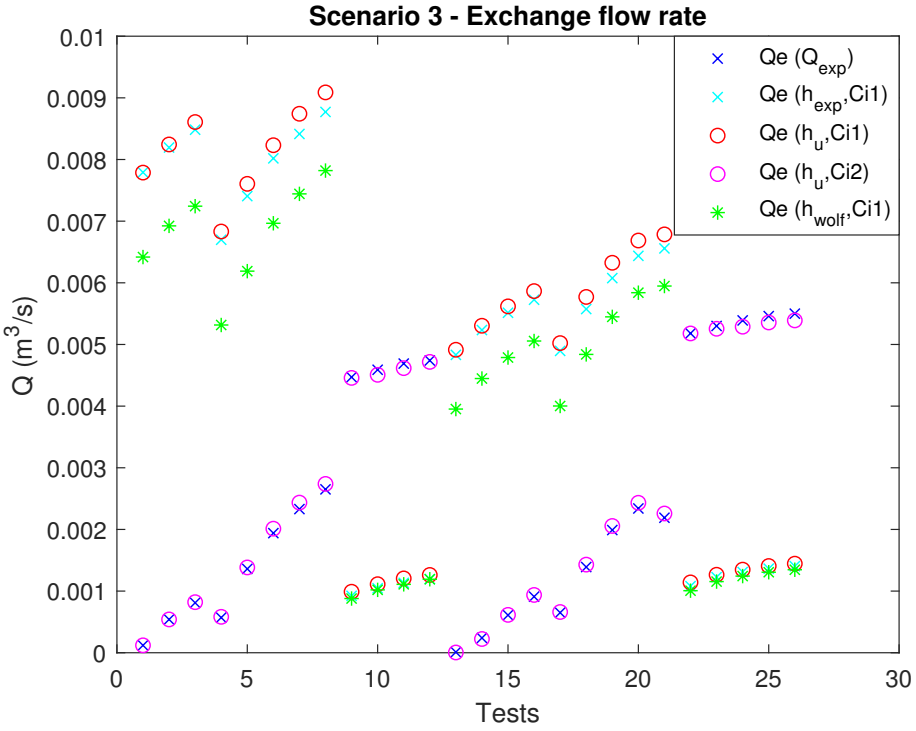

Figure B.3: Results of numerical simulations for Scenario 3 in term of exchange flow rate

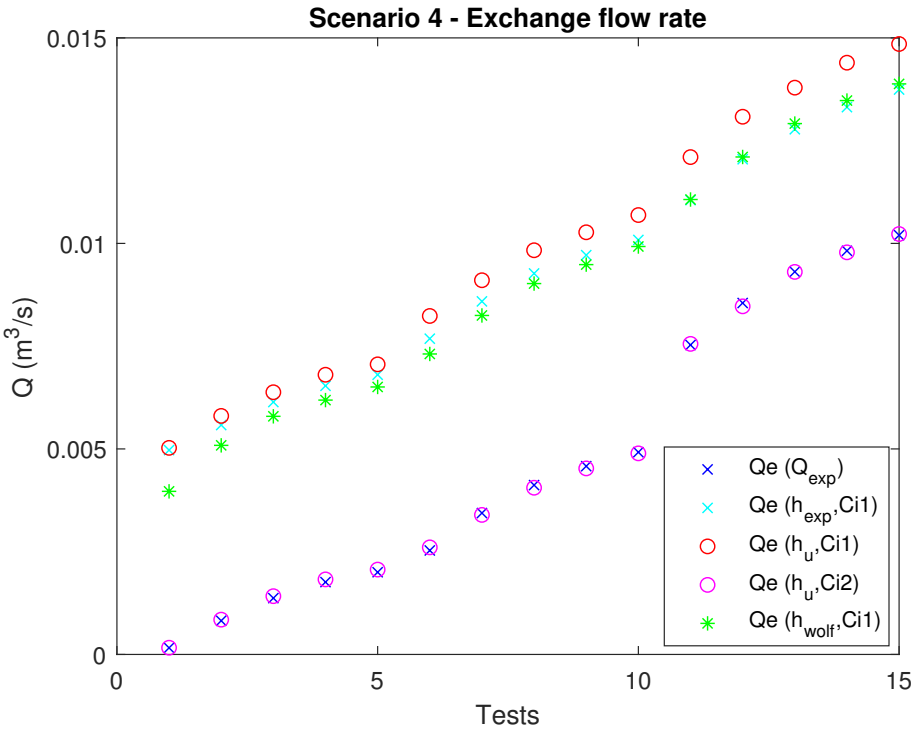

Figure B.4: Results of numerical simulations for Scenario 4 in term of exchange flow rate

B.2 Unsteady state simulations

B.2.1 Matlab code

```
%Author : Fantine Fontaine
%Date : May-June 2019
%Subject : Calculation of surface uniform depth that will be implemented in
%the calculation of exchange sewer-surface flow rate in unsteady state
%conditions

close all;
clear all;
clc

%% Experimental data

depths = xlsread('depths.xlsx','26-52'); %26-52 26-76 43-52 43-76 (4 excel
depths = depths/1000; %m
flowrates = xlsread('Flowrates.xlsx','26-52'); %26-52 26-76 43-52 43-76 (4
flowrates = flowrates/1000; %m^3/s

%% Parameters

Ci1 = 0.55; %0.5-0.6 scenario 1
Ci2 = 0.05; %0.02-0.05 scenario 2
Ci3 = 0.07; %0.06-0.16 scenario 3

%% Calculation of Qe(hu,Ci) and Qe(hexp,Ci)

for k = 1:12

    [Qexp,hs_exp,Qexch,Qexchcalc,hs,Time,Test,SC] = exchange(Ci1,Ci2,Ci3,k,

    ERRQ = (Qexch-Qexp)./Qexch*100;
    ERRh = (hs-hs_exp)./hs*100;

    PEAK = Test(4);
    DUR = Test(3);
    VALVE = Test(2);

    %% Plot

    figure(k)
    subplot(2,1,1);
    plot(Time,smooth(Qexch));
    hold on
    plot(Time,-Qexp);
    plot(Time,smooth(Qexchcalc));
    hold off
    legend('Qe (h_u,Ci)','Qe (Q_{exp})','Qe (h_{exp},Ci)');
```

```
    title(['Test = Peak : ',num2str(PEAK),'m^3/s - Duration : ',num2str(DUR
    ylabel('Q (m^3/s)');
    xlabel('Time (s)');
    subplot(2,1,2);
    plot(Time,hs);
    hold on
    plot(Time,smooth(hs_exp));
    hold off
    legend('hs (h_u)','hs (h_{exp})');
    title(['Test = Peak : ',num2str(PEAK),'m^3/s - Duration : ',num2str(DUR
    ylabel('h (m)');
    xlabel('Time (s)');

end


%Author : Fantine Fontaine
%Date : May-June 2019

function [Qexp,hs_exp,Qexch,Qexchcalc,hs,Time,Test,SC] = exchange(Ci1,Ci2,C

hp = depths(6:end,(2*k-1))';
hp(isnan(hp)) = []; %m

Qin = flowrates(2:end,(5*k-3))';
Qin(isnan(Qin)) = []; %m^3/s

hs_exp = depths(6:end,2*k)';
hs_exp(isnan(hs_exp)) = []; %m

Qexp = flowrates(2:end,(5*k))';
Qexp(Qexp == 0) = []; %m^3/s

Test = depths(1:4,(2*k-1))*1000;
Time = 0:0.05:length(Qin)*0.05-0.05; %s
Qexch = zeros(1,length(Qin)); %m^3/s
Qexchcalc = zeros(1,length(Qin)); %m^3/s
SC = zeros(1,length(Qin)); %scenarios

%% Parameters

g = 9.81;
L = 4; %m
K = 1/0.009; %Manning
s = 1/1000; %slope
Dm = 0.24; %m manhole diameter
Am = 0.0452; %m^2 manhole area
Zcrest = 0.478; %m

%% Calcuation of hu
%(the same during time because Q surface doesn't change)
```

```
syms x
eq = x^5/(2*x+L)^2 == mean(Qin)^3/(L^5*K^3*s^(3/2)); %Manning
solx = solve(eq,x);
hu = vpa(solx);
hu = double(hu(5,1));
hs = hu*ones(1,length(Qin));

%% Linking equations

for i = 1:length(Qin)

    disp(i/length(Qin)*100);

    % Linking equations for hu

    if hp(i) < (Zcrest+hs(i))
        if hp(i) < Zcrest %free weir eq
            Qexch(i) = -2/3*Ci1*pi*Dm*sqrt(2*g*hs(i)^3);
            SC(i) = 1;
        else
            if hs(i) < (Am/(pi*Dm))  %Submerge weir eq
                Qexch(i) = -Ci2*pi*Dm*hs(i)*sqrt(2*g*(Zcrest+hs(i)-hp(i)));
                SC(i) = 2;
            else  %Submerge orifice eq
                Qexch(i) = -Ci2*Am*sqrt(2*g*(Zcrest+hs(i)-hp(i)));
                SC(i) = 2;
            end
        end
    else  %Orifice eq
        Qexch(i) = Ci3*Am*sqrt(2*g*(-hs(i)-Zcrest+hp(i)));
        if Qin(i) == 0
            SC(i) = 4;
        else
            SC(i) = 3;
        end
    end

    % Linking equations for hexp

    if hp(i) < (Zcrest+hs_exp(i))
        if hp(i) < Zcrest   %free weir eq
            Qexchcalc(i) = -2/3*Ci1*pi*Dm*sqrt(2*g*hs_exp(i)^3);
        else
            if hs_exp(i) < (Am/(pi*Dm))   %Submerge weir eq
                Qexchcalc(i) = -Ci2*pi*Dm*hs_exp(i)*sqrt(2*g*(Zcrest+hs_exp
            else   %Submerge orifice eq
                Qexchcalc(i) = -Ci2*Am*sqrt(2*g*(Zcrest+hs_exp(i)-hp(i)));
            end
        end
```

```
    else    %Orifice eq
        Qexchcalc(i) = Ci3*Am*sqrt(2*g*(-hs_exp(i)-Zcrest+hp(i)));
    end

end

end
```

B.2.2 Numerical results

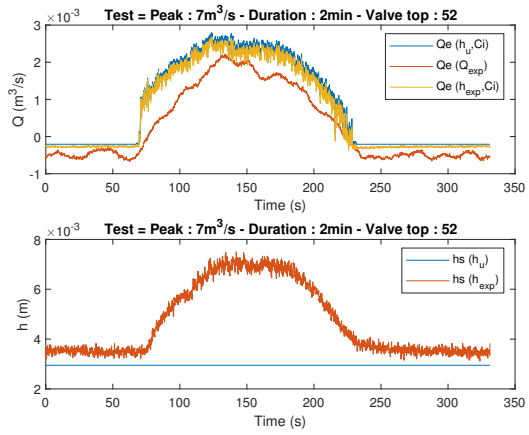

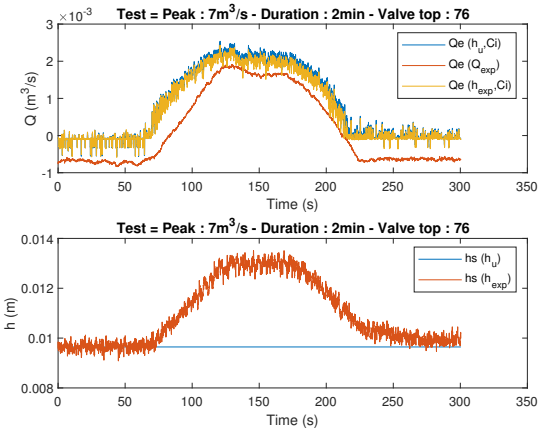

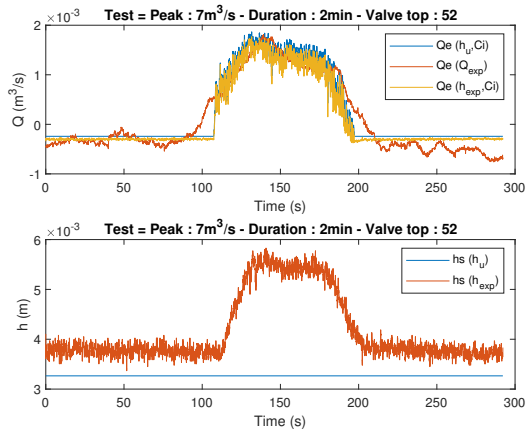

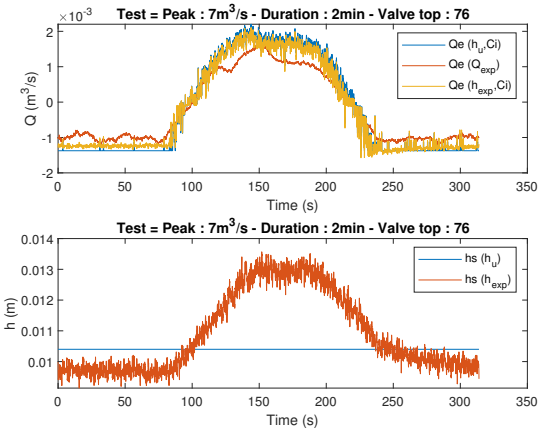

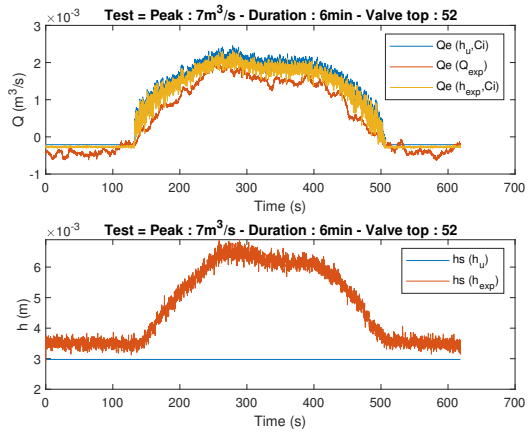

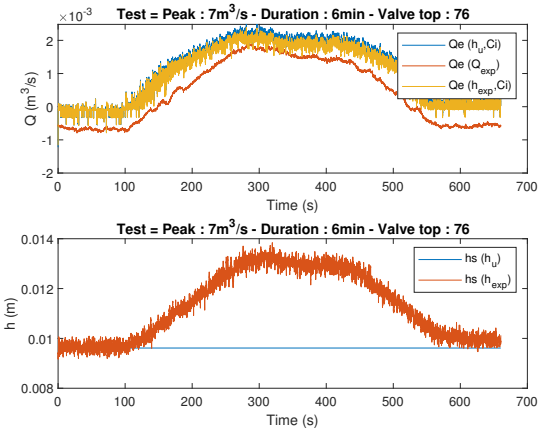

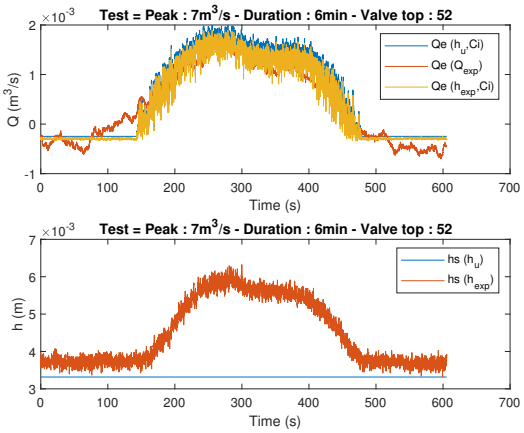
Test = Peak : 7m3/s - Duration : 6min - Valve top : 52
Qe (hu,Ci)
Qe (Qexp)
Qe (hexp,Ci)
Q (m3/s)
Time (s)
Test = Peak : 7m3/s - Duration : 6min - Valve top : 52
hs (hu)
hs (hexp)
h (m)
Time (s)

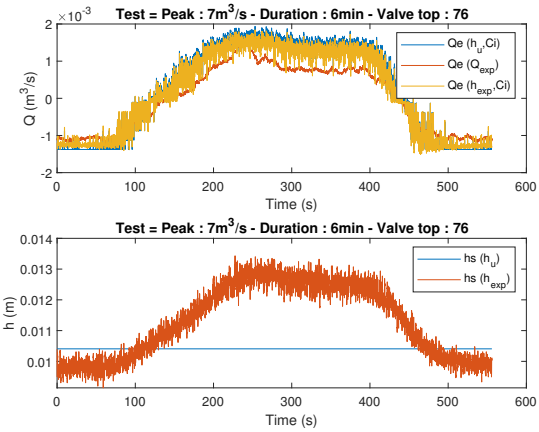
Test = Peak : 7m3/s - Duration : 6min - Valve top : 76
Qe (hu,Ci)
Qe (Qexp)
Qe (hexp,Ci)
Q (m3/s)
Time (s)
Test = Peak : 7m3/s - Duration : 6min - Valve top : 76
hs (hu)
hs (hexp)
h (m)
Time (s)

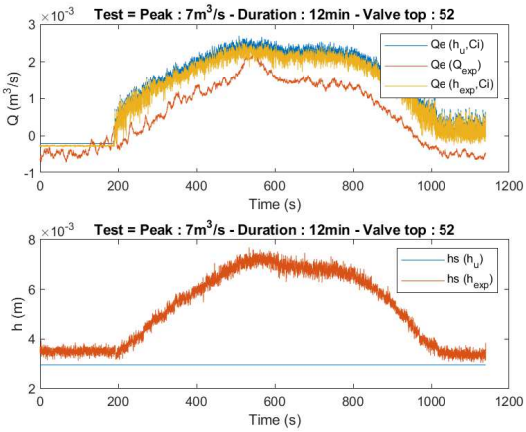
Test = Peak : 7m3/s - Duration : 12min - Valve top : 52
Qe (hu,Ci)
Qe (Qexp)
Qe (hexp,Ci)
Q (m3/s)
Time (s)
Test = Peak : 7m3/s - Duration : 12min - Valve top : 52
hs (hu)
hs (hexp)
h (m)
Time (s)

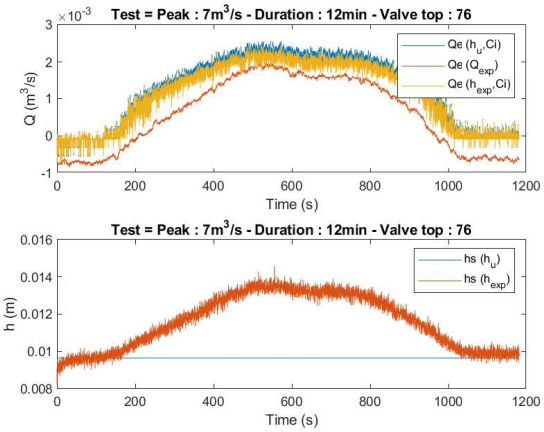
Test = Peak : 7m3/s - Duration : 12min - Valve top : 76
Qe (hu,Ci)
Qe (Qexp)
Qe (hexp,Ci)
Q (m3/s)
Time (s)
Test = Peak : 7m3/s - Duration : 12min - Valve top : 76
hs (hu)
hs (hexp)
h (m)
Time (s)

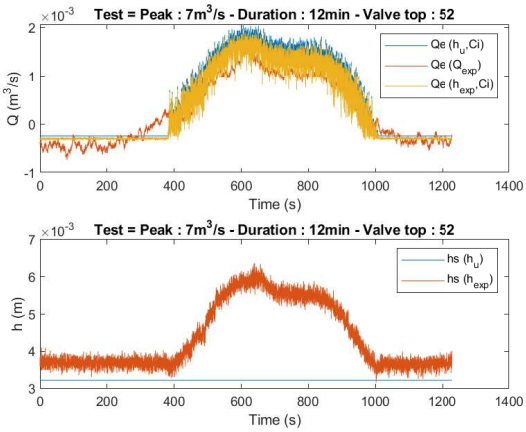
Test = Peak : 7m3/s - Duration : 12min - Valve top : 52
Qe (hu,Ci)
Qe (Qexp)
Qe (hexp,Ci)
Q (m3/s)
Time (s)
Test = Peak : 7m3/s - Duration : 12min - Valve top : 52
hs (hu)
hs (hexp)
h (m)
Time (s)

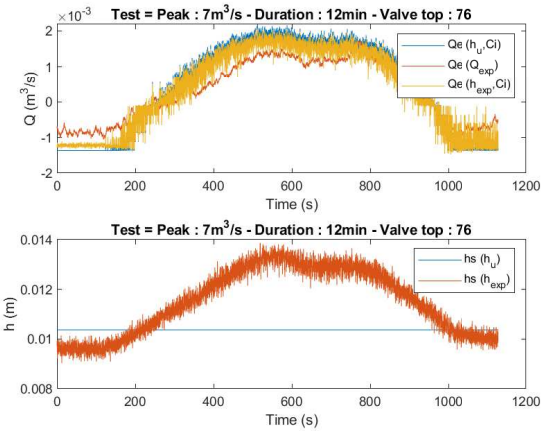
Test = Peak : 7m3/s - Duration : 12min - Valve top : 76
Qe (hu,Ci)
Qe (Qexp)
Qe (hexp,Ci)
Q (m3/s)
Time (s)
Test = Peak : 7m3/s - Duration : 12min - Valve top : 76
hs (hu)
hs (hexp)
h (m)
Time (s)

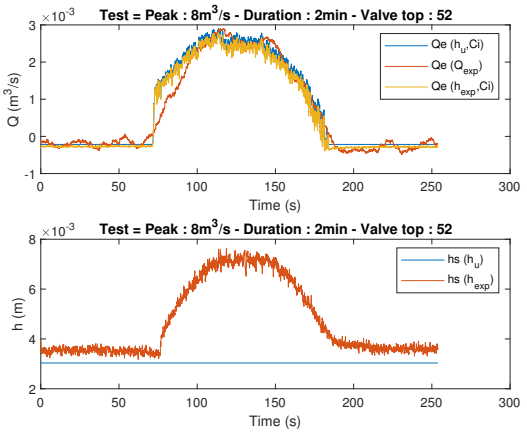
Test = Peak : 8m3/s - Duration : 2min - Valve top : 52
Qe (hu,Ci)
Qe (Qexp)
Qe (hexp,Ci)
Q (m3/s)
Time (s)
Test = Peak : 8m3/s - Duration : 2min - Valve top : 52
hs (hu)
hs (hexp)
h (m)
Time (s)

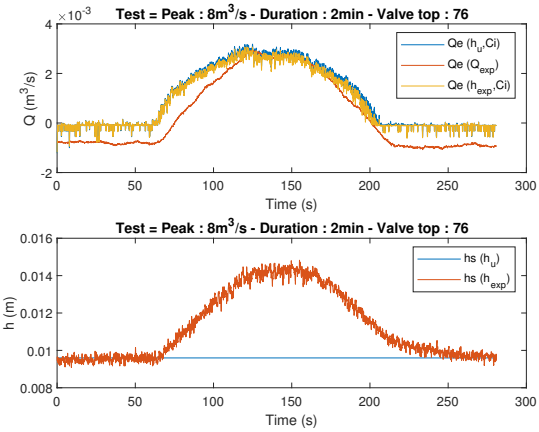
Test = Peak : 8m3/s - Duration : 2min - Valve top : 76
Qe (hu,Ci)
Qe (Qexp)
Qe (hexp,Ci)
Q (m3/s)
Time (s)
Test = Peak : 8m3/s - Duration : 2min - Valve top : 76
hs (hu)
hs (hexp)
h (m)
Time (s)

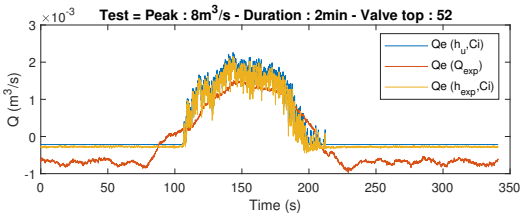
Test = Peak : 8m3/s - Duration : 2min - Valve top : 52
Qe (hu,Ci)
Qe (Qexp)
Qe (hexp,Ci)
Q (m3/s)
Time (s)

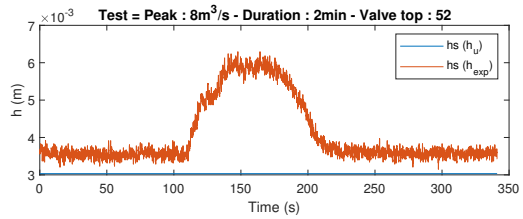
Test = Peak : 8m3/s - Duration : 2min - Valve top : 52
hs (hu)
hs (hexp)
h (m)
Time (s)

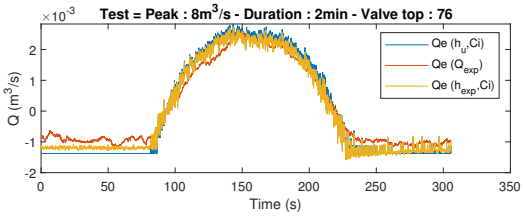
Test = Peak : 8m3/s - Duration : 2min - Valve top : 76
Qe (hu,Ci)
Qe (Qexp)
Qe (hexp,Ci)
Q (m3/s)
Time (s)

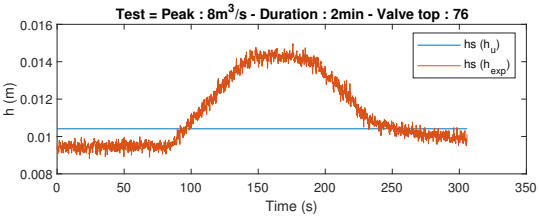
Test = Peak : 8m3/s - Duration : 2min - Valve top : 76
hs (hu)
hs (hexp)
h (m)
Time (s)

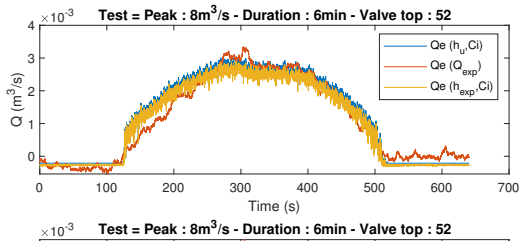
Test = Peak : 8m3/s - Duration : 6min - Valve top : 52
Qe (hu,Ci)
Qe (Qexp)
Qe (hexp,Ci)
Q (m3/s)
Time (s)

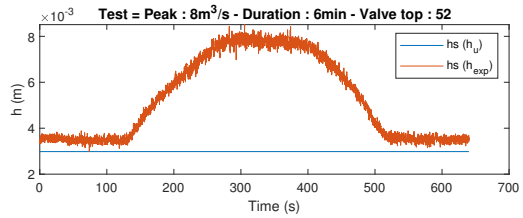
Test = Peak : 8m3/s - Duration : 6min - Valve top : 52
hs (hu)
hs (hexp)
h (m)
Time (s)

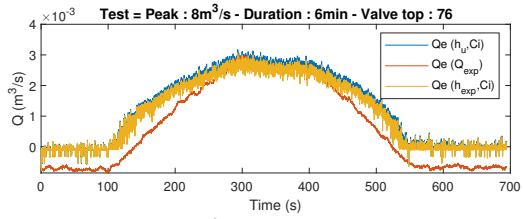
Test = Peak : 8m3/s - Duration : 6min - Valve top : 76
Qe (hu,Ci)
Qe (Qexp)
Qe (hexp,Ci)
Q (m3/s)
Time (s)

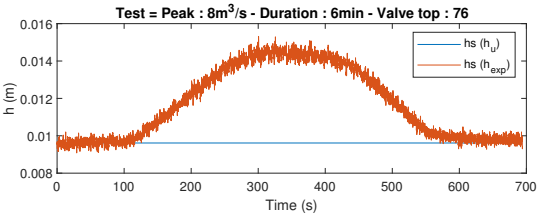
Test = Peak : 8m3/s - Duration : 6min - Valve top : 76
hs (hu)
hs (hexp)
h (m)
Time (s)

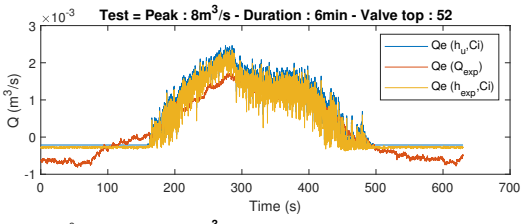
Test = Peak : 8m3/s - Duration : 6min - Valve top : 52
Qe (hu,Ci)
Qe (Qexp)
Qe (hexp,Ci)
Q (m3/s)
Time (s)

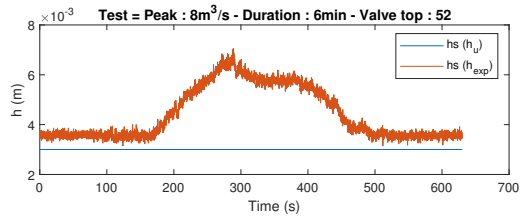
Test = Peak : 8m3/s - Duration : 6min - Valve top : 52
hs (hu)
hs (hexp)
h (m)
Time (s)

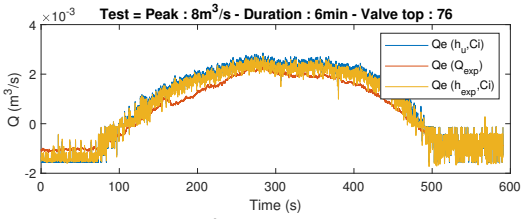
Test = Peak : 8m3/s - Duration : 6min - Valve top : 76
Qe (hu,Ci)
Qe (Qexp)
Qe (hexp,Ci)
Q (m3/s)
Time (s)

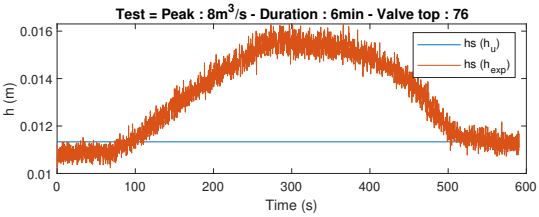
Test = Peak : 8m3/s - Duration : 6min - Valve top : 76
hs (hu)
hs (hexp)
h (m)
Time (s)

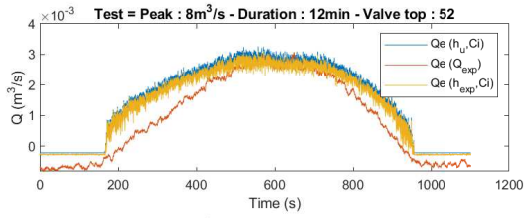
Test = Peak : 8m3/s - Duration : 12min - Valve top : 52
Qe (hu,Ci)
Qe (Qexp)
Qe (hexp,Ci)
Q (m3/s)
Time (s)

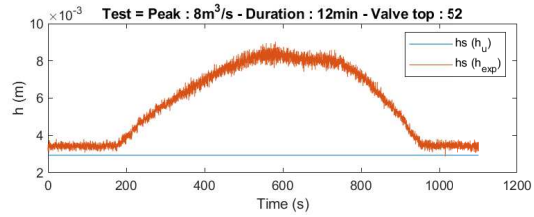
Test = Peak : 8m3/s - Duration : 12min - Valve top : 52
hs (hu)
hs (hexp)
h (m)
Time (s)

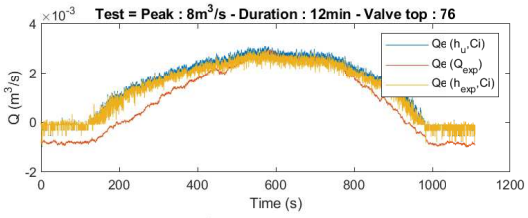
Test = Peak : 8m3/s - Duration : 12min - Valve top : 76
Qe (hu,Ci)
Qe (Qexp)
Qe (hexp,Ci)
Q (m3/s)
Time (s)

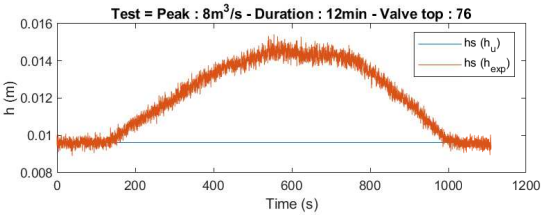
Test = Peak : 8m3/s - Duration : 12min - Valve top : 76
hs (hu)
hs (hexp)
h (m)
Time (s)

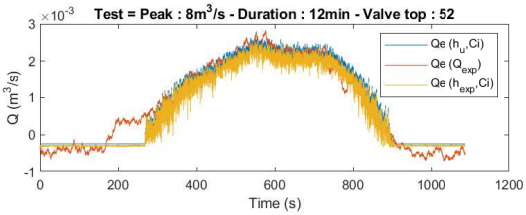
Test = Peak : 8m3/s - Duration : 12min - Valve top : 52
Qe (hu,Ci)
Qe (Qexp)
Qe (hexp,Ci)
Q (m3/s)
Time (s)

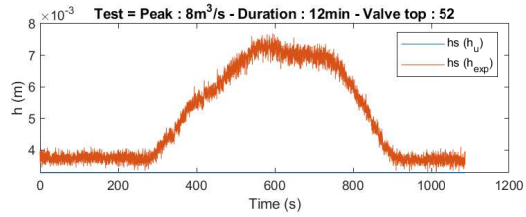
Test = Peak : 8m3/s - Duration : 12min - Valve top : 52
hs (hu)
hs (hexp)
h (m)
Time (s)

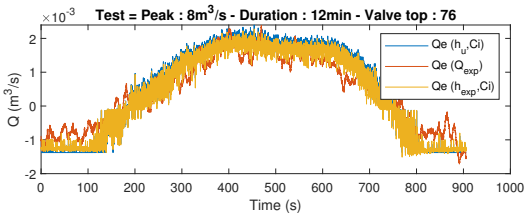
Test = Peak : 8m3/s - Duration : 12min - Valve top : 76
Qe (hu,Ci)
Qe (Qexp)
Qe (hexp,Ci)
Q (m3/s)
Time (s)

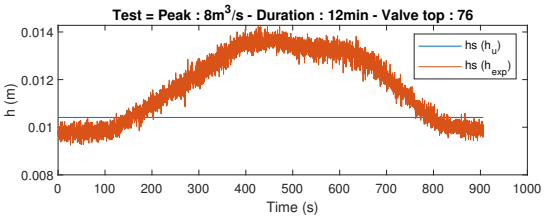
Test = Peak : 8m3/s - Duration : 12min - Valve top : 76
hs (hu)
hs (hexp)
h (m)
Time (s)

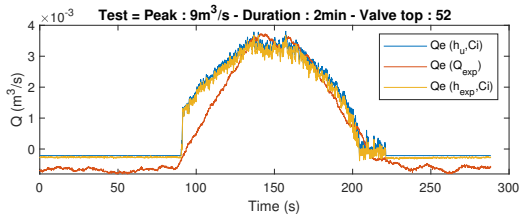
Test = Peak : 9m3/s - Duration : 2min - Valve top : 52
Qe (hu,Ci)
Qe (Qexp)
Qe (hexp,Ci)
Q (m3/s)
Time (s)

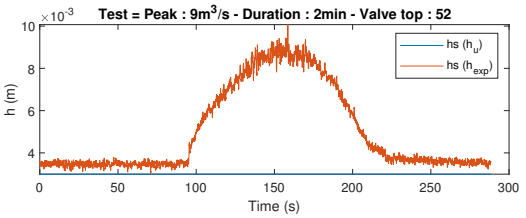
Test = Peak : 9m3/s - Duration : 2min - Valve top : 52
hs (hu)
hs (hexp)
h (m)
Time (s)

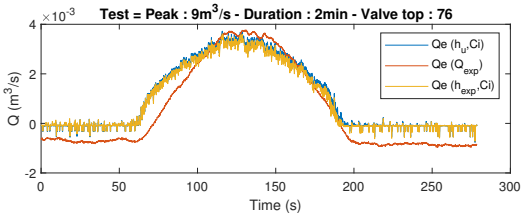
Test = Peak : 9m3/s - Duration : 2min - Valve top : 76
Qe (hu,Ci)
Qe (Qexp)
Qe (hexp,Ci)
Q (m3/s)
Time (s)

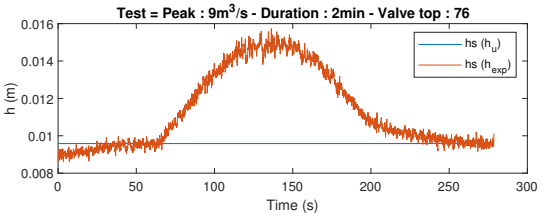
Test = Peak : 9m3/s - Duration : 2min - Valve top : 76
hs (hu)
hs (hexp)
h (m)
Time (s)

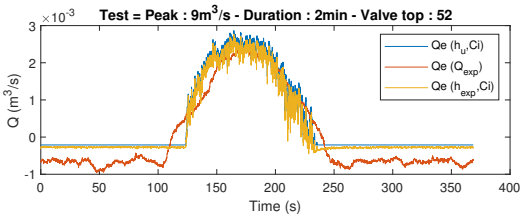
Test = Peak : 9m3/s - Duration : 2min - Valve top : 52
Qe (hu,Ci)
Qe (Qexp)
Qe (hexp,Ci)
Q (m3/s)
Time (s)

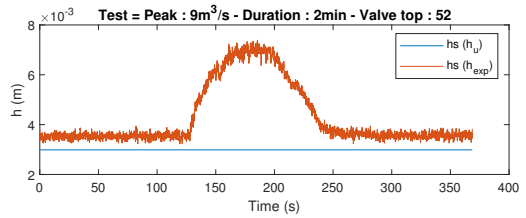
Test = Peak : 9m3/s - Duration : 2min - Valve top : 52
hs (hu)
hs (hexp)
h (m)
Time (s)

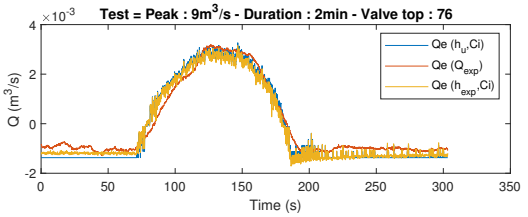
Test = Peak : 9m3/s - Duration : 2min - Valve top : 76
Qe (hu,Ci)
Qe (Qexp)
Qe (hexp,Ci)
Q (m3/s)
Time (s)

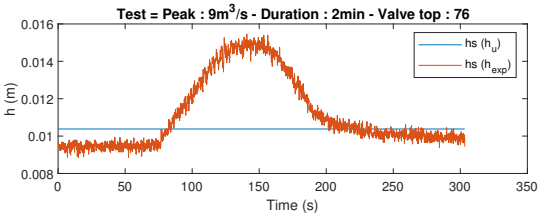
Test = Peak : 9m3/s - Duration : 2min - Valve top : 76
hs (hu)
hs (hexp)
h (m)
Time (s)

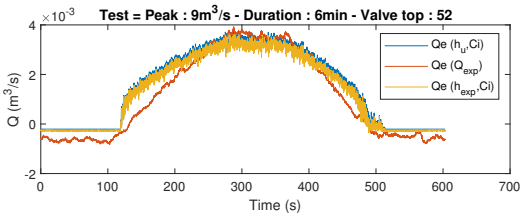
Test = Peak : 9m3/s - Duration : 6min - Valve top : 52
Qe (hu,Ci)
Qe (Qexp)
Qe (hexp,Ci)
Q (m3/s)
Time (s)

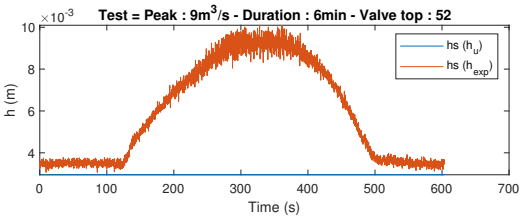
Test = Peak : 9m3/s - Duration : 6min - Valve top : 52
hs (hu)
hs (hexp)
h (m)
Time (s)

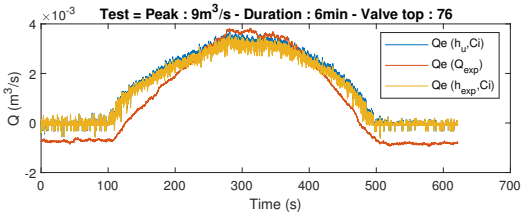
Test = Peak : 9m3/s - Duration : 6min - Valve top : 76
Qe (hu,Ci)
Qe (Qexp)
Qe (hexp,Ci)
Q (m3/s)
Time (s)

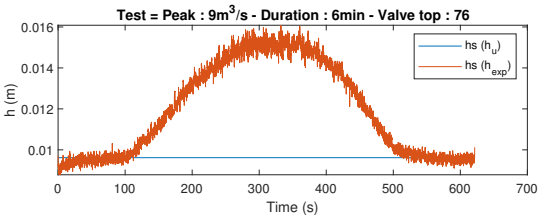
Test = Peak : 9m3/s - Duration : 6min - Valve top : 76
hs (hu)
hs (hexp)
h (m)
Time (s)

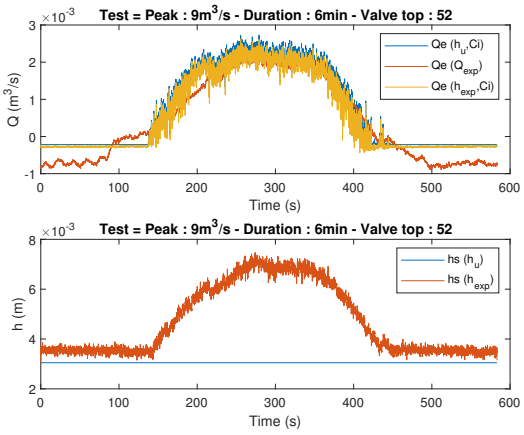
Test = Peak : 9m3/s - Duration : 6min - Valve top : 52
Qe (hu,Ci)
Qe (Qexp)
Qe (hexp,Ci)
Q (m3/s)
Time (s)
Test = Peak : 9m3/s - Duration : 6min - Valve top : 52
hs (hu)
hs (hexp)
h (m)
Time (s)

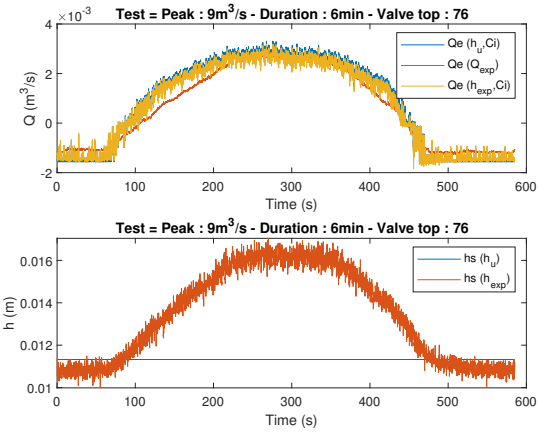
Test = Peak : 9m3/s - Duration : 6min - Valve top : 76
Qe (hu,Ci)
Qe (Qexp)
Qe (hexp,Ci)
Q (m3/s)
Time (s)
Test = Peak : 9m3/s - Duration : 6min - Valve top : 76
hs (hu)
hs (hexp)
h (m)
Time (s)

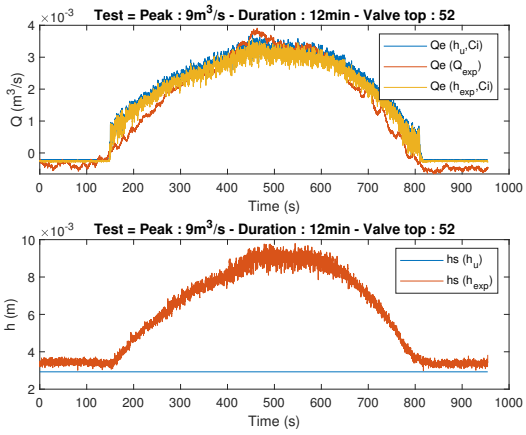
Test = Peak : 9m3/s - Duration : 12min - Valve top : 52
Qe (hu,Ci)
Qe (Qexp)
Qe (hexp,Ci)
Q (m3/s)
Time (s)
Test = Peak : 9m3/s - Duration : 12min - Valve top : 52
hs (hu)
hs (hexp)
h (m)
Time (s)

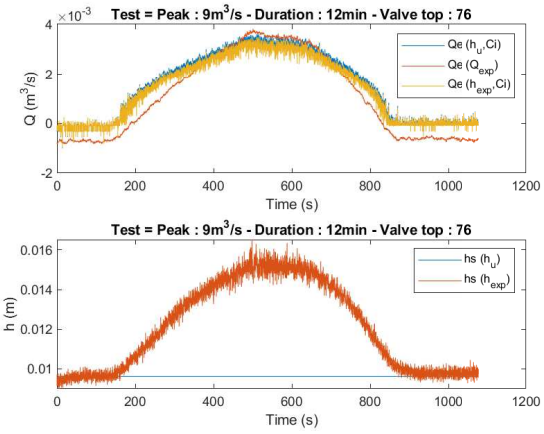
Test = Peak : 9m3/s - Duration : 12min - Valve top : 76
Qe (hu,Ci)
Qe (Qexp)
Qe (hexp,Ci)
Q (m3/s)
Time (s)
Test = Peak : 9m3/s - Duration : 12min - Valve top : 76
hs (hu)
hs (hexp)
h (m)
Time (s)

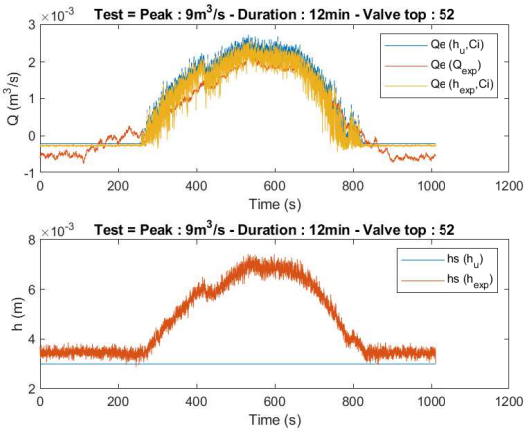
Test = Peak : 9m3/s - Duration : 12min - Valve top : 52
Qe (hu,Ci)
Qe (Qexp)
Qe (hexp,Ci)
Q (m3/s)
Time (s)
Test = Peak : 9m3/s - Duration : 12min - Valve top : 52
hs (hu)
hs (hexp)
h (m)
Time (s)

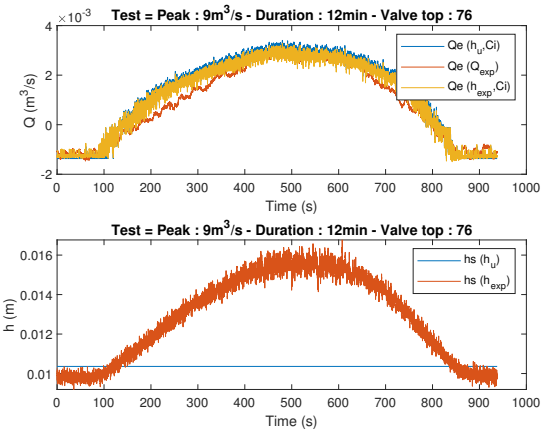
Test = Peak : 9m3/s - Duration : 12min - Valve top : 76
Qe (hu,Ci)
Qe (Qexp)
Qe (hexp,Ci)
Q (m3/s)
Time (s)
Test = Peak : 9m3/s - Duration : 12min - Valve top : 76
hs (hu)
hs (hexp)
h (m)
Time (s)

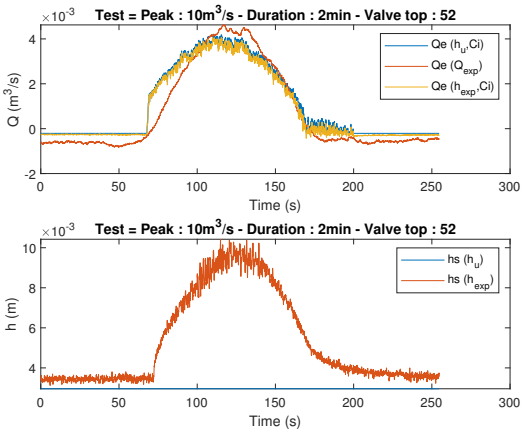
Test = Peak : 10m3/s - Duration : 2min - Valve top : 52
Qe (hu,Ci)
Qe (Qexp)
Qe (hexp,Ci)
Q (m3/s)
Time (s)
Test = Peak : 10m3/s - Duration : 2min - Valve top : 52
hs (hu)
hs (hexp)
h (m)
Time (s)

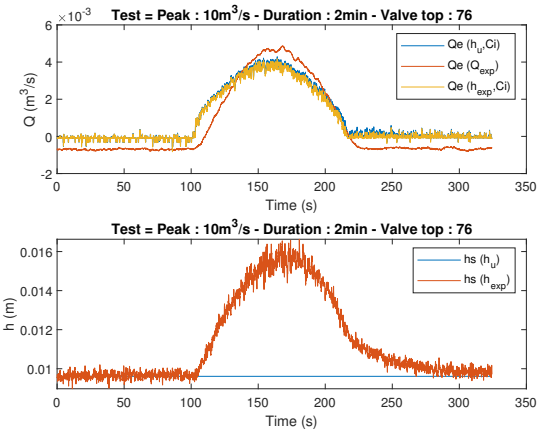
Test = Peak : 10m3/s - Duration : 2min - Valve top : 76
Qe (hu,Ci)
Qe (Qexp)
Qe (hexp,Ci)
Q (m3/s)
Time (s)
Test = Peak : 10m3/s - Duration : 2min - Valve top : 76
hs (hu)
hs (hexp)
h (m)
Time (s)

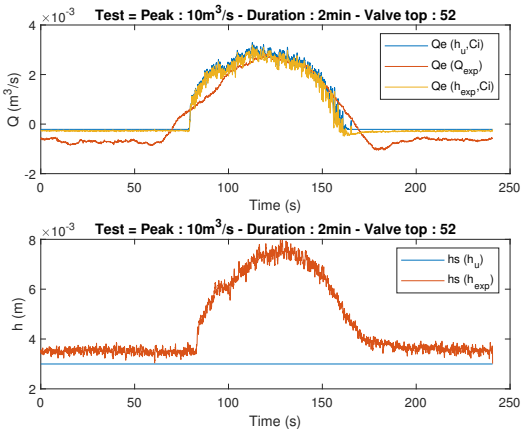
Test = Peak : 10m3/s - Duration : 2min - Valve top : 52
Qe (hu,Ci)
Qe (Qexp)
Qe (hexp,Ci)
Q (m3/s)
Time (s)

Test = Peak : 10m3/s - Duration : 2min - Valve top : 52
hs (hu)
hs (hexp)
h (m)
Time (s)

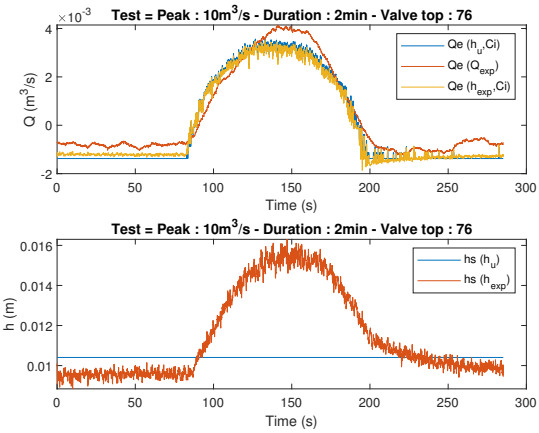
Test = Peak : 10m3/s - Duration : 2min - Valve top : 76
Qe (hu,Ci)
Qe (Qexp)
Qe (hexp,Ci)
Q (m3/s)
Time (s)

Test = Peak : 10m3/s - Duration : 2min - Valve top : 76
hs (hu)
hs (hexp)
h (m)
Time (s)

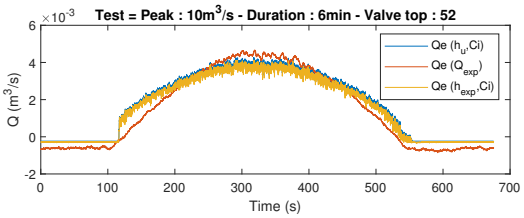
Test = Peak : 10m3/s - Duration : 6min - Valve top : 52
Qe (hu,Ci)
Qe (Qexp)
Qe (hexp,Ci)
Q (m3/s)
Time (s)

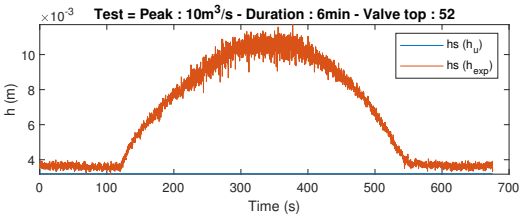
Test = Peak : 10m3/s - Duration : 6min - Valve top : 52
hs (hu)
hs (hexp)
h (m)
Time (s)

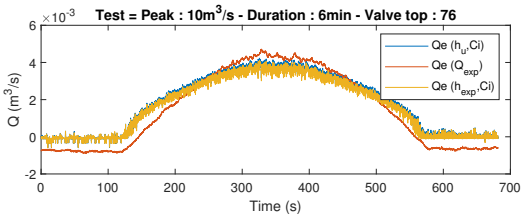
Test = Peak : 10m3/s - Duration : 6min - Valve top : 76
Qe (hu,Ci)
Qe (Qexp)
Qe (hexp,Ci)
Q (m3/s)
Time (s)

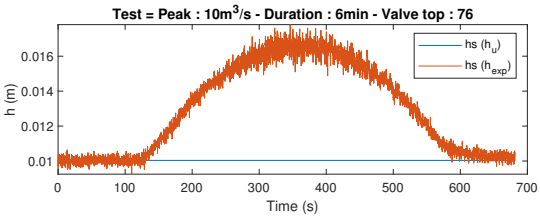
Test = Peak : 10m3/s - Duration : 6min - Valve top : 76
hs (hu)
hs (hexp)
h (m)
Time (s)

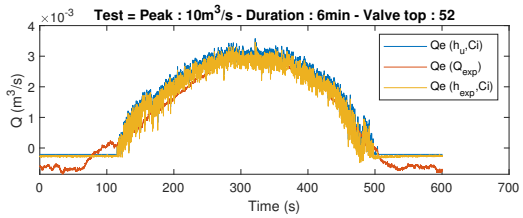
Test = Peak : 10m3/s - Duration : 6min - Valve top : 52
Qe (hu,Ci)
Qe (Qexp)
Qe (hexp,Ci)
Q (m3/s)
Time (s)

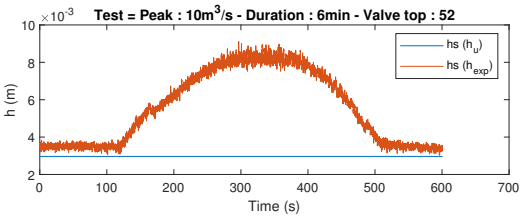
Test = Peak : 10m3/s - Duration : 6min - Valve top : 52
hs (hu)
hs (hexp)
h (m)
Time (s)

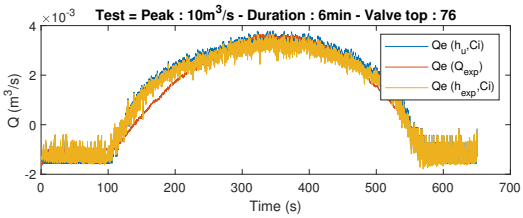
Test = Peak : 10m3/s - Duration : 6min - Valve top : 76
Qe (hu,Ci)
Qe (Qexp)
Qe (hexp,Ci)
Q (m3/s)
Time (s)

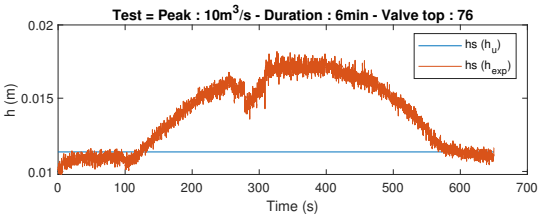
Test = Peak : 10m3/s - Duration : 6min - Valve top : 76
hs (hu)
hs (hexp)
h (m)
Time (s)

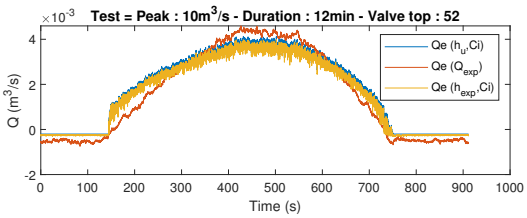
Test = Peak : 10m3/s - Duration : 12min - Valve top : 52
Qe (hu,Ci)
Qe (Qexp)
Qe (hexp,Ci)
Q (m3/s)
Time (s)

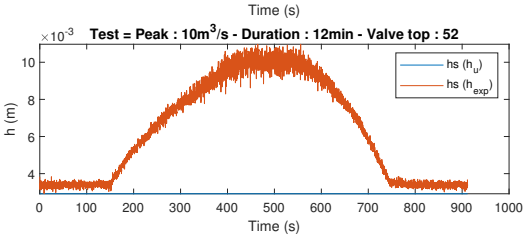
Test = Peak : 10m3/s - Duration : 12min - Valve top : 52
hs (hu)
hs (hexp)
h (m)
Time (s)

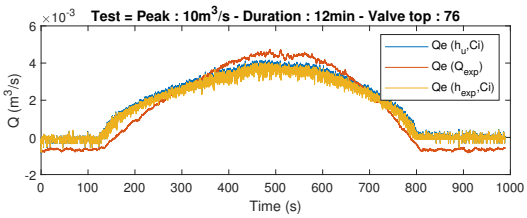
Test = Peak : 10m3/s - Duration : 12min - Valve top : 76
Qe (hu,Ci)
Qe (Qexp)
Qe (hexp,Ci)
Q (m3/s)
Time (s)

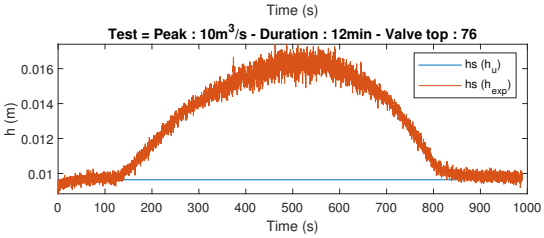
Test = Peak : 10m3/s - Duration : 12min - Valve top : 76
hs (hu)
hs (hexp)
h (m)
Time (s)

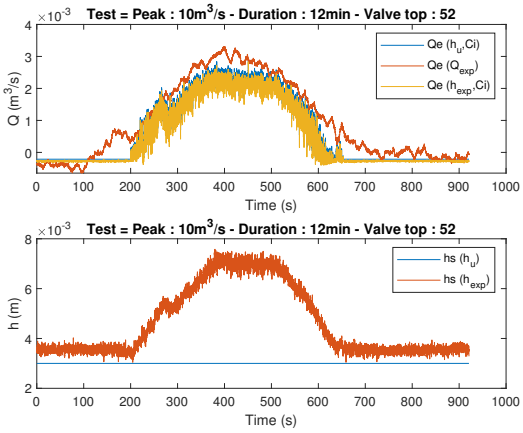
Test = Peak : 10m3/s - Duration : 12min - Valve top : 52
Qe (hu,Ci)
Qe (Qexp)
Qe (hexp,Ci)
Q (m3/s)
Time (s)
Test = Peak : 10m3/s - Duration : 12min - Valve top : 52
hs (hu)
hs (hexp)
h (m)
Time (s)

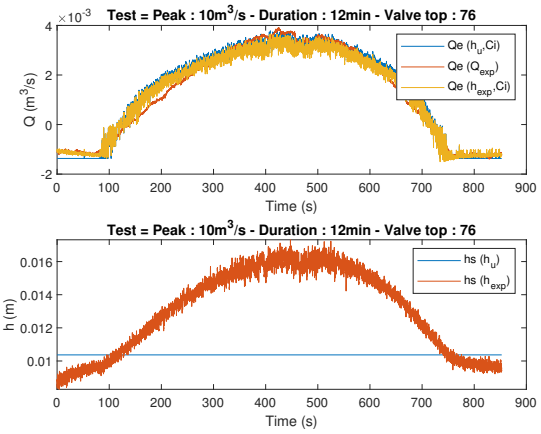
Test = Peak : 10m3/s - Duration : 12min - Valve top : 76
Qe (hu,Ci)
Qe (Qexp)
Qe (hexp,Ci)
Q (m3/s)
Time (s)
Test = Peak : 10m3/s - Duration : 12min - Valve top : 76
hs (hu)
hs (hexp)
h (m)
Time (s)

Bibliography

[1] Asztely, M. (1995). *Literature Review of Energy Losses in Manholes,* Report Series B: 60, ISSN 0348–1069. Department of Hydraulics, Chalmers University of Technology, Goteborg.

[2] Bazin, P.-H., Nakagawa, H., Kawaike, K., Paquier, A., Mignot, E. (2014). Modeling flow exchanges between a street and an underground drainage pipe during urban floods. *Journal of Hydraulic Engineering 140(10),* 04014051.

[3] Beg, M. N. A., Carvalho, R. F., Leandro, J. (2017). Effect of surcharge on gully-manhole flow. *Journal of Hydro-environment Research.*

[4] Djordjevic, S., Ivetic, M., Maksimovic, C., Prodanovic, D. (2005). SIPSON - Simulation of Interaction between Pipe flow and Surface Overland flow in Networks. *Water Science and Technology 52 (5),* 275–283.

[5] Fraga, I., Cea, L., Puertas, J. (2017). Validation of a 1D-2D dual drainage model under unsteady part-full and surcharged sewer conditions. *Urban Water Journal 14 (1),* 74–84.

[6] JinNoh, S., Lee, S., An, H., Kawaike, K., Nakagawa, H. (2016). Ensemble urban flood simulation in comparison with laboratory-scale experiments: Impact of interaction models for manhole, sewer pipe, and surface flow. *Advances in Water Resources 97,* 25–37.

[7] Marsalek, J. (1984). Head losses at sewer junction manholes. *Journal of Hydraulic Engineering 110(8),* 1150-1154.

[8] O'Loughlin, G., Stack, B. (2002). Algorithms for pit pressure changes and head losses in stormwater drainage systems. 9th International Conference on Urban Drainage, Portland, United States.

[9] Payet, M. (2019). *Echanges égouts/surface : Ecoulements stationnaires et instationnaires.* Internal report of the University of Liège.

[10] Pfister, M., Gisonni, C. (2014). Head losses in junction manholes for free surface flows in circular conduits. *Journal of Hydraulic Engineering 140(9),* 06014015.

[11] Rubinato, M. (2015). *Physical scale modelling of urban flood systems.* PhD Thesis.

[12] Rubinato, M., Martins, R., Kesserwani, G., Leandro, J., Djordjevic, S., Shucksmith, J. (2017). Experimental calibration and validation of sewer/surface flow exchange equations in steady and unsteady flow conditions. *Journal of Hydrology, 552 (2017),* 421-432.

[13] Rubinato, M., Martins, R., Shucksmith, J. (2018). Quantification of energy losses at a surcharging manhole. *Urban Water Journal, 15 (3),* 234-241.

[14] Saldarriaga, J., Bermúdez, N., Rubio, D. P. (2012). Hydraulic behaviour of junction manholes under supercritical flow conditions. *Journal of Hydraulic Research,* 50:6, 631-636.

[15] Sangster, W. M., Wood, H. W., Smerdan, E. T., Bossy, H. G. (1958). Pressure changes at storm drain junctions. *Engineering series Bulletin* No. 41.

[16] Wang, K. H., Cleveland, T. G., Towsley, C., Umrigar, D. (1998). Head Loss at manholes in surcharged sewer systems. *Journal of the American Water Resources Association 34,* 1391–1400.